UNIVERSITY OF SOUTHAMPTON

Faculty of Engineering and Physical Sciences
School of Electronics and Computer Science

EEG-based Brain Connectivity Analysis for Identifying Neurodevelopmental Disorders

by

Noura Meshaan Alotaibi

MSc in Computer science

ORCiD: 0000-0003-3815-3814

A dissertation for the degree of
Doctor of Philosophy

April 2022

UNIVERSITY OF SOUTHAMPTON

ABSTRACT

FACULTY OF ENGINEERING AND PHYSICAL SCIENCES
School of Electronics and Computer Science

Doctor of Philosophy

EEG-BASED BRAIN CONNECTIVITY ANALYSIS FOR IDENTIFYING NEURODEVELOPMENTAL DISORDERS

by Noura Meshaan Alotaibi

This dissertation aims to identify the neurological biomarkers that could assist in providing reliable, automated and objective prediction of neurodevelopmental disorders (NDDs) in early infancy. Quantitative electroencephalography analysis (qEEG), mainly phase synchronisation-based functional brain connectivity estimated using phase locking value (PLV) and weighted phase lag index (WPLI), were investigated to deduce whether it can be used for the early prediction of such disorders. The resulting connectivity network was quantitatively characterised using complex graph-theoretical features, namely transitivity, global efficiency, radius, diameter, and characteristic path length. These features were then fed into the machine learning algorithms such as linear discriminant analysis (LDA), support vector machine (SVM), decision tree and k-nearest neighbour to examine their discriminant capability in classifying /predicting NDDs. The proposed framework has gained initial validation in classifying autism spectrum disorders (ASD) from an experimentally obtained EEG data set of 24 children. Then, the framework was utilised to predict the appearance of cerebral palsy (CP) at two years of age. The EEG data were recorded within the first week after birth from a cohort of infants born with hypoxic-ischaemic encephalopathy (HIE). The exploration results revealed that the proposed analytical methodology successfully predicted the infants that would develop CP with a performance of 84.6% accuracy, 83% sensitivity, 85% specificity, 84% balanced accuracy and 0.85 area under the curve (AUC) in the delta band, with a close result also obtained in the theta and alpha bands. The WPLI and graph parameters were then used to predict the cognitive scores of infants born with HIE by developing the regression framework correlating these EEG features and a cognitive profile completed in a follow-up assessment at two years of age. The regression analysis showed that the radius feature yielded the best performance (root mean square error (RMSE)= 16.78, mean absolute error (MAE)= 12.07 and R-squared= 0.24). Although this study has successfully demonstrated that the qEEG features could be considered potential biomarkers for identifying the brain deficits causing the NDDs, it has a certain limitation due to the size of the data set. It needs to be validated on large trials with a statistically significant population.

Contents

List of Figures

List of Tables

Declaration of Authorship

I, Noura Meshaan Alotaibi, declare that this thesis and the work presented in it is my own and has been generated by me as the result of my own original research.

I confirm that:

1. This work was done wholly or mainly while in candidature for a research degree at this University;
2. Where any part of this thesis has previously been submitted for a degree or any other qualification at this University or any other institution, this has been clearly stated;
3. Where I have consulted the published work of others, this is always clearly attributed;
4. Where I have quoted from the work of others, the source is always given. With the exception of such quotations, this thesis is entirely my own work;
5. I have acknowledged all main sources of help;
6. Where the thesis is based on work done by myself jointly with others, I have made clear exactly what was done by others and what I have contributed myself;
7. Parts of this work have been published as: (Alotaibi & Maharatna 2021), (Bakheet et al. 2021) and (Alotaibi et al. 2022)

Signed:..... Date:07/04/2022.....

Acknowledgements

All praise be to Almighty Allah for all blessing who provided to me, and without His blessing I could not complete this challenging journey.
This research work would not be accomplished without the support and help of numerous individuals. I am very grateful to be surrounded by those people who motivated and believed in me. First and foremost, I will never be thankful enough to Prof. Koushik Maharanta to give me the opportunity to be PhD student under his supervision. His patient, uninterrupted guidance, support, encouragement, and kindness accompanied me through the life obstacles and scientific challenges faced during the PhD journey.
I acknowledge the valuable help of Dr Daniel Konn in providing the EEG data set for this research, along with a lot of practical comments and helpful discussions. I am also grateful to Dr Brigitte Vollmer for providing the neurological evaluation information for the infants' data set used in this research, along with helpful advice and comments.
I also have to express my gratitude to my colleagues in my research group for their cooperation, help and suggestions.
I would express my gratitude to my family. I owe more to them than I can express in words and am truly grateful for all they do and continue to do. I am deeply indebted to my father and mother for their prayers, support, encouragement, and for their being with me every step of the way in my life. I owe a deep sense of gratitude to my brothers (Abdullah, Mohammed and Abdulrahman) and my sisters (Sheemah, Reem, Joud and Retaj) for their continuous and unparalleled love, help and support.
Last but not least, from the bottom of my heart, I would like to thank my close friends Tarfah Alrashed, Ghada Alzaydi, Dalal Bakheet, Kholoud Alghamdi, and Muna Altharwi for their help, support and for being with me through the tough times and the happy moments. I could not have completed this dissertation without their supports.
I would also like to extend my deepest gratitude to my friend Dalal Bakheet who provided stimulating discussions about the research directions, was co-author in several manuscripts, helped me cope with being away from my family for these years and provided happy distractions to rest my mind outside of my research.

To my family, friends and supervisor . . .

Definitions and Abbreviations

ACC	Accuracy
ADHD	Attention-Deficit/Hyperactivity Disorder
ADI-R	Autism Diagnostic Interview-Revised
ADOS-G	Autism Diagnostic Observation Schedule-Generic
aEEG	amplitude-integrated Electroencephalogram
ASD	Autism Spectrum Disorders
AUC	Area Under the Curve
BOLD	Blood Oxygenation Level Dependence
BSITD-III	Bayley Scales of Infant and Toddler Development III
CAR	Common Average Reference
cEEG	conventional Electroencephalogram
CP	Cerebral Palsy
DBP	Digital Bandpass Filter
DCM	Dynamic Causal Modelling
DFA	Detrended Fluctuation Analysis
DSM-IV-TR	Diagnostic and Statistical Manual of Mental Disorders: Text Revision
DSM-5	Diagnostic and Statistical Manual of Mental Disorders, fifth Edition
DTF	Direct Transfer Function
ECG	Electrocardiogram
EEG	Electroencephalogram
EMD	Empirical Mode Decomposition
ERP	Event-Related Potentials
FBC	Functional Brain Connectivity
FFT	Fast Fourier Transform
FIR	Finite Impulse Response
fMRI	functional Magnetic Resonance Imaging
fNIRS	functional Near Infrared Spectroscopy
GC	Granger Causality
HCoh	Intrahemispheric Coherence
HIE	Hypoxic-Ischemic Encephalopathy
IC	Independent Component
ICA	Independent Component Analysis

ICoh	Interhemispheric Coheerence
IIF	infinite impulse response
ImCoh	Imaginary Component of Coherence
IMF	Intrinsic Mode Functions
KNN	K-Nearest Neighbour
LDA	Learning Discriminant Analysis
LOOCV	Leave-One-Out-Cross-Validation
MAE	Mean Absolute Error
MCN	modified combinatorial nomenclature
MEG	Magnetoencephalography
MEMD	Multivariate Empirical Mode Decomposition
MRI	Magnetic Resonance Imaging
NA-MEMD	Noise-Assisted Multivariate Empirical Mode Decomposition
NDDs	Neurodevelopmental Disorders
PDC	Partial Direct Coherence
PDD-NOS	Pervasive Developmental Disorder-not Otherwise Specified
PET	Position Emission Tomography
PLI	Phase Lag Index
PLV	Phase Locking Value
qEEG	quantitative EEG
rs-fMRI	resting-state fMRI
RMSE	Root Mean Square Error
RUSBoost	Random Under-Sampling Boosting
SNS	Sensitivity
SPC	Specificity
STFT	Short-Time Fourier Transform
SVM	Support Vector Machine
TD	Typically Developing
t-fMRI	task-based fMRI
TNR	True Negative Rate
TPR	True Positive Rate
UHS	University Hospital of Southampton
WPLI	Weighted Phase Lag Index

Chapter 1

Introduction

Neurodevelopmental disorders (NDDs) are a group of conditions caused by atypical brain growth and functions, and their onset occurs in the developmental period (often in a pre-school age) (Tran & Miyake 2017). According to the Diagnostic and Statistical Manual of Mental Disorders, Fifth Edition (DSM-5), NDDs include cerebral palsy (CP), attention-deficit/hyperactivity disorder (ADHD), autism spectrum disorders (ASD), learning disabilities, and communication and motor disorders (Tran & Miyake 2017). An individual with an NDD could suffer from impairments in cognition, intelligence, learning ability, social skills, and in certain cases, motor skills. Some of these impairments could be permanent, while others might alter or become more extensive during an individual's lifetime (Klimkeit et al. 2008). Although still a matter of some controversy—and not always clear—the causes of NDDs may, in some cases, be associated with risk factors including genetic, social, environmental, and other factors (Blackburn et al. 2012). Poor pregnancy outcomes, such as low birth weight and delivery complications, which are influenced by genetic and social factors, are usually associated with NDDs (Blackburn et al. 2012). Hypoxic-ischaemic encephalopathy (HIE), one of the most severe birth complications affecting infants, is considered the leading cause of NDDs (Byeon et al. 2015).

Recent years have seen a rise in the prevalence of NDDs. In the UK, for example, the prevalence of ASD, ADHD and learning disorders has increased from around 50,000 in 1995 to approximately 210,000 in 2012 (Blackburn et al. 2012). In England in particular, the prevalence of NDDs among children is estimated to be around 3 - 4% (Blackburn et al. 2012). This disability has significant impacts on an affected individual's quality of life, as well as on the parents, and its increased incidence affects society as a whole. A disabled individual faces many barriers in health, education, employment and social participation, including an inadequate environment, insufficient funding for money and poor attitudes from others (Blackburn et al. 2012). Furthermore, caring for an individual with NDDs has negative economic impacts as parents and society pay a high

cost for health care, special education services and losses in productivity. Services cost the UK between £23.7 and £152.15 per week for each child [1] (Gov.uk 2021)

Early diagnosis of NDDs, mainly in early infancy, is crucial for establishing the appropriate early intervention strategies and providing parents with more accurate prognostic information and counselling. Ultimately, early intervention may improve the neurodevelopmental outcomes and prevent severe symptoms in young children. It would also help to reduce the high financial costs associated with caring for the affected person. The mechanism behind intervention strategies is attributed to the plasticity of the developing brain could be optimised in early infancy (Glass et al. 2021). Brain plasticity can be defined as the ability of the brain to modify its structure and functions (Cioni et al. 2016). The critical period of brain plasticity is during its maturation when the structural connections in the brain are continually shaped by synaptic modifications to neuronal growth under the influences of learning and experience (Cioni et al. 2016). Early intervention, therefore, attempts to utilise this property by providing suitable learning and behavioural training to alter the developmental trajectory and modify structural connections.

Traditionally, the diagnosis of an NDD occurs following the manifestation of symptoms, which is, on average, at around age 4.5 years and typically after parents or the child's school have flagged symptoms, depending on their vigilance (Duda et al. 2016). The most active brain plasticity period has passed by this time, and so the faulty brain connections are mostly set, making any changes with behavioural intervention much more difficult. Clinical assessments that include behavioural tests, developmental tests and neurological examinations are currently used for diagnosing NDDs. These assessments are usually lengthy, subjective, and they require a multidisciplinary team to assess the behavioural, historical and parental report information (Falkmer et al. 2013).

It follows that in recent years, researchers have sought methods to evaluate brain function in early infancy, utilising their findings to aid the early prognosis of neurodevelopmental outcomes. One technique to feature in several recent studies is neuroimaging, which is utilised to identify infants with neurodevelopmental delay (Ouyang et al. 2020, Potharst et al. 2012, Slaughter et al. 2016). Alongside neuroimaging methods, electroencephalogram (EEG) is a widely used technique for capturing brain activity and identifying brain deficits because it is relatively inexpensive, portable, non-invasive, user-friendly and comparatively easy to use. Therefore, EEG analysis is now being used in predicting neurodevelopmental outcomes in several studies as reported in the review of Ouwehand et al. (2020). Nevertheless, the interpretation of the prognostic value of these methods remains subjective, however.

[1] This statistic was taken from a number of recipients of Disability Living Allowance, which is the UK state benefit for people needing extra care and support in their daily lives.

Researchers are therefore keen to find approaches that can identify the neurological biomarkers of NDDs that could potentially assist in providing an objective prediction of neurodevelopmental outcomes. Quantitative EEG (qEEG) could provide objective, reproducible, and reliable biomarkers to characterise the brain activities related to these disorders. Limited previous studies have, in fact, shown that such qEEG features can satisfactorily predict the long-term neurodevelopmental outcomes (Hayashi-Kurahashi et al. 2012, Lloyd et al. 2016). However, this field has yet to find a reliable biomarker suitable to be introduced into clinical practice. Because detailed explorations of qEEG for identifying NDDs in infancy age are limited, more studies are needed, with particular attention given to qEEG features and their efficiency in providing insights into the brain developmental state.

In the following sections, a brief description of the aim and the objectives, together with the challenges and overall contributions of this research, are provided. The chapter concludes with an outline of the dissertation.

1.1 Aim and Objectives

This research aims to overcome the shortcomings outlined above by exploring the feasibility of the qEEG features-based machine learning framework to early predict neurodevelopmental outcomes in term-born infants at high-risk (specifically those born with HIE). The ultimate aim of this proposed framework is to provide the early prediction of NDDs, which in turn facilitate providing the tailored intervention. This aim is supported by the World Health Organization, which stated that identifying infants at risk for NDDs is crucial to establishing a close relationship between parents and health care providers and providing early intervention (Cioni et al. 2016, Organization 2011). A coherence systematic review provided by Spittle et al. (2015) also showed a significant association between the early interventions protocol and the positive effects on cognitive development, but effects tend to disappear after preschool age (Cioni et al. 2016). Mainly, the goal of early intervention is to prevent or reduce the motor, cognitive and emotional impairments in young children, and this would have a significant improvement in the patient's quality of life (Cioni et al. 2016, Kiiski et al. 2018). In addition, the early intervention could provide the promotion of parent-infant interaction, reduce the parent stress, anxiety and depression, and afford a supportive environment (Hadders-Algra 2021).

This dissertation tests the hypothesis that the qEEG feature, mainly functional brain connectivity (FBC), specifically the phase-based connectivity characterised by graph-theoretical metrics, could be used as a biomarker for identifying the NDDs. This approach reflects the underlying information flow between different areas in the brain

network by measuring the functional interactions between the distant and distinct brain regions. Characterising these interactions using the graph theory parameters provides a better understanding of the brain functions and topological properties of the brain network. As developmental delay stems from disruption of the functional brain network, the FBC with the graph theory analysis is chosen to employ in this research to reveal the individual's brain network properties and explore the early development of the organisational brain paradigm. At the same time, any alteration in these network characteristics is investigated within the machine learning framework to examine whether it could be used as a biomarker for identifying the neurodevelopmental delay. The machine learning techniques were employed in this dissertation as a framework to assess the FBC and complex network measures as predictors of NDDs. These techniques were utilised to assist in developing EEG-based biomarkers for automated and objective prediction of NDDs at the individual subject level. The performance of the machine learning technique was used as a metric to evaluate the diagnostic efficiency of the FBC and complex network measures (Chaitra et al. 2020).

In order to ascertain the validity of the proposed approach, the starting point of this research is to design a basic framework to classify children with ASD and typically developing (TD) groups in an experimentally obtained EEG data set of twenty-four children, twelve with ASD and twelve TD. Even though the aim of this work is the early prediction of NDDs, this data set is chosen to validate the proposed framework because it is considered proven data set and has been previously employed in several studies (Apicella et al. 2013, Jamal et al. 2014, Khuntia et al. 2019). The second phase involves investigating the utility of this framework in predicting neurodevelopmental outcomes at two years of age from a neonatal EEG recording at the first week after birth. The main purpose of the study is to identify the infants who developed CP at two years of age by validating the neonatal EEG analysis against the clinical labels assessed at that age. The phase-based FBC is necessarily calculated from the single scale of the EEG spectra—a complex signal composed of multiple frequency oscillators—to characterise the overlapping time-frequency brain dynamics associated with CP. Thus, some form of prefiltering into narrowband is necessary before estimating the instantaneous phase. Traditionally, the digital bandpass filter (DBP) has been utilised for this purpose, relying on the predefined traditional brain waves. Quantification of phase synchronisation calculated from the DBP filter is compared with the adaptive decomposition algorithm (without a priori selection of the filter cut-offs), namely noise-assisted multivariate empirical mode decomposition (NA-MEMD) in CP prediction. The final part of the research investigates the effectiveness of the neurological biomarkers—identified in the previous phase—to predict the cognitive outcome. This can be established by finding the association between neonatal EEG and the individual cognitive profiles that were completed at a follow-up visit at 24 months of age.

The dissertation objectives can therefore be restated as follows:

- To investigate the effectiveness of FBC analysis employed within a machine learning framework in discriminating between children with ASD and TD.
- To inspect the feasibility of quantitative EEG-based FBC on the basis of a machine learning framework in finding a biomarker that helps in the early prediction of CP from high-risk term-born infants with neonatal HIE and who were diagnosed either as having or not having CP at twenty-four months of age.
- To explore whether incorporating the biomarkers identified in the previous step with the regression-based model could predict the cognitive outcome at twenty-four months of age.
- To examine the effectiveness of the NA-MEMD algorithm in decomposing EEG signals into their intrinsic components and compare its results in CP prediction with the traditional DBP filter.
- To establish the graph-theoretic framework to quantify the topographical characteristics of FBC and identify the highest impact network measures in: 1) discriminating between ASD and TD, 2) classifying between CP and normal, and 3) predicting the later cognitive outcome at two years of age.
- To identify the association between frequency ranges and dysfunction of FBC in: 1) children with ASD, 2) infants diagnosed later with CP, and 3) infants associated with cognitive outcome at two years of age.

Figure 1.1 illustrates a schematic diagram giving a generalised view of the blocks required to achieve the research objectives.

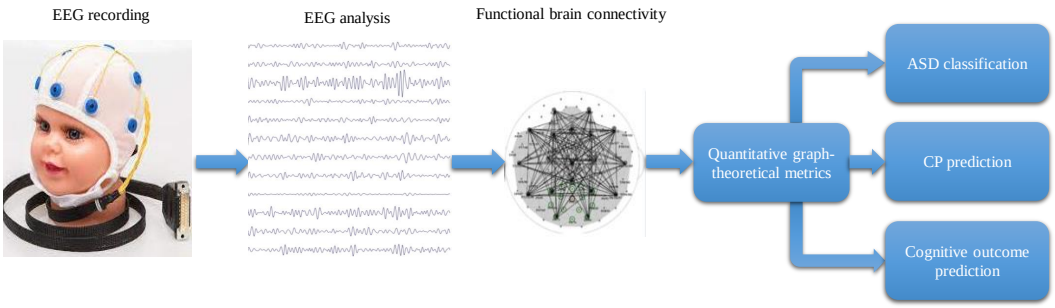

FIGURE 1.1: Schematic diagram of core issues in the prediction of NDDs, as proposed in this research. The first step in the proposed prediction framework is the EEG recording from the two populations: children and infants. Then the recorded EEG signals are preprocessed to enhance the quality of signals and remove the artefacts. After that, the desired qEE features are extracted using phase-based FBC and graph theoretical features. These features are fed into several machine learning algorithms to investigate their ability in ASD classification, CP prediction and cognitive outcome prediction.

1.2 Contributions

The contributions of this dissertation are outlined below.

- Validates using the phase-based FBC characterised by global graph-theoretical attributes as features in a machine learning framework to distinguish between and classify ASD and TD groups.
- Establishes a novel machine learning framework for predicting, at two years of age, the neurodevelopmental outcomes from neonatal EEG of infants born with HIE highlighting a potential approach that could serve as an aiding tool for earlier prediction of neurodevelopmental outcomes; subsequently assisting in establishing the tailored intervention programme at an early stage to improve the outcome.
- Shows that the quantitative graph-theoretical features derived from phase-based FBC networks could provide additional evidence (markers) for early predicting the long-term outcomes (CP and cognitive deficits). It is hoped that this study will lay the ground for more research that could provide a direct assessment of the brain using EEG and lead to new insights into automating the neurodevelopmental delay prediction before the prodromal stage.
- Demonstrates, for the first time, that NA-MEMD could be used for defining the pairwise synchrony between a multiple time-series of infants in order to quantify the synchronisation across data-driven modes /frequencies that are consistent across all the signals. Using this algorithm contributes to the existing knowledge by providing an approach that adaptively decomposes the time-series. All potentially meaningful subject-specific brain dynamics inherent in the signals are thus included in the analysis, and the issue of variations in neural oscillation ranges among individuals—particularly in infants—could be settled.

1.3 Dissertation Outline

The remainder of the dissertation is organised as follows: Chapter 2 includes the background and literature review of EEG analysis, functional brain connectivity, and graph theory analysis. The chapter also provides the basic concept of the machine learning framework and its relevant application in diagnosing pathological conditions. Further, it reviews the current state-of-the-art techniques for predicting neurodevelopmental disorders and then describes the shortcomings of these techniques that are motivated for proposing the methodology in this study. Chapter 3 describes the proposed framework based on FBC and complex network measures and its application in diagnosing

ASD. Chapter 4 goes on to validate the previously established framework in predicting the neurodevelopmental outcome, particularly CP, in newborns affected by HIE. Chapter 5 presents the sophisticated signal processing technique, namely NA-MEMD, in order to investigate its efficiency in calculating phase-based FBC. The chapter then also provides a comparison of NA-MEMD results with the traditional approach DBP filter used in Chapter 4. The methodology of early predicting the cognitive outcomes in infants with neonatal HIE and its results are described in Chapter 6. The final chapter brings together the threads of upon the entire dissertation and highlights the possible areas for further research.

Chapter 2

Background and Literature Review

2.1 Introduction

This chapter reviews the theoretical background and the basic concepts regarding brain functions and EEG signals processing. The background covers the description of the brain components and their functions, the techniques used for capturing brain activity, and the fundamental EEG signal analysis. The brain connectivity and its types are also included. Usually, the brain connectivity network is characterised by graph-theoretical attributes to provide an abstraction and better understanding of brain network topology. Hence, the overview of graph theory analysis is presented to demonstrate its basic concept. The chapter also explains the machine learning framework and the state-of-the-art studies of its application in predicting neurodevelopmental outcomes. Since the first stage in this research focuses on classifying ASD children, a brief description of ASD symptoms and current diagnosis protocols are provided. An introduction to HIE, its complications, and the state-of-the-art approaches used for the outcome prediction of newborns at-risk of developing neurodevelopmental deficits later in life are also provided.

The chapter is structured as follow: section 2.2 demonstrates the components of the human brain and its functions. The types of brain connectivity and the state-of-the-art studies that have used brain connectivity in studying brain disorders are reviewed in section 2.3. The graph theory analysis and its application in investigating the pathological brain functions are described in section 2.4. The basic concept of the machine learning framework and its application for automating the diagnosis /prediction of the neurodevelopmental outcomes are provided in section 2.5. Section 2.6 gives the background of the pathological conditions under investigation in this work and reviews the studies classifying and predicting them. An overview of the proposed study is illustrated in section 2.7.

2.2 The Human Brain: Introduction and Measurement techniques

Neurons are the basic unit of the brain responsible for triggering the events from outside or inside the body, sending motor commands to the muscles, and transforming information to other neurons at every step in between. The human brain consists of many neuronal cells connected forming a complex network with an estimated 100 trillion synaptic connections between them (Northcutt 1989). Typical neurons need both electrical and chemical stimulation for excitation and initiating interaction with other neurons. An interaction commences when the neuron is triggered by the external or internal stimulus evoking the physical or physiological response, producing an electrical impulse. This electrical impulse then travels along the neuron's axon until it reaches the dendrite of the next neuron at a synapse. In addition to electrical communication, the neurons can interact through chemical transmission using neurotransmitters acting as the chemicals that carry the signals across the synapses between neurons. Figure 2.1 shows the neuron structure.

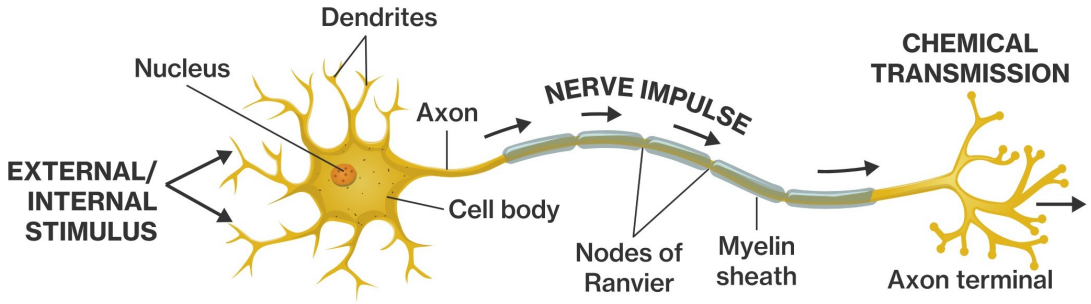

FIGURE 2.1: Neuron structure and how the neuronal signal transfer along with the neuron cells. Image was taken from McGuire (2021).

The neural activities can be measured directly by registering the electrical and magnetic currents produced simultaneously from each neuron during communication with others. In addition, they can be measured indirectly by capturing the functional and physiological effects related to brain activities. EEG is the time-series data of the electrical signals generated by intercommunications between neurons recorded by scalp electrodes (Covarrubias 2017). The electrodes measure the difference of potential between dipoles formed by axons and dendrites, and a selected reference. The magnetic field is generated simultaneously with initiated electrical current from each neuron which can be measured by magnetoencephalography (MEG).

On the other hand, brain activities can be measured indirectly by quantifying the change

in blood flow. Functional magnetic resonance imaging (fMRI), positron emission tomography (PET) or functional near-infrared spectroscopy (fNIRS) are examples of imaging techniques that rely on this mechanism. fMRI measures brain activities by detecting the changes associated with blood flow. PET measures the metabolic change in the cells of brain tissues by using the tracer (radioactive drug). PET scanning allows seeing how the brain is working and detecting abnormalities by identifying the inactive brain areas that consume energy (glucose) at a lower level than the active ones. fNIRS measures brain activity by estimating the changes in the light absorption of different haemoglobin species. Generally, EEG and fMRI are the most commonly used methods in measuring and studying brain activities; hence, the following sections describe these techniques in more detail.

2.2.1 fMRI

fMRI is based on the magnetic resonance imaging (MRI) technique that uses nuclear magnetic resonance coupled with gradients in a magnetic field to show the image of the brain's structure. fMRI measures brain activity based on blood oxygenation levels that change in response to neural activity. The active neurons in the brain consume more oxygen than inactive ones, and the blood flow is increased to this active brain area to meet this increased demand for oxygen (since the oxygen is delivered to neurons by haemoglobin in red blood cells). The variation of oxygen concentration in haemoglobin between the neurons that consume high amounts of oxygen and those that supply it is called blood oxygenation level-dependent (BOLD). Practically, the BOLD contrast results from the difference in the magnetic field surrounding the red blood cell depending on the oxygen state in the haemoglobin (Glover 2011). As a result, fMRI deduces brain activity by monitoring the brain region with more blood oxygenation, i.e., producing the brain activation maps showing which parts of the brain are involved in a particular mental process.

The brain activity can be measured using fMRI during two experimental paradigms: task-based fMRI (t-fMRI) or resting-state (rs-fMRI). In t-fMRI, the brain activities are scanned during manipulating different tasks such as visual, auditory or other stimuli to induce the different neural states in the brain (Glover 2011). In rs-fMRI, brain activities are measured during resting-state, i.e., in the absence of external stimuli or demands of imposed tasks. Generally, fMRI has been widely used for investigating several brain disorders such as ASD (Assaf et al. 2010, Bos et al. 2014, Chaitra et al. 2020, Doyle-Thomas et al. 2015, Gooskens et al. 2021, Iidaka 2015, Keown et al. 2013, Lau et al. 2019, Shao et al. 2021), ADHD (Cao et al. 2014, Lake et al. 2019, Luo et al. 2020) and learning disorders (Yin et al. 2020).

The most prominent advantage of fMRI is its relatively high spatial resolution in the

order of 3 - 4 mm that helps provide an anatomical scanning of the brain with high resolution in the same session, which makes fMRI is optimal for source localisation (Glover 2011). Furthermore, fMRI is a non-invasive technique widely available for clinicians and researchers. However, it has a limited temporal resolution attributed to haemodynamic response time. Typically, the BOLD response has a width of approximately 3s and a peak occurring around 5 - 6s after the onset of a neural stimulus which is much slower than the underlying neural processes, and temporal information is thereby heavily blurred (Glover 2011). Additionally, the equipment used in this technique is large and much more expensive than other neuroimaging techniques.

2.2.2 EEG

EEG is a technique used for a direct measure of brain activities. It registers the electrical current from the scalp using a set of electrodes. Several electrode system configurations are used to record the EEG, such as the 10-20 system and HydroCel Geodesic Sensor. The 10-20 system is a standard electrode system configuration used to record the electrical potentials from the scalp. It uses anatomical landmarks on the skull, as shown in Figure 2.2. The name of this system is derived from the distance interval between electrode positions which is determined based on the interval between the subject's nasion and inion; where nasion is the delve at the top of the nose, and inion is the bony lump at the back of the head (Malmivuo & Plonsey 1995). This long interval is divided into 10% and 20% segments, and the electrodes are placed at both endpoints of each segment, as depicted in Figure 2.2. The standard 21 electrodes of 10-20 system can be extended to incorporate a large number of electrodes, which are placed between the 21 electrodes with the same intermediate 10% interval distance as shown in Figure 2.3.

It should be noted that the EEG signals recorded from the human brain are attenuated due to different factors such as the several brain layers, which they have to pass through until they reach the scalp. The amplifier is used to resolve this issue and regulate the signals in the displaying units.

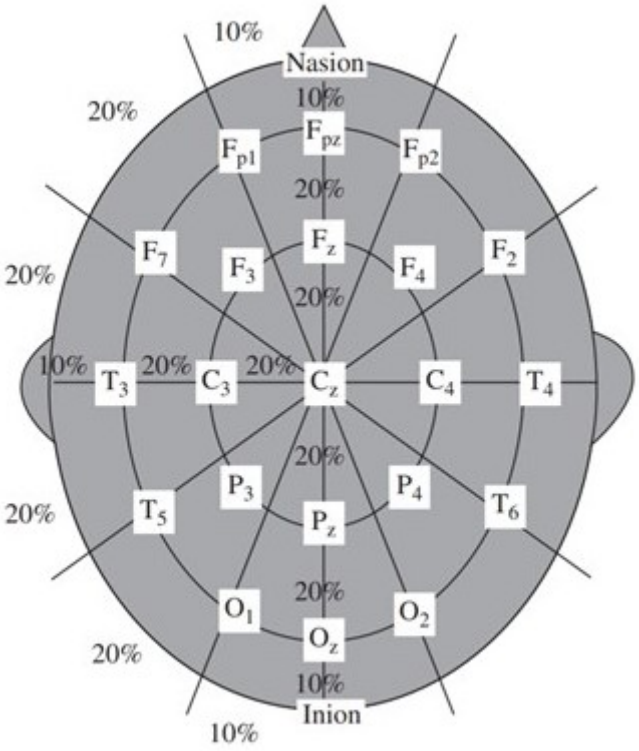

FIGURE 2.2: Conventional 10-20 EEG electrode positions for the placement of 21 electrodes (Sanei & Chambers 2013).

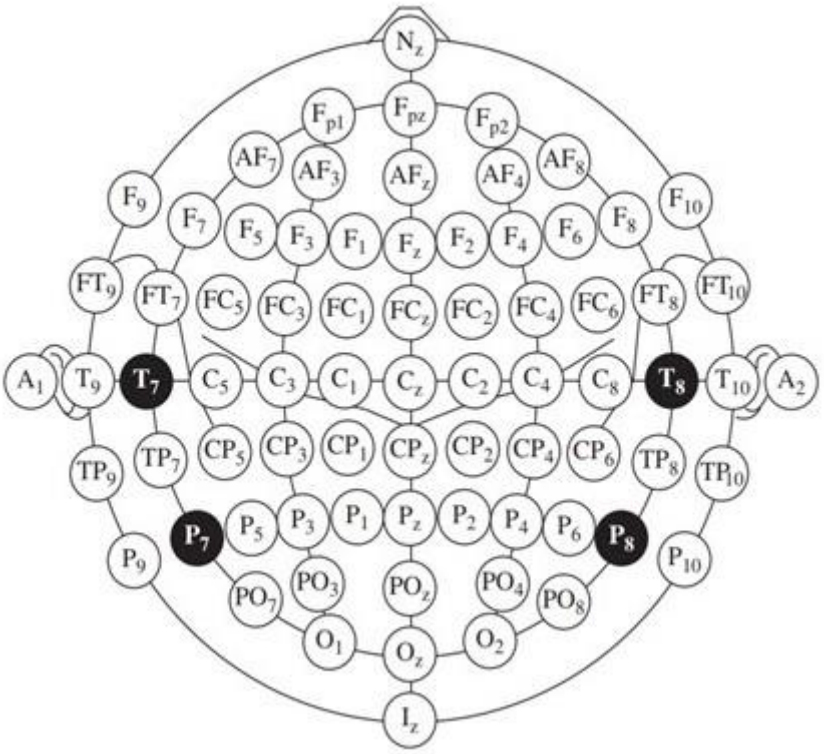

FIGURE 2.3: A diagrammatic representation of the extended version of 10-20 system using modified combinatorial nomenclature (MCN). It contains 75 electrodes, including the reference electrodes. The MCN system renames four electrodes of the 10–20 system: T3 is now T7, T4 is now T8, T5 is now P7, and T6 is now P8 (Sanei & Chambers 2013).

The electrical activity recorded from the brain occurs at different well-known frequencies called brain waves. Traditionally, they are classified into five components differentiated from each other by frequency range, namely: delta (δ), theta (θ), alpha (α), beta (β), and gamma (γ). Table 2.1 shows the frequency band associated with each type of brain wave (Sanei & Chambers 2013) and Figure 2.4 shows their wave patterns.

TABLE 2.1: Five traditional EEG wave patterns and their frequency ranges.

Brain Waves	Frequency range
Delta	0.5 - 4 Hz
Theta	4 - 8 Hz
Alpha	8 - 13 Hz
Beta	13 - 30 Hz
Gamma	above 30 Hz

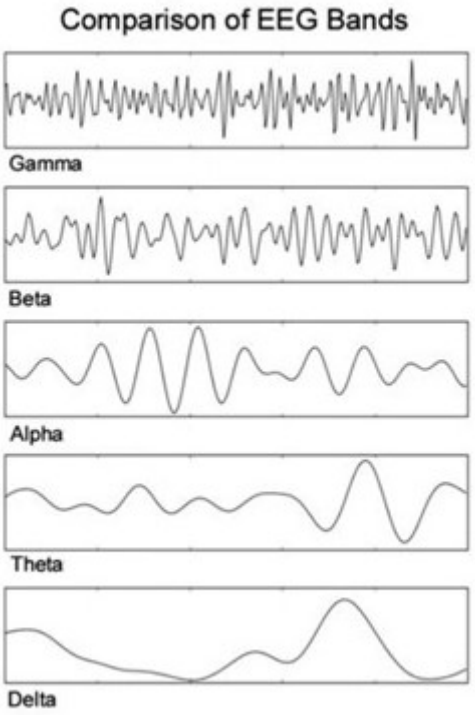

FIGURE 2.4: Typical brain normal rhythms.

The characteristics of these brain waves vary with an individual's age and mental state. Delta waves are observed in infants and adults during deep sleep (Sanei & Chambers 2013). Theta waves are associated with deep meditation, drowsiness or arousal in older children and adults. Studying the change of theta wave plays an essential role in maturational and emotional studies. Alpha waves are usually observed during relaxed awareness when attention or concentration is absent. It is produced in most subjects when closing eyes. In contrast, it is usually reduced by opening the eyes, by hearing unfamiliar sounds, by anxiety or mental concentration or attention. Beta waves appear in typical adults and are associated with active thinking, active attention, focusing on the outside world, or solving concrete problems. The frequency ranges between 30 - 45 Hz corresponds to a gamma wave. It rarely occurs and is associated with low amplitude (Sanei & Chambers 2013).

Advanced signal processing algorithms can be applied to decompose and separate the broadband EEG signal into desired waveforms. The most used techniques for this purpose are: DBP filter, short-time Fourier transform (STFT) (Gabor 1946), wavelet transform (Mallat 1989) and empirical mode decomposition (EMD) (Huang et al. 1998).

Event-related potentials (ERPs) are another important neurophysiological feature of EEG. ERPs measure the response of brain activity that are evoked due to specific events, stimulus (visual, auditory or somatosensory), cognitive tasks or motor events (Cohen

2014). They are voltage fluctuations in EEG emanated from the brain as a sum of several numbers of action potentials that are time-locked to the events mentioned above (Sanei & Chambers 2013). The basic concept underlying the computation of the ERPs is the use of a signal-averaging procedure. Each trial contains signal and noise, and noise can be cancelled out by averaging several trials; thus, the signal to noise ratio will be improved.

ERPs can be divided into two categories, exogenous response and endogenous response (Sur & Sinha 2009). An exogenous response consists of the early waves or components, peaking roughly within the first 100 ms after the stimulus onset. In contrast, the endogenous response is the wave produced after evaluating the stimulus. On the other hand, the ERP signals could be either positive represented by the letter P such as P300, P200 and P50 or negative referred to by the letter N such as N100 (Sur & Sinha 2009). The digits after the letter in those ERP examples indicate the response time in milliseconds after the stimulus onset (Sanei & Chambers 2013).

Generally, EEG studies rely on the two basic experimental paradigms: resting-state and task dependant EEG. In the resting-state, the background activity of EEG (such as the traditional brain waves mentioned above) is recorded in the absence of any task or stimulus, whereas in the task-dependant, the EEG activity is recorded while presenting the stimulus. In recent years, utilising EEG analysis in studying neurodevelopmental disorders has been thriving. For example, several studies have been conducted for investigating the ASD (Abdolzadegan et al. 2020, Lavanga et al. 2021, Peters et al. 2013, Righi et al. 2014, Schwartz et al. 2017), ADHD (Barry et al. 2003, Janssen et al. 2017, Mahmoud et al. 2021, Moghaddari et al. 2020), and learning disorders (Kaisar 2020, Suchetha et al. 2021, Xue et al. 2020).

The main advantage of EEG compared to the fMRI technique is the high temporal resolution in the order of a millisecond, providing a high ability for quantifying the fast, dynamic and temporally sequenced neural oscillations. Further, EEG is inexpensive, portable, non-invasive, user-friendly, and comparatively easy to use. However, EEG has limited spatial resolution (in order of cm) as it records the signal from the scalp, which reflects the underlying electrical potentials from a large population of active neurons. Thus, EEG is not suited for localising the signal source and studying the brain's deep structures (Cohen 2014).

2.3 Brain Connectivity

The human brain is a complex system consisting of regions that are functionally and structurally connected to process information during either a behavioural /cognitive

task or in a resting-state (Mohammad-Rezazadeh et al. 2016). This concept is called brain connectivity, and it was first addressed in the literature in the early 1960s (Adey et al. 1961). Studying brain connectivity is essential to understand how the brain executes its primary functions and what the roles of different brain regions are (Hamedi et al. 2016). It can be categorised into structural, effective and functional connectivity.

- **Structural connectivity**
  Structural connectivity describes a set of physical connections through synaptic contacts between neighbouring neurons (Mohammad-Rezazadeh et al. 2016). These connections generally refer to the white matter of fibre tracts that connect the spatially distributed neurons. Usually, the structural connectivity is measured by MRI, particularly diffusion tensor imaging (Sakkalis 2011). The structural connectivity has been used in studying the brain structure in several brain disorders such as ASD (D'Albis et al. 2018, Moradimanesh et al. 2021, Valenti et al. 2020), ADHD (Beare et al. 2017, Bos et al. 2017, Griffiths et al. 2021) and learning disorders (Banker et al. 2021).

- **Effective connectivity**
  With effective connectivity, the effects of one neural system on another can be understood. Effective connectivity reflects the causal interactions between activated brain areas providing both magnitude and directions of the interaction (Lang et al. 2012), and is usually measured by EEG, MEG and fMRI techniques. Generally, effective connectivity can be estimated based on the model specifying the causal link known as the model-based approach, directly from the signal known as a data-driven approach or by using information theory measures. The model-based approach is a theoretical model that is generated from the neurobiological evidence, and it provides insights into the way that the brain regions interact and influence each other (Sakkalis 2011). The most popular method is dynamic causal modelling (DCM) (Friston et al. 2003) which measures non-linear interactions between brain regions (Hamedi et al. 2016). In DCM, the response of a dynamic system is modelled by a network of discrete but interacting neuronal sources described in terms of a neural mass or conductance-based model (Sakkalis 2011).

  On the other hand, the data-driven approach does not require any assumption of the underlying model or prior knowledge regarding the spatial and temporal relationships (Sakkalis 2011). Granger causality (GC) (Granger 1969), partial direct coherence (PDC) (Baccalá & Sameshima 2001) and direct transfer function (DTF) (Kamifiski & Bfinowska 1991) are the most common methods for this approach. GC is based on the idea that causes precede their effects in time (Sakkalis 2011). It investigates whether one time-series can correctly predict another (Mehdizadehfar & Fallah 2016). The general forms of GC are PDC and DTF. Both approaches

can deal with multivariate signals, i.e., they take into consideration an estimate of the activity flow in a given direction between all channels simultaneously (Mehdizadehfar & Fallah 2016). The difference between the two methods is that DTF shows only the direct interactions between channels while the PDC shows both direct and indirect interactions.

Information theory measure is based on the concept of Shannon entropy (Shannon 1948) which measures the amount of the information contained in the variable. The best-known methods in this class are transfer entropy (Schreiber 2000), partial transfer entropy, mutual information and minimum description length. Transfer entropy and partial transfer entropy are directed measures of interaction, while mutual information and minimum description are non-directed measures of interaction (they are classified as the class of FBC).

Transfer entropy is a model-free measure, and it measures the information flow from source X into target Y, conditioned on the past of the target (Niso et al. 2013). It is based on transition probability and does not assume any *prior* kind of dependence.

Partial transfer entropy measures the amount of directed information flow from X to Y in the presence of a variable Z. Hence if Z is independent of both variables X and Y, the partial transfer entropy is equivalent to the transfer entropy (Niso et al. 2013).

Several studies have been carried out to investigate the effectiveness of effective connectivity in studying ASD (Rolls et al. 2020), ADHD (Muthuraman et al. 2019, Wang et al. 2021), and learning disorders (Liu et al. 2010, Morken et al. 2017).

- **Functional brain connectivity**
  FBC measures the temporal correlation among neuronal activities of distant and distinct brain regions (Mohammad-Rezazadeh et al. 2016). It does not consider any physical connection between the brain areas as in the aforementioned structural connectivity, but it measures the statistical dependency between different neuronal signals. It can be recorded using several techniques: EEG, MEG, PET, and fMRI (Sakkalis 2011). EEG-based FBC was preferable in this research because EEG has a high temporal resolution. Hence, it could capture the statistical dependencies that are highly time-dependent and fluctuate on multiple time scales ranging from milliseconds to seconds, as in the case of neural activities. In addition, EEG has other advantages that were mentioned in section 2.2.2. However, the critical challenge that faces EEG-based FBC is volume conduction. It is a problem that induces the mixing of signals in electrodes that distort the actual neuronal activities. The cause of volume conduction is that recording EEG by

electrodes does not provide direct access to the source of the signal. However, they record the linear and spontaneous superposition of multiple sources in the brain (Hamedi et al. 2016). In addition, the electrical field spreads tangentially through the skull, skin, and scalp, thus affecting adjacent electrodes and leading to distortions of the electrical signal. As a result, the potential of existing spurious connectivity could be high. Figure 2.5 illustrates the effects of the volume conduction.

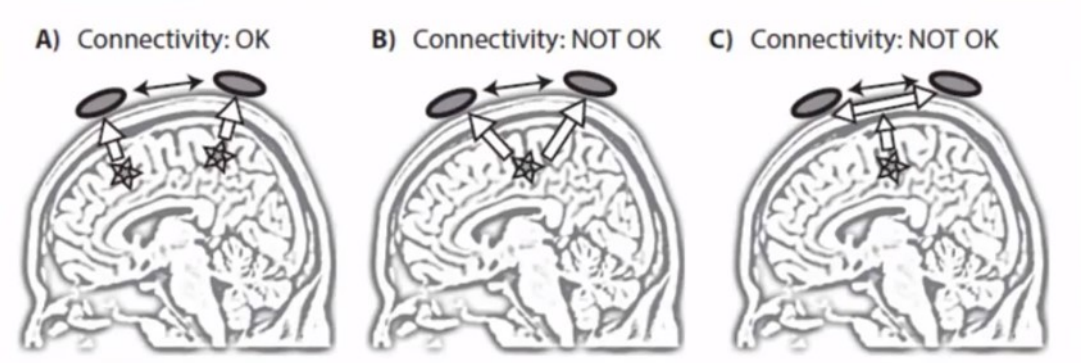

FIGURE 2.5: Illustration of the volume conduction effects. The black/grey rings represent electrodes; the black arrow represents the measured connectivity; the stars represent neural sources in the brain; the white arrows illustrate the path of electrical activity from these sources to electrodes. Panel A shows that each electrode measures only neural activity below the source; therefore, the measured connectivity between two electrodes reflects the true connectivity between two physically distinct brain regions. In panel B, both electrodes measure the activity from the same neuronal source. In panel C the electrical field spreads horizontally through the skull/scalp; the measured connectivity is spurious since both neighbour electrodes measure the same signal from a single source. The image was taken from Cohen (2014).

Computational methods used to measure the FBC can be classified into three categories: linear, non-linear and information-based techniques (Hamedi et al. 2016). The Linear FBC approach provides a linear measure of FBC, and it consists of three methods: correlation, cross-correlation and coherence (Hamedi et al. 2016). Correlation estimates the linear relationship between two signals using Pearson's correlation coefficient, where a higher correlation indicates a stronger functional relationship between the corresponding brain regions. Similarly, the cross-correlation calculates the linear dependency, but with respect to the time, i.e., it recovers to Pearson correlation when the time delay equals zero.

In contrast, coherence measures the linear correlation between two variables as a function of frequency. It quantifies the relationship between two time-series based on phase consistency, i.e., if phase change in one signal, the coherence value would be reduced, while if the phases are stabilised over time between the two signals, the coherence value would be high (Hamedi et al. 2016). In practice, coherence measures the linear relationship between two signals by using a linear time invariant transformation, i.e., a constant amplitude ratio and phase shift, in

each frequency band (Duffy et al. 2017). A high coherence indicates strong connectivity between two time-series signals and vice versa.

Generally, the primary advantage of linear FBC is that they are well-known and computationally fast (Niso et al. 2013). However, they are highly affected by VC and restricted with the assumption of the stationarity and linearity of the signal. A large and growing body of literature has investigated the linear FBC in detecting the brain deficits in several disorders such as ASD (Buckley et al. 2015, Carson et al. 2014, Coben et al. 2008, Murias et al. 2007, Lazarev et al. 2015, Léveillé et al. 2010, Righi et al. 2014), ADHD (Sato et al. 2012), and learning disorders (Gaudet et al. 2020).

Non-linear FBC methods are designed to measure the dynamics, non-linear and non-stationary properties of EEG (Hamedi et al. 2016). The most common non-linear FBC method is synchronisation. It is based on interacting chaotic oscillators (Hamedi et al. 2016), initially introduced by Pikovsky (1984) and Pecora & Carroll (1990). One of the most significant advantages of synchronisation is that it provides an amplitude-independent measure of connectivity between cortical regions. Thus it is less susceptible to the effects of artefacts and inter-trial /inter-subject amplitude variability (Hamedi et al. 2016). It is classified into two broad categories: generalised synchronisation and phase-based synchronisation (Hamedi et al. 2016). Generalised synchronisation estimates the coupled interaction between two stochastic oscillators by the specific function F. Considering the first dynamical time-series Y is the function of another X as $Y = F(X)$ where F is unknown, maybe complex, and change over time (Niso et al. 2013). The existence of generalised synchronisation between X and Y indicates that if the temporal patterns in x(t) at times t_i and t_j are similar, in like manner, the pattern in y(t) at these exact times will be similar. Generalised synchronisation can be computed via several indices, such as S Index, H Index, N Index, M Index and L Index. Niso et al. (2013) study contained more detail about these indices.

On the other hand, the phase-based synchronisation approach uses to calculate the strength of phase coupling between two stochastic oscillators regardless of uncorrelated amplitude (the major EEG characteristic in calculating the linear FBC) (Niso et al. 2013). The most common phase-based synchronisation methods used in neuroscientific literature are phase-locking value (PLV), phase lag index (PLI), and weighted phase lag index (WPLI) (Niso et al. 2013). PLV is a classical measure of phase-based synchronisation, and it was first described for EEG by Lachaux et al. (1999). It measures the strength of phase synchronisation between two time-series based on the absolute phase difference. Although PLV

can deal with the dynamics of the brain and the non-stationarity of its EEG signal, it is sensitive to volume conduction. Typically this issue is reflected as the zero-phase lag between two time-series signals. PLI was proposed by Stam et al. (2007) to alleviate the effect of volume conduction and other common sources of noise. It quantifies the extent that the phase leads and lags between signals from two sources as non-equiprobable, instead of considering the magnitude of the phase leads and lags. PLI is hindered by the discontinuity of the measure caused by small perturbation of phases that would change the signs of the phase differences having small magnitudes; accordingly, the PLI value would be changed. The most recent method of quantifying phase synchronisation is WPLI. It was defined by Vinck et al. (2011) as an improved version of the PLI index by weighting the contribution of the observed phase lag or lead with the magnitude of the imaginary component of the cross-spectrum. Although the WPLI is based on amplitude in its calculation, it is still classified as a member of the phase-based synchronisation family. WPLI provides a robust estimation of phase synchronisation against the VC and other sorts of noise.

Although in principle, the WPLI and PLI could be the optimal choices for quantifying phase-based synchronisation based on their characteristics, PLV estimates absolute phase differences between two time-series, reflecting the meaningful neurological coupling between them. Thus, there is no evidence about the optimal method for quantifying phase-based synchronisation.

The third class of FBC techniques is the information-based measures that capture linear and non-linear interactions between signals (Hamedi et al. 2016). A standard method of this group is the cross mutual information which measures the mutual dependence between two signals by quantifying the amount of information gained about one signal by measuring the other as a function of the delay between them (Sakkalis 2011). It is based on the probability distribution to detect the correlation between two sources. Another measure is minimum description length that estimates the interdependency between two sources by measuring the degree of predictability of the two signals as a function of the other (Hamedi et al. 2016).

2.4 Application of Graph Theory in Characterising Functional Brain Connectivity

Graph theory is often applied to FBC to describe the network architecture. It provides the visualisation of the brain network, which facilitates understanding of its properties. Furthermore, the graph theory gives an abstraction that could reduce the complexity

in understanding the neural networks and help to identify similarities and differences in their organisation (Kaiser 2011). In the graph theory analysis, the brain can be represented as a network where the nodes correspond to distinct brain regions (or EEG electrodes in EEG-based FBC derivation). The edge is the link between neighbouring nodes representing the strength of the brain functional connections. The graph can be categorised as directed or undirected, according to the direction of the edges, and as weighted or binary, based on the weight of the edges (Islam et al. 2017). In the weighted graph, each edge has a weight that represents the strength of the correlation, and this form is the most accurate in the real applications (Kaiser 2011). Figure 2.6 illustrates these different categories of networks.

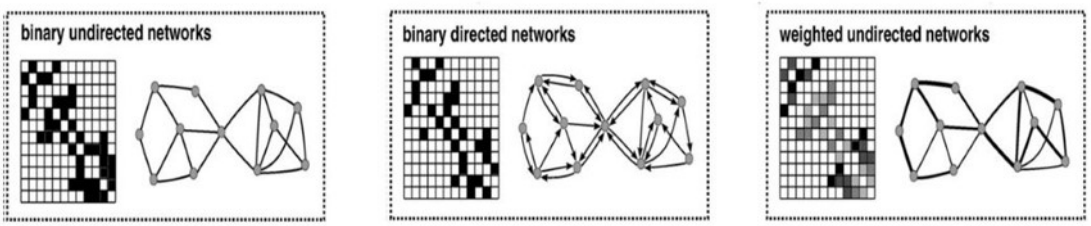

FIGURE 2.6: Illustration of different graph categories. The graph is commonly represented by a matrix. The left panel shows the binary and undirected graph. In a binary graph, the edge represented by the black entry in the corresponding matrix is only considered, regardless of the weight of the edge. An undirected graph is a graph that contains a set of nodes connected with bidirectional links, i.e., the direction is not important in this type of graph. The middle panel depicts the binary directed graph. A directed graph is a graph that its nodes are connected through a direct edge. The right panel represents a weighted undirected graph containing nodes connected with weighted and directed edges. The greyscale represents the edge weight in the corresponding matrix (Rubinov & Sporns 2010).

The graph theory analysis can adequately characterise the brain network and its topology and provide quantitative information about the network properties. The graph-theoretical parameters measure these topological properties on both local and global scales. Local attributes identify the topological features of the single node, such as node degree and centrality. In contrast, the global metrics reveal the information flow over the whole network and any specialised local processing. Examples of global network attributes are transitivity, global efficiency and characteristic path length.

Graph theory analysis has been used in many studies to investigate brain neurodevelopmental disorders such as ASD (Barttfeld et al. 2011, Han et al. 2017, Kessler et al. 2016, Lavanga et al. 2021, Zeng et al. 2017), ADHD (Janssen et al. 2017, Kim et al. 2021) and learning disorders (Xue et al. 2020).

2.5 Machine Learning Framework

Machine learning can be classified into two categories: supervised machine learning and unsupervised machine learning. In supervised machine learning, the model is trained in a known label of observations and known response (output data) to generate the predictions class of new data. In general, supervised machine learning is divided into two approaches: classification and regression. In classification, the model is trained with specific features to predict the corresponding category of a given observation, while in regression, the model is trained to predict the continuous response. Various classification and regression algorithms are different from each other based on the learning functions and underlying assumptions. For example, linear discriminant analysis (LDA), support vector machine (SVM), decision tree and K-nearest neighbour (KNN) are the most popular classification algorithms. On the other hand, examples of well-known regression models are linear regression, regression trees, regression support vector machines, and ensemble regression trees.

In machine learning frameworks, after training the model on specific features from the training set, the next step is to validate it in the testing set. In order to mitigate the effect of overfitting and ensure that the model performs well without bias, it is important to train and test the model independently, i.e., the testing data set must not be used in the training process. Another important factor for obtaining an optimal performance is that the model should train as much training data as possible (Rashid & Calhoun 2020). One known challenge in the clinical realm is getting an adequate sample size, i.e., the training data size is usually small. To deal with the limited number of instances in the data set and avoid overfitting, cross-validation is often used to train the model by dividing the data set into two sets, one for training and another for testing in a repeated fashion. K-fold cross-validation and leave-one-out-cross-validation (LOOCV) are the most common cross-validation approaches. In K-fold cross-validation, the data set is divided into K partitions, where K-1 partitions are used to train the model, and the remaining one is used to evaluate its performance. This process is repeated until each partition has been used as testing data. In LOOCV, K is equal to the number of instances in the data set, and every instance in the data set is left out once for testing the model. This procedure is repeated K times, leaving out the data of a different instance each time. Finally, the model performance is obtained by averaging the K independent results.

Class imbalance is a common problem in machine learning, where sample distribution across the classes is biased. The class with large data samples is known as a majority class, and the one with a small number is a minority class. A typical model would often be ineffective in classifying the observation that belongs to the minority class. Several approaches have been proposed to alleviate the problem of imbalanced data. Three

such approaches are data level, algorithm level, and hybrid level. The data level approach balances the data distribution by either over-sampling—adding more instances into the minority class—or under-sampling—removing the instances from the majority class. Then the conventional classifiers are applied without any changes in the classifier's logic (Gosain & Sardana 2017). Several techniques have been employed for performing over-sampling and under-sampling. For example, random under-sampling is the most popular under-sampling technique. Random over-sampling and synthetic minority over-sampling techniques are frequently used for over-sampling the data. At the algorithm level, the new classification algorithms are designed, or the existing ones are modified to handle the class imbalance problem without any prior changes to the data set. Several algorithms have been designed for addressing the imbalance problem, such as boosting and bagging algorithms. The hybrid approach combines the data level approach and algorithm level approach into a single algorithm to obtain an optimal solution for the imbalance problem (Gosain & Sardana 2017). Random under-sampling boosting (RUSBoost) and synthetic minority over-sampling boosting are examples of hybrid data sampling with boosting algorithms.

On the other hand, unsupervised machine learning algorithms aim to cluster the unlabelled input data into different groups according to similarity measures such as Euclidean or probabilistic distance (MathWorks 2018). Common algorithms for unsupervised learning are the k-means algorithm, Gaussian mixture models, and the hidden Markov model (MathWorks 2018).

In recent years, there has been a great tendency to use machine learning frameworks to provide an automatic, objective, and robust aiding tool for classifying /predicting NDDs. In these frameworks, the individual with the developmental delay is automatically discriminated from the TD group. In the literature, these have been extensively investigated in an attempt to provide diagnostic-focused predictive analysis of NDDs in general and particularly ASD (Abdolzadegan et al. 2020, Grossi et al. 2017, Jamal et al. 2014, Kang et al. 2020), ADHD (Ahmadi et al. 2021, Chen et al. 2019, Tenev et al. 2014) and learning disabilities (Dimitriadis 2016, Kaisar 2020).

2.6 Pathological Conditions

As described in section 1.1, the study was conducted on two data sets: firstly, the data set of children with ASD and secondly, the data set of infants born with HIE. The ASD data set was chosen as a starting point for this exploration because ASD is one of the most commonly occurring NDDs. Moreover, the ASD data set used in the investigation of the proposed framework is well-proven, and it can be viewed as a benchmark for evaluating the proposed analysis. This section describes the general pathological

information and symptoms and reviews the current approaches used to diagnose ASD. The overview of pathophysiology, experimental treatments and complications of HIE is provided in section 2.6.2. The frequent consequence outcomes of HIE are described in sections 2.6.3 and 2.6.4.

2.6.1 Autism Spectrum Disorders

ASDs are a group of lifelong neurodevelopmental disorders including the following subtypes: autistic disorder, Asperger syndrome, childhood disintegrative disorder, and pervasive developmental disorder-not otherwise specified (PDD-NOS) (Gurau et al. 2017). A lack of social communication characterises them and language acquisition, in addition to restricted interests and repetitive behaviour (Mohammad-Rezazadeh et al. 2016). Furthermore, people with ASD suffer from stereotypic behaviour and nonverbal communicative behaviour impairment, which impact social interaction. Symptoms of ASD may be identified in early childhood but are often diagnosed at school-age (World Health Organization 2021). The prevalence of ASD has been rising over the last four decades (Kern et al. 2015, Klimkeit et al. 2008). According to the The National Autistic Society (2016) report, around 700,000 individuals in the UK had an ASD.

Traditionally, ASD is diagnosed after onset of the symptoms using behavioural assessment techniques. The Autism Diagnostic Interview-Revised (ADI-R), the Developmental, Dimensional and Diagnostic Interview and the Autism Diagnostic Observation Schedule-Generic (ADOS-G) are widely adopted by clinicians to diagnose ASD. More details of these tools can be found in (Falkmer et al. 2013, Zwaigenbaum & Penner 2018). These clinical diagnostic tools are time-consuming, requiring multidisciplinary teams (including a psychologist, a physician and a speech-language pathologist), and the heterogeneity of the ASD symptoms hampers their efficiency.

With advancements in technology, several studies have recently begun to explore the feasibility of qEEG in diagnosing ASD. Gurau et al. (2017) conducted a systematic review to examine the evidence for the efficiency of qEEG signal analysis in ASD diagnoses, classifying EEG analysis methods into three classes: spectral analysis, information dynamics, and FBC. They found that these analysis methods could be utilised in characterising ASD. However, different limitations hampered the progress and the possibilities of using these methods in clinical practice to diagnose ASD. Spectral analysis is a linear approach that might not be optimal for characterising the non-linear and non-stationary properties of the EEG. On the other hand, the information dynamics are non-linear techniques but more challenging to perform and generally less well-known as signal analysis tools. Moreover, they measure the complexity of each EEG independently, providing a deep understanding of the dynamic process underlying specific brain areas rather than giving a broad view of the neural connectivity over the whole

brain. Thus, this approach is not adopted well for understanding the dynamical process underlying ASD that affects the whole brain (Kana et al. 2014). In FBC, most studies used coherence for estimating neural connectivity (Fingelkurts et al. 2005). Coherence is a linear measure used with the assumption of signal stationarity, highly sensitive to volume conduction and limited temporal resolution. Furthermore, coherence is positively affected by either change in power or phase of signals as it quantifies the stability of the relationship between two time-series regarding power asymmetry and phase relationship. Indicating coherence does not directly reveal the true relationship between the two signals.

Phase synchronisation based FBC is a non-linear measure of neural activity capable of detecting the dynamic and non-stationary characteristics of EEG. It has gained increased attention in neuroscience literature due to evidence suggesting that phase-based connectivity analysis could reveal information exchange topography in the human brain, which could offer insight into pathological brain states. Ahmadlou et al. (2012) used the fuzzy synchronisation likelihood within the machine learning framework to classify the ASD children of age between 7-13 years, and this method was validated on the EEG data recorded during eye-closed in resting-state condition. Buckley et al. (2015) compared different brain connectivity methods, including PLI between ASD children, children with developmental delay and TD group of age between 2-6 years, during the resting-states condition in three states fully awake, drowsy and sleeping. Han et al. (2017) and Zeng et al. (2017) investigated the brain connectivity measured via PLI characterised by graph theory attributes with EEG data recorded during resting-state from ASD children and TD with 3-11 years and 7-13 respectively. Orekhova et al. (2014), and their replicated study by Haartsen et al. (2019) used a debiased weighted phase lag index to study the EEG-based brain connectivity in high-risk infants aged between 13-18 months, while the data were recorded during the presenting of video streaming. Jamal et al. (2014) proposed a phase synchronisation states (synchrostates) approach in the machine learning environment for differentiating between ASD and TD children aged between 6-13 years, while the EEG was recorded during the presentation of three types of stimuli: happy, fearful and neutral.

Researchers have elucidated that the core deficits of ASD are associated with impairments in sensory processing, which is related to deficiencies in social cognition that may define this disorder (Jeste & Nelson 2009). Mainly, ASD children show severe impairment in emotional facial expression processing compared to TD children. Sysoeva et al. (2018) examined the face processing abnormalities in ASD children compared to control based on the amplitude and latency of ERP components. Monteiro et al. (2017) provided a systematic review to examine the EEG-based ERP features in emotional facial expression processing in ASD and confirmed the deficits of facial emotion processing associated with individuals who have ASD.

A closer look at the literature shows that many studies have investigated the EEG-based FBC for classifying ASD. Although these studies exist, such phenomenological evidence is yet to be brought into clinical practice. Moreover, a detailed exploration of the change in the task-dependent FBC to classify ASD is not that extensive. Notably, other than the study of Jamal et al. (2014), to the best of the author's knowledge, no previous study has investigated the non-linear dynamics of ERP components in emotional facial expression processing. In addition, very few studies have been carried out on discriminating between the ASD and the control groups using machine learning techniques.

2.6.2 Hypoxic-Ischaemic Encephalopathy

HIE is one of the most severe birth complications causing neonatal brain damage. The incidence of HIE has increased in recent years, occurring at approximately 1-6 per 1000 live births (Byeon et al. 2015). It is caused by insufficient blood flow to the infant's brain as a result of a hypoxic-ischaemic event during the prenatal, intrapartum or postnatal periods (Allen & Brandon 2011). The signs of HIE in early postnatal life include abnormal fetal heart rate, poor umbilical cord gas (pH $<$ 7.0 or base deficit $\geqslant$ 12 mmol/L), slow Apgar scores, presence of meconium stained fluid, or the need for respiratory support within the first several minutes of postnatal life (Allen & Brandon 2011). The severity of encephalopathy is measured using the Sarnat staging criteria in conjunction with neuroimaging techniques during the first days after birth. Generally, HIE treatment is limited to supportive medical therapy to maintain cardiopulmonary function and manage seizure activity (Allen & Brandon 2011, Dereymaeker et al. 2019). The most prominent treatment is the therapeutic hypothermia technique provided through either selective head or whole-body cooling of the infant (Allen & Brandon 2011). The procedure of hypothermia treatment involves decreasing the infant's body temperature to between 33°C and 36.5°C for two to three days. Then the infant is rewarmed gradually to prevent complications such as hypotension. Regrettably, with these treatments, up to 40% to 60% of infants die by two years or have severe neurodevelopmental impairments including CP, cognitive impairment, behavioural difficulties, visual or hearing impairment, and epilepsy (Schreglmann et al. 2020). Early prediction of developmental delay is crucial due to it plays an essential role in providing successful therapeutic interventions (Doyle et al. 2010). However, it is considered challenging and is traditionally identified by neurological examination. The following sections review the current approaches used to predict the frequent consequences of HIE being CP, and cognitive deficits.

2.6.3 Cerebral Palsy

CP is the most common subsequent neuromotor impairment of HIE. It is a movement and posture disorder frequently associated with epilepsy, impairment of sensation, cognition, communication, and behaviour (Morris 2007). As a lifelong condition, it has a severe socio-economic impact on families and health care systems (Tonmukayakul et al. 2018). Early identification of infants with neonatal HIE who are at high-risk of developing CP later in life is important for appropriate planning of intervention strategies (Hadders-Algra 2014), which ultimately may lead to improved outcomes.

The most frequently used assessment methods for early prediction of CP are (a) neurological and neuromotor assessments, (b) neuroimaging, and (c) neurophysiological tests (Hadders-Algra 2014). Even though neurological and neuromotor assessments have been widely used in diagnosing CP and their prediction value is generally good, they are subjective and often require longitudinal series of tests to detect the abnormalities.

Alternatively, neuroimaging techniques have been used as promising tools for the early prediction of CP in infants who are at high-risk (Hadders-Algra 2014), and MRI has been the preferred imaging technique used for this purpose (Ouwehand et al. 2020, van Laerhoven et al. 2013). Several studies have employed neurophysiological tests with infants at risk of adverse neurodevelopmental outcomes. Conventional grading electroencephalogram (cEEG) and amplitude-integrated electroencephalogram (aEEG) modalities have been found to predict outcomes well (Hayashi-Kurahashi et al. 2012, Maruyama et al. 2002, Ouwehand et al. 2020, Pisani & Spagnoli 2016, van Laerhoven et al. 2013). However, interpretation of the prognostic value of these methods remains subjective (Dereymaeker et al. 2019).

On the other hand, qEEG analysis could provide objective, reproducible and reliable biomarkers for characterising the brain activities related to CP. Spectral power, FBC (particularly coherence) and complexity analysis of EEG signals are the most common features used in this field (Gao, Jia, Wu, Yu & Feng 2017). These measures have been suggested to be the gold standard biomarker for identifying CP. Gao, Wu, Feng & Jia (2017) and Gao, Jia, Wu, Yu & Feng (2017) studied linear-complexity measures to assess the temporal and spatial correlations of EEG signals in adolescent patients with CP and the control group. Coherence-based measures and spectral power were used to study the EEG characteristics in CP children in several studies. Koeda & Takeshita (1998) investigated the change in spectral power and coherence connectivity in children with CP from resting-state EEG within a machine learning framework. Kułak et al. (2005), and Kulak & Sobaniec (2005) performed the studies to investigate the spectral power and

coherence-based measures in children with CP. Sajedi et al. (2013) carried out the machine learning study to determine the linear and non-linear changes in brain dynamics related to CP. Their study employed spectral power as a linear analysis and fractal dimension as a non-linear analysis.

However, the detailed exploration of using qEEG to identify CP at the age of infancy was rarely investigated (George et al. 2020). Moreover, different limitations hampered the progress of analysing the cognitive process of CP individuals using these methodologies. As mentioned in section 2.6.1, EEG is a non-linear and non-stationary signal in its nature (Sanei & Chambers 2013), and such linear-based measurements are not well adapted for its analysis. Mainly, volume conduction has been reported to significantly affect EEG coherence estimations (Gao, Jia, Wu, Yu & Feng 2017). Thus, there are still many works required to explore the pathological mechanisms of CP using qEEG analysis.

2.6.4 Cognitive Outcomes

Neurodevelopmental impairment is a composite outcome that includes cognitive, behavioural, educational, and motor impairments. Cognitive deficit is considered one of the most common outcomes usually associated with NDDs (Slaughter et al. 2016), featured by slow information processing speed, deficits in working memory, attention, and executive function. Moderate to severe HIE is one of the leading causes of later cognitive impairment in children at school-age. Schreglmann et al. (2020) provided a systematic review, which suggested that up to 60% of children without CP have a cognitive impairment following HIE.

Early identification of infants at high-risk can help to provide targeted early intervention aimed at improving cognitive outcomes by taking advantage of the neuroplasticity of the developing brain in early infancy. Yet, the accurate diagnosis of cognitive impairments cannot be carried out before 3 to 5 years of age (He et al. 2018). Recently, there has been increased interest in exploring methods for assessing brain function in early infancy and using them as an aiding tool for the early prediction of cognitive impairments. Neuroimaging techniques have been used in several studies to identify infants at high-risk of cognitive impairment (He et al. 2018, Moeskops et al. 2017, Slaughter et al. 2016).

Along with neuroimaging methods, several studies have used EEG analysis to predict cognitive outcomes. Kong et al. (2018) conducted a systematic review highlighting the two basic approaches currently adopted for the early prediction of cognitive outcomes. One is the analysis of EEG features to identify the biomarkers that could help classify the subject as either cognitively impaired or normal. Second is the analysis of EEG

characteristics to estimate the specific scores for the continuous cognitive measure to predict cognitive performance and deficit level. Compared with binary classification, prediction of the cognitive development reflects the difference among individuals in brain functions and level of cognitive impairment, rather than determining the group as in the classification case, which can be more challenging (Sui et al. 2020).

Limited previous studies have shown that the early quantitative analysis of EEG can satisfactorily predict the long-term cognitive outcome. Lloyd et al. (2021) employed serial, multichannel video EEG to predict outcome in preterm infants by finding the association between the grading of EEG background activity—where EEG was recorded soon after birth and continued over the first three days—and the developmental scores, which were assessed at two years of age. Suppiej et al. (2017) compared spectral EEG values of infants born near term with infants born at extremely low gestational age, aiming to investigate whether spectral EEG features were related to neurological outcomes. The EEG data were recorded at 35 weeks post-conception, and the outcome was evaluated at one year of age by Griffiths' scales. Cainelli et al. (2021) also carried out the longitudinal six-year study to evaluate the feasibility of neonatal spectral EEG in predicting the developmental delay in premature infants. The EEG data were recorded at 35 weeks post-conception. The outcome was assessed at six years after the perinatal period (school-age period) using the Wechsler Preschool and Primary Scale of Intelligence III and neurological test. West et al. (2005) conducted the regression-based analysis to predict outcomes at 18 months of forty-four preterm infants using the quantitative measure of EEG continuity recording in the first four days after birth. Kühn-Popp et al. (2016) investigated the relation between brain maturation processes and the epistemic language skills (evaluated at 48 months) using EEE coherence measured at 14 months.

Although these attempts have paved the way to early prediction of cognitive development, methodological limitations hinder further progress. The EEG grading system is still subjective and dependent on interpretation by an expert. Alternatively, the spectral power, amplitude and coherence-based measures could provide an objective measure for predicting the associated cognitive outcome. Nevertheless, as mentioned earlier, its linearity has hampered its progress in this field. Therefore, further works are required to find the objective and reliable biomarkers for the early prediction of cognitive outcomes.

2.7 The Basis of this Work

This work is conducted to find the objective and reliable multivariate brain network features for the early prediction of NDDs. A closer look at the literature reveals some

gaps and shortcomings. The prognostic value of qEEG analysis in identifying long-term outcomes at the age of infancy was rarely investigated. Furthermore, the previously adopted qEEG features (as coherence and spectral analysis) for classifying /predicting neurodevelopmental outcomes are linear by their nature. They would be more meaningful under the assumption of stationarity and linearity of the signal. EEG is non-linear and non-stationary, and dealing with these characteristics (non-stationarity and non-linearity) is essential for understanding the dynamic process underlying pathological change. Thus, the qEEG features mentioned above are not optimal for capturing the EEG characteristics. Moreover, adopting the qEEG features in the machine learning framework for classifying /predicting the NDDs could make considerable progress in providing automated and objective decisions. However, machine-based identification studies are limited.

The main purpose of this study is to explore the effectiveness of non-linear qEEG features within a machine learning framework for identifying neurodevelopmental outcomes. Mainly, phase synchronisations (PLV and WPLI) characterised by graph-theoretical parameters are proposed to quantitatively characterise the individual's brain connectivity from the EEG, either in task-dependent (in the case of children's data set of an ASD study) or resting-state (in the case of infants' data set of neurodevelopmental outcomes studies). These chosen features could capture the complex properties of the EEG signal. They are then used to train and test several machine learning algorithms to show how useful they could be in the practical classification /prediction of neurodevelopmental outcomes.

2.8 Summary

This chapter reviewed the basic concepts related to NDDs and their current diagnostic approaches. The first part of the chapter offered a brief description of the human brain and the measurement techniques used for recording brain activities. The detail of the brain connectivity approach and its crucial role in understanding the dynamics of the brain system were highlighted. The graph theory analysis is usually utilised to characterise brain network topology. It facilitates the visualisation of functional brain networks and provides the abstract of the network architecture, which could help detect the network irregularity; thus, a brief background of graph theory analysis was provided. This was followed by an overview of the machine learning framework. The summary of the current state-of-the-art approaches used for classifying /predicting several pathological conditions were also reviewed. The following chapters illustrate the proposed approaches to classify children with ASD and predict CP and cognitive outcome at two years of age from infants' EEG born with HIE.

Chapter 3

Classification of Autism Spectrum Disorders from EEG-based Functional Brain Connectivity Analysis

3.1 Introduction

The starting point of this research is an attempt to design and establish a machine learning framework to classify children with ASD. Specifically, the phase-based task-dependent functional brain connectivity is investigated to measure the functional coupling of neural populations through the strength of phase synchronisation; hence, the abnormal synchronisation could be considered a hallmark of several brain disorders. Evidence has shown that the phase-based FBC analysis could reveal a task-dependent information exchange topography in the human brain, which could help to give insight into pathological brain states (Farahmand et al. 2018). Furthermore, the phase-based connectivity analysis is fast to compute and requires few assumptions and parameter selections (Cohen 2014).

Thus, the phase-based task-dependent FBC and graph-theoretical measures are adopted in this research to deduce the characteristics of the brain's network and then utilise these characteristics to classify ASD and TD. Specifically, the feasibility of using three proposed PLV-based FBC—trial-averaged PLV, average trial-averaged PLV and time-points-averaged PLV— is investigated. Furthermore, the study aims to find the most discriminating graph metrics (markers) to be used as the features for training a classification model. The association between frequency bands and brain connectivity dysfunction in children with ASD is also investigated.

Methodology for the proposed PLV-based FBC consists of the following steps. Firstly the EEG signals are decomposed into five frequency bands. Then, connectivity maps are formulated separately by three phase synchronisation approaches trial-averaged PLV, average trial-averaged PLV and time-points-averaged PLV. Graph theory indices characterise each connectivity map for every subject in each frequency band. These graph-theoretical measures are then used as features fed into classifiers to evaluate the proposed approaches in ASD classification. The results from this chapter have been reported in (Alotaibi & Maharatna 2021).

This chapter is organised as follows: the experimental design, the data set and preprocessing techniques are described in section 3.2. Formulating phase-based functional connectivity procedures is illustrated in section 3.3. Fundamental graph-theoretical measures are reviewed in section 3.4. Section 3.5 describes the proposed feature extraction schemes. Results analysis is depicted in section 3.7 and discussed in 3.8. Section 3.9 concludes the chapter.

3.2 Experimental Design and Data set

EEG data used in this study were obtained from Jamal et al. (2014)—a modified data set from that used by Apicella et al. (2013)—which studied EEG characteristics in ASD and TD children with respect to face perception tasks. It was chosen, in this exploration, because the impairment in social processing is a core difficulty in ASD, which can be conveyed by emotions showing on the face. This could be strictly connected to disruption of the ability to activate specific brain circuits during facial processing (Jamal et al. 2014).

The data were collected from twenty-four subjects, twelve children (seven boys and five girls) with ASD and twelve TD children (seven boys and five girls). The children with ASD were aged between six to thirteen years (mean age= 10.2 years), and their neurotypical peers age-matched group were aged between six to thirteen years (mean age= 9.7 years). The participants having ASD were diagnosed according to the Diagnostic and Statistical Manual of Mental Disorders (DSM-IV-TR) criteria and confirmed by ADOS-G and ADI-R (Apicella et al. 2013).

Facial images with three types of emotion were displayed for each subject during the EEG recording. The images showed the standardised emotional facial expressions: happy, neutral, and fearful. Thirty faces were taken from ten subjects (five male and five female) acquired from the widely used database of standardised face expressions (Tottenham et al. 2009). The experiment consisted of three blocks, each composed of

ten happy faces, ten fearful faces and ten neutral faces. Each stimulus was presented for 850 ms with an inter-stimulus interval of 150 ms. EEG data were sampled at 250 Hz and recorded using 128 channels HydroCel Geodesic Sensor Net (HGSN), as shown in 3.1 (Apicella et al. 2013).

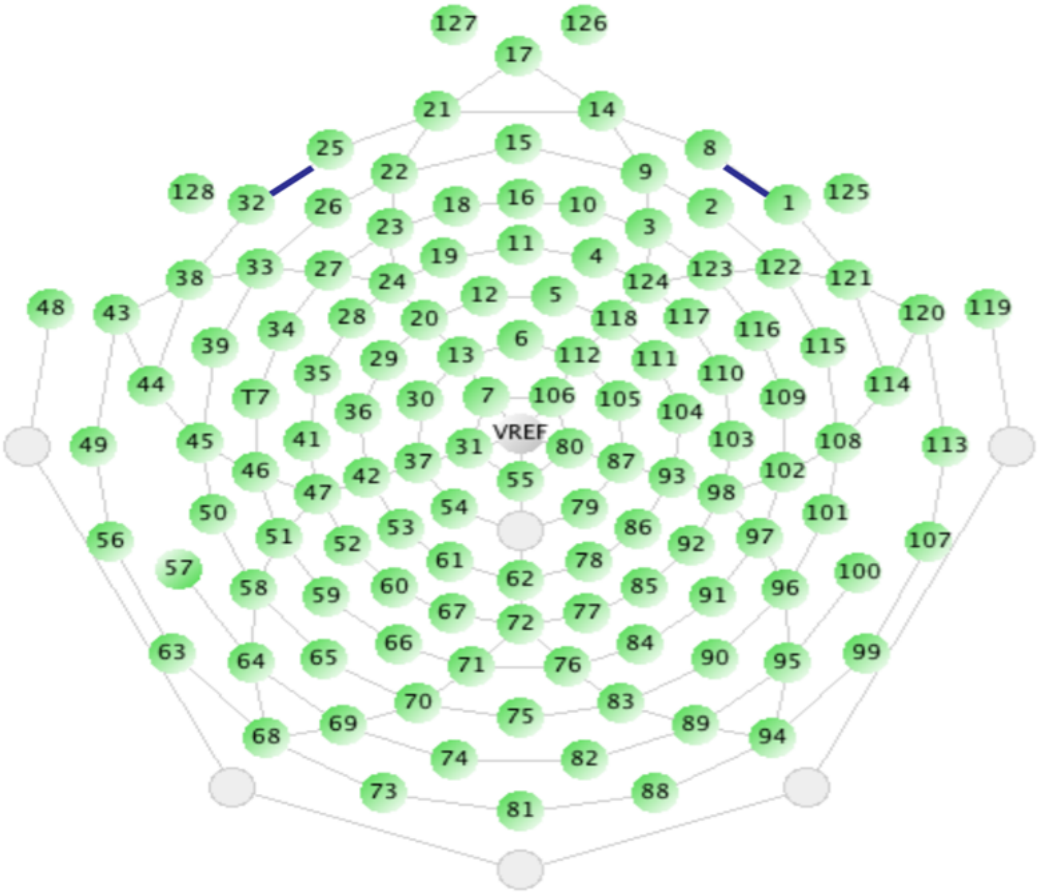

FIGURE 3.1: HGSN sensor layout including 128 electrodes (Apicella et al. 2013).

Data were filtered through a finite impulse response (FIR) bandpass filter with the cut-off frequencies of 0.5 Hz and 50 Hz. FIR filter has a finite response which means that its response ends at some point (Cohen 2014). It was chosen for filtering the data over the infinite impulse response (IIF) because it is more stable and less likely to introduce non-linear phase distortions (Cohen 2014). The filter order was determined according to the following equation:

$$filterorder = round(3 \times (srate/lowerFilterBound)) \tag{3.1}$$

where srate is the sampling rate, which is equal to 250 Hz, and lowerFilterBound is the lower frequency bound which is equal to 0.5 Hz. Thus, the filter order according above equation was equalled 1500.

TABLE 3.1: FIR filter order corresponding to each brain waves.

Brain wave #	Filter order
Delta (0.5 – 4 Hz)	1500
Theta (4 – 8 Hz)	188
Alpha (8 – 13 Hz)	94
Beta (13 - 30 Hz)	58
Gamma (30 - 45 Hz)	26

The continuous EEGs were segmented into 1000 ms epochs (150 ms of baseline and 850 ms of stimulus presentation) as 1000 ms is a reasonable epoch length typically used in ERP research to capture the entire temporal dynamics of the ERP (Apicella et al. 2013). Any segment containing signals above a threshold of 200 μV was considered contaminated by artefacts such as blinking or eye movement and was not used in further analysis (Jamal et al. 2014). Next, the FIR bandpass filter was used to decompose EEG signals into its five traditional narrowband frequencies, described in section 2.2.2, namely delta (0.5 – 4 Hz), theta (4 – 8 Hz), alpha (8 – 13 Hz), beta (13 - 30 Hz) and gamma (30 - 45) (Wang et al. 2016). The filter order corresponding to each traditional narrowband frequency is shown in Table 3.1. This decomposition step is necessary to get a proper phase value and obtain its intended physical interpretation.

3.3 PLV-based Functional Brain Connectivity

PLV is a classical approach for quantifying phase synchronisation, which is a key strategy for estimating FBC. The strength of phase synchronisation is measured by the absolute value of the mean of the phase difference between two signals (Aydore et al. 2013). PLV value ranges between zero and one - 0 when the two signals are totally independent and 1 when the two signals are strongly coupled (Aydore et al. 2013). The first step in PLV calculation is to compute the instantaneous phase $\Phi(t)$, often calculated using Hilbert or complex wavelet transform. Both approaches yielded the same result with the same efficiency (Bruña et al. 2018). In this study, the Hilbert transform was used for this purpose, which is defined as:

$$\tilde{x}_i(t) = \frac{1}{\pi} PV \int_{-\infty}^{\infty} \frac{x_i(\tau)}{t-\tau} d\tau \tag{3.2}$$

where, $\tilde{x}_i(t)$ is the Hilbert transform of the original signal $x_i(\tau)$, and the transformation is calculated using the integration of division of the original signal over the time-shifted by τ (Brunner et al. 2006). PV is the Cauchy principal value used to avoid the error in

calculation due to improper integration. The instantaneous phase can then be calculated as:

$$\Phi(t) = \arctan \frac{\tilde{x}_i(t)}{x_i(t)} \tag{3.3}$$

where $\Phi(t)$ is the phase extracted from each time-point $t[1, \dots T]$, trial $n[1, \dots N]$, and for each frequency band. Upon completing the phase extraction, the exponentiation is calculated to obtain the unit phase difference vector between each pair of channels. Hence, the series of phases difference vectors induce a connectivity matrix as the following equation:

$$PLV = \mid \langle exp(j\triangle\Phi) \rangle \mid \tag{3.4}$$

In the above definition, $\triangle\Phi$ denotes the phase difference between two signals and $\langle\rangle$ is an expectation operator (Brunner et al. 2006). Lachaux et al. (1999) defined PLV as a time-dependent measure to estimate the inter-trial variability of phase at time t. Hence, Equation (3.4) can be written as:

$$PLV_t = \frac{1}{N} \left| \sum_{n=1}^{N} exp(j\{\Phi_1(t) - \Phi_2(t)\}) \right| \tag{3.5}$$

3.4 Fundamental Graph-Theoretical Measures

After describing the basic concept of calculating brain connectivity, it would be quite valuable to transform the connectivity matrix into a complex network. This transformation is an established approach for getting insight into the process of information propagation amongst the brain areas—the underpinning mechanism of the working principle of the brain. As described in Chapter 2, in this approach, the electrodes are represented as nodes in the network, and the edge between two nodes is weighted by the functional connectivity measures, particularly the phase-based connectivity matrix entries. Fundamental graph-theoretical measures are used to quantitatively characterise the brain network. They help understand a network's topology, thus facilitating the network's proprieties comparison between typical subjects and those with brain disorders (Matlis et al. 2015). Typically, these metrics are categorised into two groups: local metrics and global features. The local features, as described in section 2.4, provide the view of the characteristics of a single node in terms of its connectivity with the neighbouring node, and the global network features characterise the network as a whole in terms of network integration and the ease of information transfer within the network.

Global network measures are particularly interesting because the neuroimaging results suggest that ASD children have long-distance hypo-connection and short-distance hyper-connection (Kana et al. 2014). The global network metrics could adequately capture these two characteristics. Thus, five global graph parameters—transitivity, global

efficiency, radius, diameter, and characteristic path length—are preferred for being adopted into this study because they are expected to provide a great insight into the essence of information flow disruptions in the brain of children with ASD.

Transitivity represents the ratio of the triangle to triplets in the network and measures the tendency of nodes to cluster together. The network with high transitivity means it contains groups of nodes that are densely connected internally. Finding such groups is significant because they reveal the functional modules. Transitivity is defined as (Rubinov & Sporns 2010):

$$T = \frac{\sum_{i \in N} 2t_i}{\sum_{i \in N} k_i \left(k_i - 1\right)} \tag{3.6}$$

where T is transitivity of the network, N is the set of all nodes in the network, k_i is a degree of node i, and t_i is the number of triangles around node i, which is calculated as follow:

$$t_i = \frac{1}{2} \sum_{j,h \in N} a_{ij} a_{ih} a_{jh} \tag{3.7}$$

where a_{ij}, a_{ih}, and a_{jh} are the connection between node i and j, i and h, and j and h, respectively. A degree of node i, k_i is equal to a number of its neighbours, and it is an important complex network measure as many graph-theoretical parameters calculated based on it, such as the transitivity in equation 3.6 (Rubinov & Sporns 2010). It is computed by the equation:

$$k_i = \sum_{j \in N} a_{ij} \tag{3.8}$$

Characteristic path length represents the average shortest path length between all possible pairs of nodes in the network. It measures the network's ability to propagate information rapidly between distributed nodes (Cao et al. 2014). Mathematically, it is defined as:

$$L = \frac{1}{N} \sum_{i \in N} L_i = \frac{1}{N} \sum_{i \in N} \frac{\sum_{j \in N, j \neq i} d_{ij}}{N - 1} \tag{3.9}$$

where L_i is the average shortest path length between node i and all other nodes, and d_{ij} is the shortest path length (distance) between the node i and j, and it is mathematically described as:

$$d_{ij} = \sum_{a_{st} \in l_{i \leftrightarrow j}} f\left(a_{st}\right) \tag{3.10}$$

where $l_{i \longleftrightarrow j}$ is the shortest path between node i and node j, which means—in a weighted graph—the path with a minimum weight between node i and j, f is a mapping function from weight to length (Rubinov & Sporns 2010).

Global efficiency is the mean of the inverse of the shortest path length. It is related to characteristic path length and used to measure network efficiency by assessing how efficiently the information is exchanged through the whole network (Liu et al. 2017). Higher global efficiency refers to higher network efficiency in information exchange.

Global efficiency can be described by the following equation:

$$E = \frac{1}{N}\sum_{i\in N} E_i = \frac{1}{N}\sum_{i\in N}\frac{\sum_{j\in N, j\neq i} d_{ij}^{-1}}{N-1} \tag{3.11}$$

where E_i is the efficiency of the node i, and d_{ij}^{-1} is an inverse of the shortest path length.

Radius is a measure of network shape, and it is defined as the minimum of network eccentricity that could be described as the maximum distance (i.e., longest shortest path) between node i and any other nodes in the network. Mathematically, it can be defined by the following equation:

$$R = min(e_i) \tag{3.12}$$

In the above equation e_i is a network eccentricity for node i, and it refers to the maximum value of each row of the dot product of d_{ij}. The network eccentricity is defined as follows:

$$e_i = \max\left(d_{ij} \cdot d_{ij}\right) \tag{3.13}$$

The diameter is another measure of network eccentricity, and it is defined as the maximum value of eccentricity:

$$D = \max\left(e_i\right) \tag{3.14}$$

3.5 PLV-based Features Extraction Process

A main stage in the proposed machine learning framework is extracting the discriminant features utilised to distinguish between ASD and TD groups. It is presented in two steps; formulating the connectivity matrices from three proposed PLV-based FBC approaches (trial-averaged PLV, average trial-averaged PLV, and time-points-averaged PLV) and deriving the graph parameters from each resulting connectivity matrix separately. Then, these graph parameters would be used as features fed into the classifier. As described in section 3.3, PLV was defined by calculating the phase difference at each time-point and then the results were averaged over the trials to get one connectivity matrix per time-point to measure the inter-trial variability of phase. The EEG data set adopted in this study was recorded while presenting a visual stimulus; typically, in the event-related experiment, the averaging process is carried out over the trials to enhance the signal to noise ratio. Thus, this study proposed adopting three different approaches to calculating the PLV matrix considering the several characteristics of EEG. These approaches, namely trial-averaged PLV, average trial-averaged PLV and time-points-averaged PLV. Detailed descriptions of each of these methods are provided in the following points. The justification behind adopting them are also clarified.

- **Trial-averaged PLV**
  In the trial-averaged PLV, the PLV connectivity matrix was computed between each pair of time-series at a specific frequency (herein, five frequency ranges that were mentioned in section 3.2 were considered), and the instantaneous phase was estimated at specific time-points across the various trials. That means, at each time-point t, the exponent of instantaneous phase difference was calculated between each pair of time-series over trials N. Then the average phase differences across trials were obtained. Mathematically, in Equation 3.5, N is a total number of trials, t is a specific time-point, n is a certain trial, and PLV_t indicates the connectivity matrix at time t. This process was repeated for each time-point at each frequency band in each stimulus. As a result, M connectivity matrices were obtained in each frequency band where M was the number of time-points (in this study, $M = 250$, which is equal to the sampling rate, i.e. the number of samples per second). Once connectivity networks were formulated from each frequency band, in each stimulus, and for each subject separately, the set of the graph-theoretical parameters (described in section 3.4)—transitivity, global efficiency, radius, diameter and characteristic path length—were extracted from each network. Brain connectivity toolbox (BCT) in MATLAB environment was used to extract these parameters (Mika 2010). These features were then used to train a set of classifiers, and their performance was analysed. A block diagram for this approach is shown in Figure 3.2.

  This approach was applied because the typical protocol followed in task-based modulations relies on averaging several trials. Hence, this study followed the same approach in connectivity analysis to get strong evidence regarding phase synchronisation by calculating connectivity in the same phase configuration on each trial (Cohen 2014).

- **Average trial-averaged PLV**
  In average trial-averaged PLV, the connectivity matrix was estimated similarly to the first approach but with slight differences. After getting N connectivity matrices, the average over N was calculated to end up with one averaged connectivity matrix. Then, the complex network was estimated, and the graph parameters were extracted from this network, as described earlier. Following that, the feature selection algorithm was run to find most of the discriminant information needed for the classification problem. Here, Fisher discriminant ratio (FDR) was employed as a criterion for ranking the features as it can quantify the ability for each feature in separation between classes (Theodoridis 2010). The features with high ranking have a greater discriminability. FDR can be defined as a ratio between-class distance to scatter within-class. Mathematically, it is computed based on the

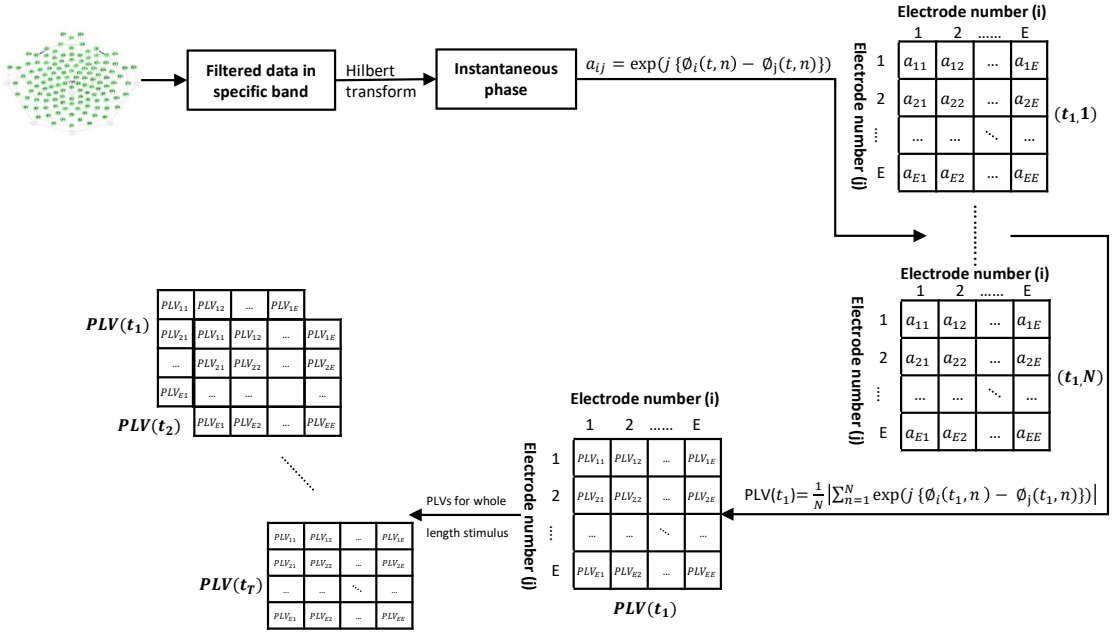

FIGURE 3.2: Schematic diagram of trial-averaged PLV. Each time-series recording from each electrode was filtered by Hilbert transform to extract the instantaneous phase. The exponent of phase difference a_{ij} between each pair of time-series i and j were computed at time-points t_1 for each trial n, and these yielded N matrices, (from $(t_1, 1)$ to (t_1, N)) where N was the number of trials. By averaging a over trials N, PLV was obtained at t_1. Repeating this process for each time-point yielded T connectivity matrices representing synchrony index related to inter-trial variability.

mean and variance of both classes as:

$$FDR = \frac{(\mu_1 - \mu_2)^2}{(\sigma_1^2 + \sigma_2^2)} \tag{3.15}$$

where μ_1 is the mean of the first class, μ_2 is the mean of the second class, σ_1^2 and σ_2^2 are the variances of first and second class respectively. The features were ranked by FDR, and the cross-correlations between the features were calculated as follows:

$$\rho_{ij} = \frac{\sum_{n=1}^{N} x_{ni} x_{nj}}{\sqrt{\sum_{n=1}^{N} x_{ni}^2 \sum_{n=1}^{N} x_{nj}^2}} \tag{3.16}$$

In the above equation, x_{nk} is the kth feature of the nth pattern, and ρ_{ij} is the cross-correlation coefficient between features i and j. The process of selecting the best discriminant features was involved the following steps (Theodoridis & Koutroumbas 2008):

- The features were ranked in descending order according to FDR, and the feature with the best rank, say x_{i_1}, was selected where i_1 is the feature's index.
- To select the second feature, the cross-correlation coefficient between x_{i_1} and the remaining features was computed, and it represented by $\rho_{i_1 j}$ where $i_1 \neq j$.

- The second feature (let say x_{i_2}) was chosen based on the following equation:

$$i_1 = \arg\max_j \{\alpha_1 C(j) - \alpha_2 |\rho_{i_1}|\}, \tag{3.17}$$

where α_1, α_2 are weighting factors and their value 0.2 and 0.8, respectively, and C is the class separability. This study considered the correlation and class separability in the feature selection process. Prior to commencing the selection process, the normalisation of features was calculated. It may be beneficial for removing bias due to features having a high value, may have a strong influence on the cost function used for designing the classifier (Theodoridis & Koutroumbas 2008). The features were normalised to zero mean and unit variance according to the following:

$$\widehat{x}_i = \frac{x_i - \bar{x}}{\sigma}, i = 1, 2, ..., N, \tag{3.18}$$

where $\widehat{x}_i$ is a normalised value, N is the number of features, x_i is the feature i, $\bar{x}$ the mean, and σ is the standard deviation. The schematic diagram for average trial-averaged approach is shown in Figure 3.3. This approach was proposed to investigate whether the graph-theoretical parameters extracted from average connectivity networks could give a refine measure to the global network properties compared to those extracted from each trial.

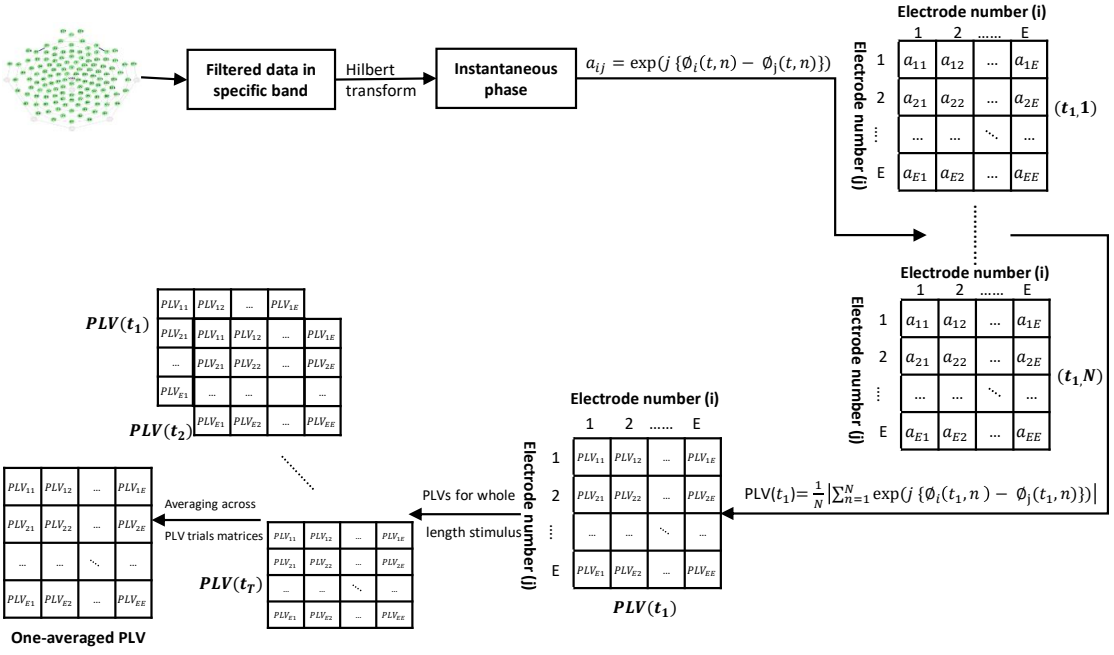

FIGURE 3.3: Schematic diagram of average trial-averaged PLV. Estimating PLV was carried out in the same manner of trial-averaged PLV with the difference in the finalising of estimation process by taking the average across the PLV matrices and ending up with one PLV matrix.

- **Time-points-averaged PLV**
  In the time-points-averaged PLV, the connectivity index was computed between all pairs of time-series for each specific trial at each frequency band. Intending, at each specific trial n, the exponentiation of the instantaneous phase difference was calculated between each pair of time-series over the time-points, and then the average of phase differences over the time-points was estimated. The phase difference was computed by Equation 3.5 where N is the number of time-points, which is equal 250. This yielded M connectivity matrices, each one corresponding to one trial. Next, the average over the M matrices was computed, resulting in one average matrix mapped into the connectivity network. In the final step, the graph parameters were inferred to find the most discriminant features between the two populations. Similar to the second approach, five features were extracted: transitivity, global efficiency, radius, diameter and characteristic path length. The feature selection algorithm was then used to rank the features and select the most informative one for feeding into the classifier. The selection process proceeded in the same manner as the second approach. This approach was proposed to investigate the variability of phase difference at trial n; if the phase difference slightly varies across the times, PLV is close to 1; otherwise, it is 0. The block diagram for the third approach is shown in Figure 3.4. This approach is the classical methodology for calculating phase synchronisation and was used to measure the intra-trial variability of phase and investigate whether it could discriminate between the two populations of ASD and TD.

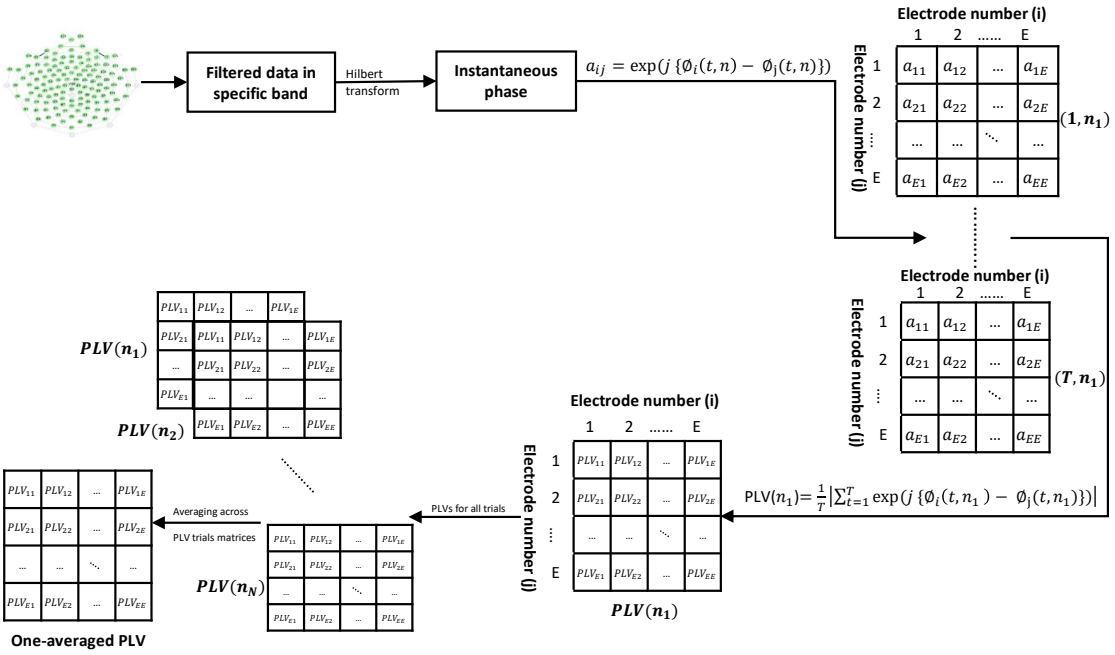

FIGURE 3.4: Schematic diagram of time-points averaged PLV. After extracting instantaneous phase by Hilbert transform, the exponents of phase differences (a_{ij}) between each pair of electrodes i and j were computed at trial n_1 for each time-point t, yielding T matrices, (from $(1, n_1)$ to (T, n_1)) where T was time-points length. By Averaging over time-points T, PLV was obtained at n_1. Repeating this process for each trial yielded N connectivity matrices representing synchrony index related to the stability of phase synchronisation over time.

3.6 Classification Algorithms

The previous section described how to form the features vector from several phase-based FBC connectivity methods. The features vector was then used to train the classification algorithm to discriminate between ASD and TD groups. Over the years, several classification algorithms have been used to separate between classes, each of which has a different learning approach, advantages and limitations. Choosing the proper algorithm for classification problem is challenging as no best algorithm fits all. Hence, this study intended to explore several classification algorithms to find the most discriminant features that can best discriminate between two groups. In particular, the study evaluated the performance of classifiers that were designed to deal with binary classification problem. These were chosen according to the needs of the study to assign each individual in the data set into one of two classes—ASD or TD. This exploration used LDA, SVM, KNN and decision tree as classifiers. A classification learner app within the statistics and machine learning toolbox in MATLAB was used to train and test the classification algorithms.

- **Linear discriminant analysis classifier**
  LDA classifier separates the data by constructing the hyperplane between two classes. It estimates the parameter of the Gaussian distribution of each class and tries to find the hyperplane that makes the distance between the mean values of the two classes as far apart as possible and the variance within each class as small as possible—this is called a Fisher criterion described earlier by Equation 3.15. The goal is to find the weight vector W that minimise the corresponding Fisher criterion as shown in the following equation:

$$J(W) = \frac{W^T S_B W}{W^T S_w W} \tag{3.19}$$

  where $J(W)$ is an objective function, W is weight vector, S_B is between-class scatter matrix, and S_w is within-class scatter matrix, which are defined as follow:

$$S_B = (m_1 - m_2)(m_1 - m_2)^T \tag{3.20}$$

$$S_w = \sum_{k=1}^{2} \sum_{i \in N_k} (x_i - m_k)(x_i - m_k)^T \tag{3.21}$$

  where m_1 is the mean of first class, m_2 is the mean of the second class and x_i is the feature vector i, $i \in 1,....,N$, N_k denoting to number of training instance in class k. The weight vector W that minimised the criterion in Equation 3.19 is defined as:

$$W = S_w^{-1}(m_1 - m_2) \tag{3.22}$$

  After inference of the discriminant vector W, the predicted class label ($y \in [-1, 1]$) can be computed by the linear discriminant functions:

$$y = Wx + b \tag{3.23}$$

  where b is the bias. If $y \geq 0$ the observation x belongs to class 1, otherwise it belongs to another class.

  Generally, a discriminant analysis classifier is preferred because it is easily computed and interpreted, fast in prediction, and works well in practice (MathWorks 2018).

- **SVM**
  SVM separates two classes by finding the best hyperplane that maximises a margin between the two classes' data points. Margin means the maximum distance between the separating hyperplane and the nearest data point of each class. This data point closest to the hyperplane is called the support vector. SVM algorithm works by mapping input data into the features space that can discriminate between classes using linear or non-linear models based on the kernel function. The

linear separating hyperplane can be computed as follow:

$$f(x) = w \cdot x + b = \sum_{i=1}^{n} w_i \cdot x_i + b = 0 \tag{3.24}$$

where sign of $f(x)$ is the decision function, n is a number of data points, w and $x \in R^l$ where l is a number of features and b is scalar. The optimal solution w is that maximise the distance between two support vectors of each class i.e margin and it obtained by minimising cost function ξ_n :

$$L(w, \xi) = \frac{1}{2}\left(w^T w\right) + C \cdot \sum_{n=1}^{Z} \xi_n \tag{3.25}$$

depending on:

$$y_i\left((x_i \cdot w) + b\right) \geqslant 1 - \xi_i, i = 1, 2, \ldots, n \tag{3.26}$$

where C is penalised error, ξ is a measure of training error, Z is the number of misclassified samples and y_i is the class label of sample i. The optimisation Equation 3.25 can be simplified as:

$$V(\alpha) = \sum_{i=1}^{n} \alpha_i - \frac{1}{2} \sum_{i,j=1}^{n} \alpha_i \alpha_j y_i y_j \,\mathrm{Ker}\left(x_i \cdot x_j\right) \tag{3.27}$$

satisfying the constraint:

$$\sum_{i=1}^{l} y_i \alpha_i = 0, C \geq \alpha_i \geq 0, i = 1, 2, \ldots, l \tag{3.28}$$

where α_i is weight of training instance i as a support vector and $\mathrm{Ker}\left(x_i, x_j\right)$ is defined as kernel function; it can be linear, quadratic, cubic and gaussian; and the SVM model is varied based on type of kernel function.

This research investigated four SVM models, linear SVM, quadratic SVM, cubic SVM, and Gaussian SVM. The SVM is most widely adopted for classifying the data with complex decision boundaries (i.e., non-linearly separable data) as it can use the higher order of kernel functions. However, the computational cost of SVM is high. Also, it is time-consuming and hard to interpret (MathWorks 2018).

- **KNN**
  The KNN is a simple supervised machine learning algorithm; it classifies the new input data based on the similarity measures of its neighbours. The distance function is used to determine such similarity. Thus, the algorithm assigns the class to the input instance by the majority voting scheme based on its nearest neighbours. The first step in calculating the KNN is selecting the number K of the neighbours (in this research, K is set to 10). Next, the distance between the input instance

and each K neighbour is calculated. The most widely used distance function is a Euclidean distance which is calculated as follow:

$$\text{Euclidian: } d(x,y) = \sqrt{\sum_{i=1}^{n} (x_i - y_i)^2} \tag{3.29}$$

where $d(x,y)$ is the distance between two points x and y, and n is the dimensionality of features space. In the final step, the new input data is assigned to the class that most K neighbours belong to it.

The advantages of the KNN are simplicity, providing good predictive accuracy in low dimensional space, and not requiring explicit training. However, the KNN is computationally expensive since it must compute the distance to all samples from the training set. It also uses a lot of memory and has a longer execution time, mainly if the data size is too large (MathWorks 2018).

- **Decision tree**
  The decision tree predicts the input data class by following a decision in a tree from a root node to the leaf node (Sahu et al. 2020). The classification process of a particular instance starts from the tree's root. At each decision, the attribute value (features) specified by the node is examined. Based on its value, moving down direction is determined (left or right branch). This process is recursively repeated in each sub-tree until the leaf node is reached, which provides an instance's class.

  The tree can be trained by splitting all input data into subsets based on attribute values (features). This partitioning is recursively repeated until only homogeneous nodes are left. Each splitting tree is evaluated by the optimising function called Gini's diversity index, and the best one is selected for building the model (MathWorks 2018). Gini's diversity index is used to measure the node impurity by checking whether all training data points belong to the same split indicating the node is pure (Sahu et al. 2020). The algorithm of the decision tree is described in Figure 3.5.

INPUT: S, **where** S = *set of classified instances*
OUTPUT: *Decision Tree*
Require: $S \neq \varnothing$, $num\_attributes > 0$

```
procedure BuildTree
    repeat
        maxGain ← 0
        splitA ← null
        e ← Entropy(Attributes)
        for all Attributes a in S do
            gain ← InformationGain(a, e)
            if gain > maxGain then
                maxGain ← gain
                splitA ← a
            end if
        end for
        Partition(S, splitA)
    until all partitions processed
end procedure
```

FIGURE 3.5: Decision tree algorithm. The image is taken from Mayo (2016).

The decision tree is easy to compute, fast to fit and predict and low in memory usage, but it could provide a low predictive accuracy (MathWorks 2018).

One of the most common problems that affect classification performance and prevent the generalisation of the model is overfitting. As mentioned in section 2.5, this problem arises when the model performs well on training data but poorly fits new ones. Overfitting risk increases for several reasons: the limited amount of available data, the number of samples used in each class not being well-balanced, or high dimensional data. LOOCV was employed herein to mitigate the effect of overfitting.

The performance of the classifiers was measured using three conventional metrics: accuracy (ACC), sensitivity (SNS), and specificity (SPC). The ACC measures the percentage of correctly classified subjects—either ASD or TD—to the total number of subjects. The SNS represents the percentage of correctly classified ASD children into the ASD class—known as a true positive rate (TPR). In contrast, the SPC measures the proportion of TD that is truly classified as typical and is known as a true negative rate (TNR). Mathematically, these measures are computed as follow:

$$\text{Sensitivity (TPR)} = \frac{TP}{P} \times 100 \tag{3.30}$$

$$\text{Specificity (TNR)} = \frac{TN}{N} \times 100 \tag{3.31}$$

$$\text{Accuracy} = \frac{TP + TN}{P + N} \times 100 \tag{3.32}$$

where TP is a true positive, representing the number of correctly classified children belonging to the ASD class, and P is the total number of instances of ASD class. TN is

a true negative, which refers to the number of correctly classified children belonging to a typical class, and N is the total number of children in the typical class.

3.7 Results

The first stage of this research examined the impact of analysing the PLV-based FBC within the machine learning framework to classify ASD. The one controversial issue about PLV performance is its sensitivity to volume conduction. It is a key challenge for EEG-based brain connectivity. The volume conduction is typically reflected as zero-phase lag; however, in this analysis, the zero-phase differences between each spatially closed pair electrode were investigated in order to mitigate the effects of volume conduction. The outcomes of employing the three proposed sets of features and the significance of the results are highlighted as follows.

- **Trail-averaged PLV**
  The features were generated from five network parameters, 250 connectivity matrices, five frequency bands, and three stimuli. The features pool was formulated using all possible parameters' combinations to identify which graph-theoretical parameters are most powerful in distinguishing between the two populations. The discriminant ability of features is determined by the class separability function and consequently the classifier result. As a result, 31 different cases in each frequency band were obtained, as shown in Table 3.2. Thus, the total number of investigated cases in each stimulus was (155 cases: 31 features × 5 frequency bands). All of these cases were fed into the classifiers described in section 3.6.

  Table 3.3 shows the best classification performance for each frequency band for each stimulus (happy, neutral and fearful). Using LOOCV, the best classification accuracy of 95.8% was achieved using the cubic SVM in the theta band calculated from the happy stimulus in case of feature combinations between transitivity, global efficiency, radius, and diameter with corresponding SNS and SPC of 100% and 92%, respectively. Same classification accuracy using the KNN classifier was achieved in two other cases: (1) a combination of all features and (2) a combination between radius, diameter, and characteristic path length. In addition, the difference between the ASD and TD groups was also observed in the delta band computed from the happy stimulus. A classification accuracy up to 83.3% was achieved using the decision tree classifier in multiple cases: (1) a combination of all features, (2) a combination between radius and diameter, (3) a combination between transitivity, radius, and diameter, (4) a combination between global efficiency, radius, and diameter, and (5) a combination between transitivity, global efficiency, and diameter. To sum up, in the happy stimulus, the best classification accuracy was achieved within the theta and delta bands.

TABLE 3.2: List of all the cases investigated in the first PLV approach (trial-averaged PLV) in each frequency band and for each stimulus.

Case	Features
1	Transitivity
2	Global efficiency
3	Radius
4	Diameter
5	Characteristic path length
6	Transitivity and global efficiency
7	Transitivity and radius
8	Transitivity and diameter
9	Transitivity and characteristic path length
10	Global efficiency and radius
11	Global efficiency and diameter
12	Global efficiency and characteristic path length
13	Radius and diameter
14	Radius and characteristic path length
15	Diameter and characteristic path length
16	Transitivity, global efficiency and radius
17	Transitivity, global efficiency and diameter
18	Transitivity, global efficiency and characteristic path length
19	Transitivity, radius and diameter
20	Transitivity, radius and characteristic path length
21	Transitivity, diameter and characteristic path length
22	Global efficiency, radius and diameter
23	Global efficiency, radius and characteristic path length
24	Global efficiency, diameter and characteristic path length
25	Radius, diameter and characteristic path length
26	Transitivity, global efficiency, radius and diameter
27	Transitivity, global efficiency, radius and characteristic path length
28	Transitivity, global efficiency, diameter and characteristic path length
29	Transitivity, radius, diameter and characteristic path length
30	Global efficiency, radius, diameter and characteristic path length
31	All features

TABLE 3.3: Best classification performance in each stimulus using trial-averaged PLV.

Stimulus	Band	ACC	SNS	SPC	Classifier
Happy	Delta	83.30%	83.00%	83.00%	Decision tree
	Theta	95.80%	100.00%	92.00%	Cubic SVM
					KNN
	Alpha	79.20%	75.00%	83.00%	Decision tree
	Beta	79.20%	75.00%	83.00%	Gaussian SVM
	Gamma	79.20%	83.00%	75.00%	Cubic SVM
Fearful	Delta	75.00%	75.00%	75.00%	Cubic SVM
			75.00%	75.00%	Quadratic SVM
			67.00%	83.00%	Gaussian SVM
			83.00%	67.00%	Quadratic SVM
	Theta	79.20%	75.00%	83.00%	Cubic SVM
			67.00%	92.00%	Gaussian SVM
	Alpha	75.00%	83.00%	67.00%	Gaussian SVM
			75.00%	75.00%	Decision tree
	Beta	70.80%	67.00%	75.00%	Decision tree
	Gamma	79.20%	75.00%	83.00%	KNN
			83.00%	75.00%	
Neutral	Delta	83.30%	83.00%	83.00%	KNN
			92.00%	75.00%	
	Theta	87.50%	92.00%	83.00%	Quadratic SVM
	Alpha	83.30%	83.00%	83.00%	Cubic SVM
	Beta	79.20%	75.00%	83.00%	Cubic SVM
	Gamma	75.00%	75.00%	75.00%	KNN
			75.00%	75.00%	KNN
			67.00%	83.00%	Decision Tree
			83.00%	67.00%	Gaussian SVM

In the neutral stimulus, the best classification performance was obtained using the quadratic SVM in the theta band with a classification accuracy up to 87.5%, with 92% SNS and 83% SPC. This result was observed in several cases: (1) a combination of transitivity, global efficiency, and diameter, (2) a combination of transitivity, diameter, and characteristic path length, and (3) a combination of global efficiency, diameter, and characteristic path length.

The optimal classification performance was observed for the fearful stimulus in the theta and gamma bands. However, classification ACC did not exceed 79.2%, which was obtained in the theta band using two sets of features: (1) the diameter feature, with 67% SNS and 92% SPC using Gaussian SVM, and (2) a combination of transitivity and characteristic path length, with 75% SNS and 83% SPC using

cubic SVM. In the gamma band, the best accuracy was observed using three sets of features: (1) a combination between transitivity and global efficiency with SNS and SPC of 83% and 75%, respectively, (2) a combination between transitivity and characteristic path length, with 83% SNS and 75% SPC, and (3) characteristic path length, with 75% SNS and 83% SPC.

- **Average trial-averaged PLV**
  The feature pool was generated from five graph metrics, and one averaged connectivity matrix, yielding a features vector consisting of only five features. Here, the features selection algorithm was applied to rank the features by how informative they are. The combinations of features based on FDR ranking were investigated in each frequency band and for each stimulus. In other words, the combination between the two highest-ranked features was firstly examined, then the three highest-ranked features, and so on. Consequently, a total of 20 different cases were investigated. Each was evaluated by feeding into a classifier to determine which feature set is optimal, which frequency band, and which stimulus. The cases involved three stimuli, the possible combination of the five highest-ranking network parameters and five frequency bands. For example, the cases examined in the happy stimulus in the delta band were (transitivity and global efficiency), (transitivity, global efficiency, and radius), (transitivity, global efficiency, radius, and characteristic path length) and (transitivity, global efficiency, radius, characteristic path length, and diameter). Thus, the overall number of cases investigated in each stimulus in a specific frequency band was four.

The rankings of the five features investigated in each frequency band corresponding to each stimulus are shown in Figures 3.6 to 3.8. The best classification performances in each stimulus and each frequency band are demonstrated in Figure 3.9. With this approach, the best classification accuracy was 87.5%, with 83% SNS and 92% SPC. This classification performance was observed in the theta band within the happy stimulus using the KNN classifier with a combination of all five features. The same classification accuracy with 100% SNS and 75% SPC was realised in the neutral stimulus in the theta band using the quadratic SVM classifier with a combination of global efficiency, transitivity, and characteristic path length. The optimal classification performance was observed in the alpha band calculated from the fearful stimulus, which achieved 83.3% ACC, 83% SNS, and 83% SPC using the quadratic SVM classifier with a combination of global efficiency, transitivity and characteristic path length.

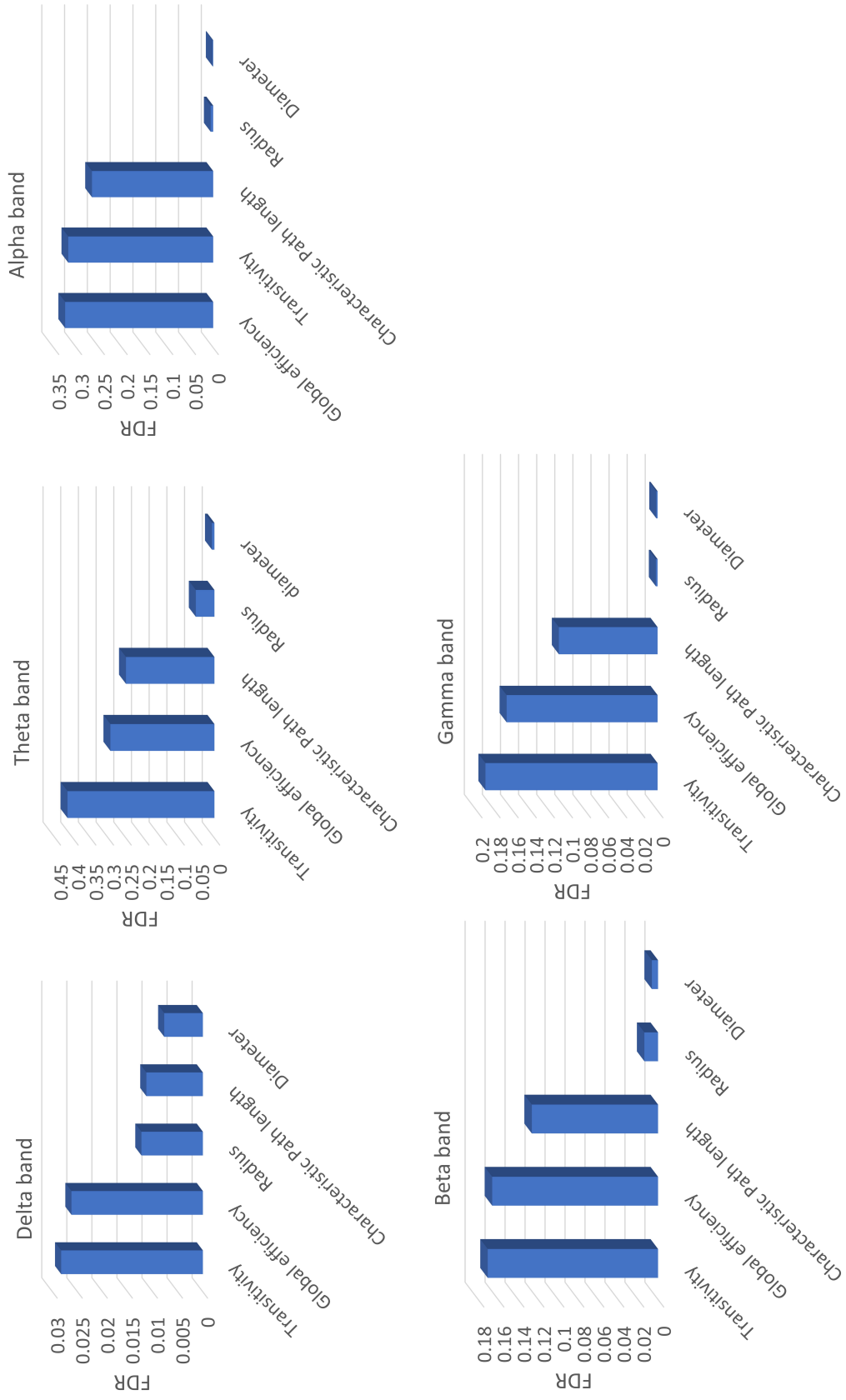

FIGURE 3.6: FDR ranking of five features in each frequency band with the happy stimulus using the average trial-averaged PLV approach.

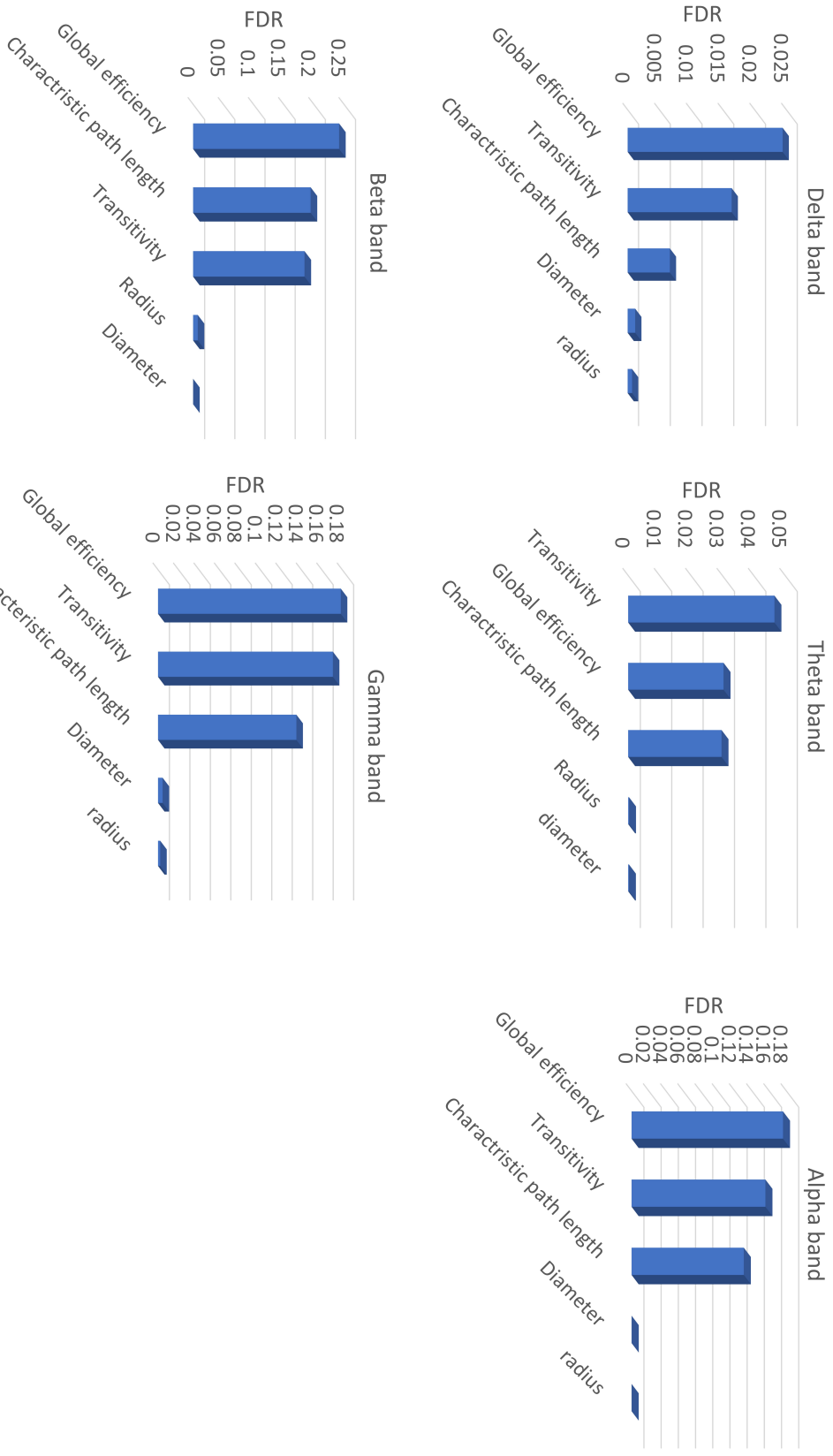

FIGURE 3.7: FDR ranking of five features in each frequency band with the neutral stimulus using the average trial-averaged PLV approach.

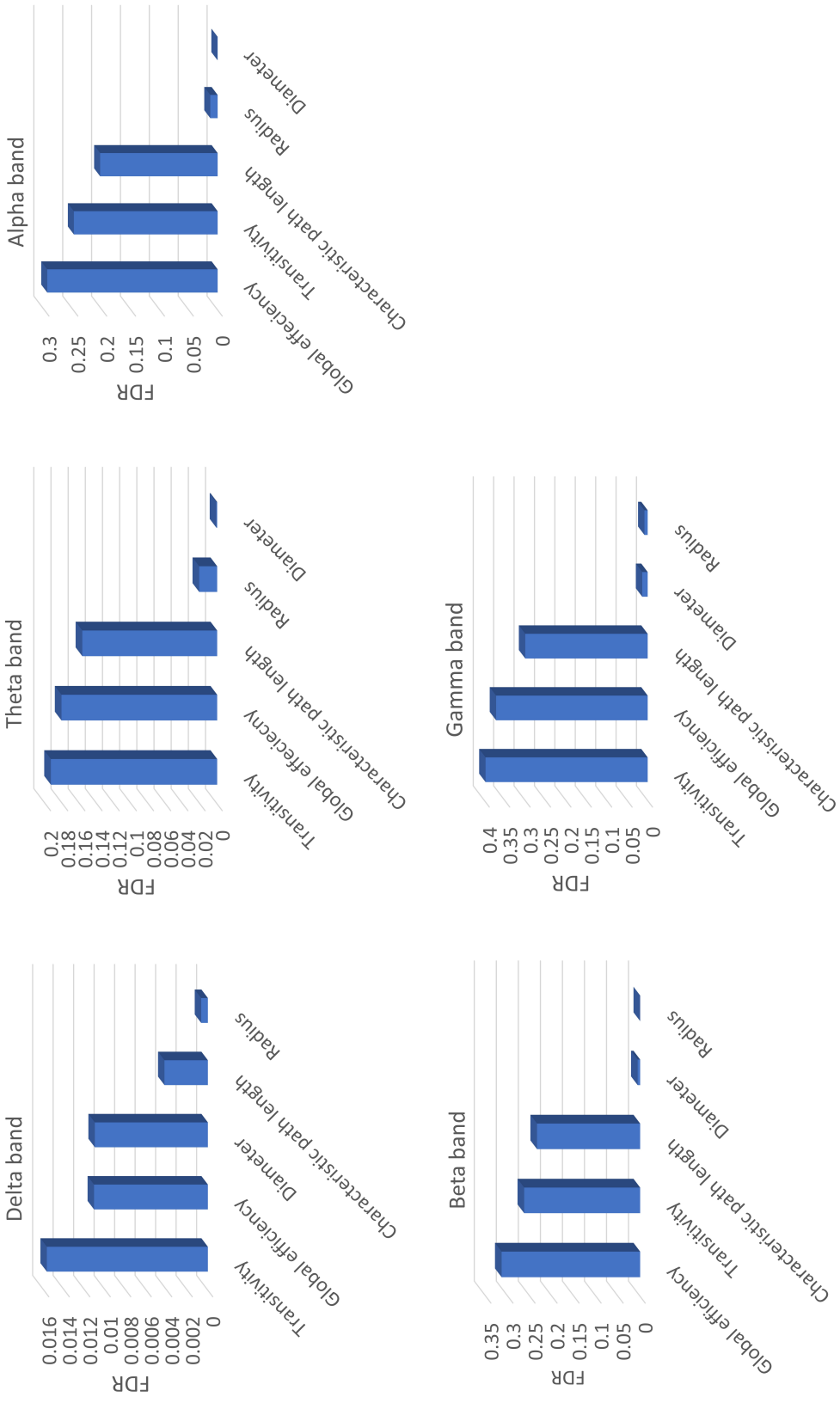

FIGURE 3.8: FDR ranking of five features in each frequency band with the fearful stimulus using average trial-averaged PLV approach.

A) Confusion matrix for happy stimulus

Delta

True class \ Predicted class	-1	1	SNS	SPC	ACC
-1	TP=10	FP=2	67%	83%	75%
1	FN=4	TN=8			

Theta

True class \ Predicted class	-1	1	SNS	SPC	ACC
-1	TP=10	FP=2	83%	92%	87.5%
1	FN=1	TN=11			

Alpha

True class \ Predicted class	-1	1	SNS	SPC	ACC
-1	TP=9	FP=3	75%	83%	79.2%
1	FN=2	TN=10			

Beta

True class \ Predicted class	-1	1	SNS	SPC	ACC
-1	TP=10	FP=2	83%	83%	83.3%
1	FN=2	TN=10			

Gamma

True class \ Predicted class	-1	1	SNS	SPC	ACC
-1	TP=10	FP=2	83%	75%	79.2%
1	FN=3	TN=9			

B) Confusion matrix for neutral stimulus

Delta

True class \ Predicted class	-1	1	SNS	SPC	ACC
-1	TP=10	FP=2	83%	75%	79.2%
1	FN=3	TN=9			

Theta

True class \ Predicted class	-1	1	SNS	SPC	ACC
-1	TP=12	FP=0	100%	75%	87.5%
1	FN=3	TN=9			

Alpha

True class \ Predicted class	-1	1	SNS	SPC	ACC
-1	TP=9	FP=3	75%	58%	66.7%
1	FN=5	TN=7			

Beta

True class \ Predicted class	-1	1	SNS	SPC	ACC
-1	TP=9	FP=3	75%	75%	75%
1	FN=3	TN=9			

Gamma

True class \ Predicted class	-1	1	SNS	SPC	ACC
-1	TP=9	FP=3	75%	83%	79.2%
1	FN=2	TN=10			

C) Confusion matrix for fearful stimulus

Delta

True class \ Predicted class	-1	1	SNS	SPC	ACC
-1	TP=9	FP=3	75%	67%	70.8%
1	FN=4	TN=8			

Theta

True class \ Predicted class	-1	1	SNS	SPC	ACC
-1	TP=9	FP=3	75%	67%	70.8%
1	FN=4	TN=8			

Alpha

True class \ Predicted class	-1	1	SNS	SPC	ACC
-1	TP=10	FP=2	83%	83%	83.3%
1	FN=2	TN=10			

Beta

True class \ Predicted class	-1	1	SNS	SPC	ACC
-1	TP=9	FP=3	75%	75%	75%
1	FN=3	TN=9			

Gamma

True class \ Predicted class	-1	1	SNS	SPC	ACC
-1	TP=9	FP=3	75%	83%	79.2%
1	FN=2	TN=10			

FIGURE 3.9: Confusion matrices of best classification performance by average trial-averaged PLV. Panel A, B, and C show each frequency band's results calculated from happy, neutral and fearful stimuli, respectively.

- **Time-points averaged PLV**
  The feature pool contained five features, ranked using FDR. Similar to the second approach, a total of 60 cases were investigated to find the best feature combinations, frequency band, and stimulus, helping to differentiate between the ASD and TD groups. Figures 3.10 to 3.12 show the ranking of the five parameters assessed in each frequency band for each stimulus. The best performances in each stimulus and each band are depicted in Figure 3.13.

  The best classification performance was observed using the decision tree classifier in the alpha band calculated from the fearful stimulus. This result was achieved using all features and reached 83.3% ACC, 75% SNS and 92% SPC. For the happy stimulus, the highest ACC did not exceed 75% in the theta band with a combination of all features. SNS and SPC were 92% and 58%, respectively. Furthermore, the same ACC was achieved in the delta band with 83% SNS and 67% SPC, with a combination of characteristic path length and diameter. In neutral stimulus, the classification performance did not exceed 75% in the alpha and beta bands.

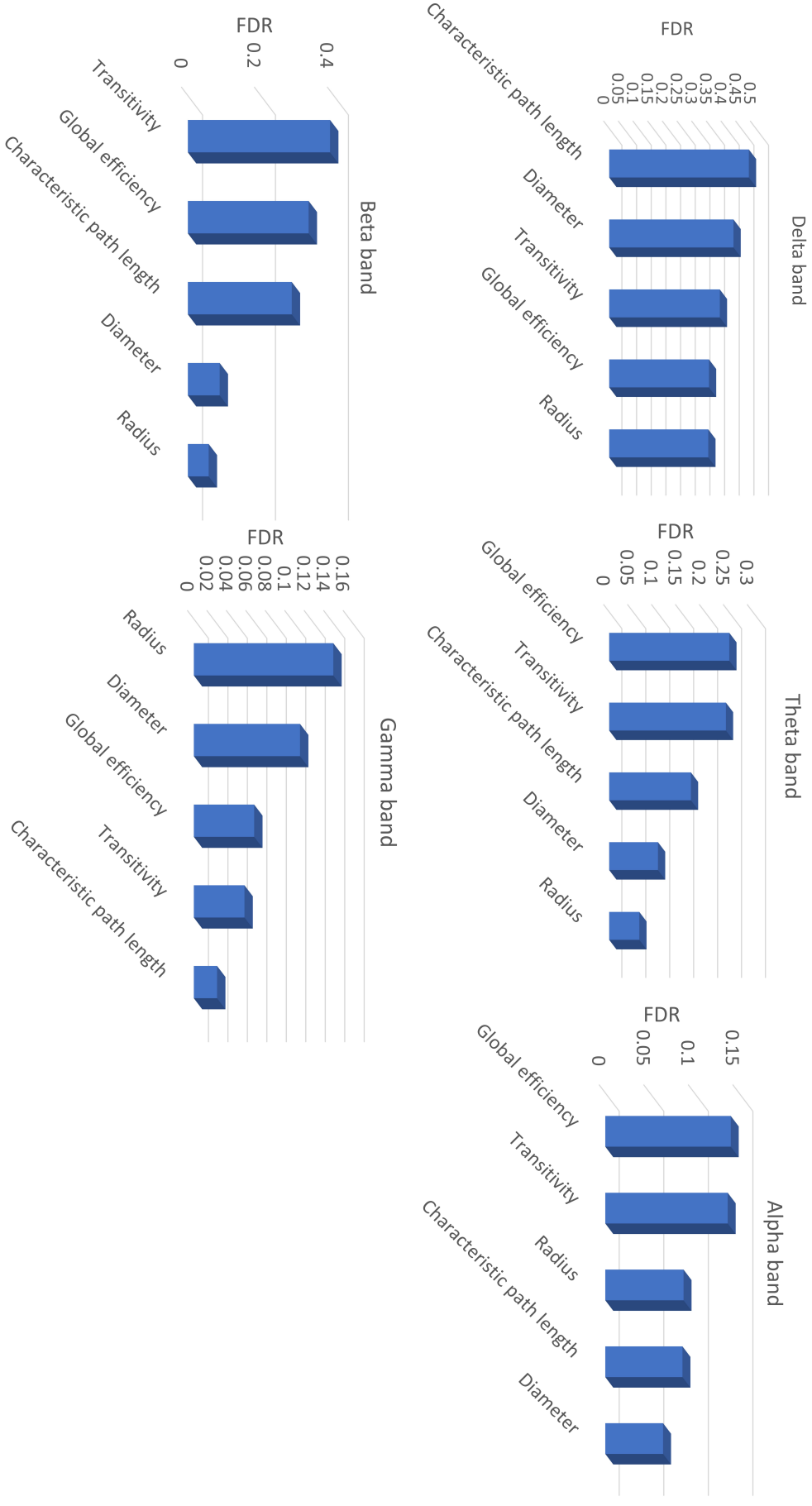

FIGURE 3.10: FDR ranking of the five features in each frequency band with happy stimulus using time-points-averaged PLV approach.

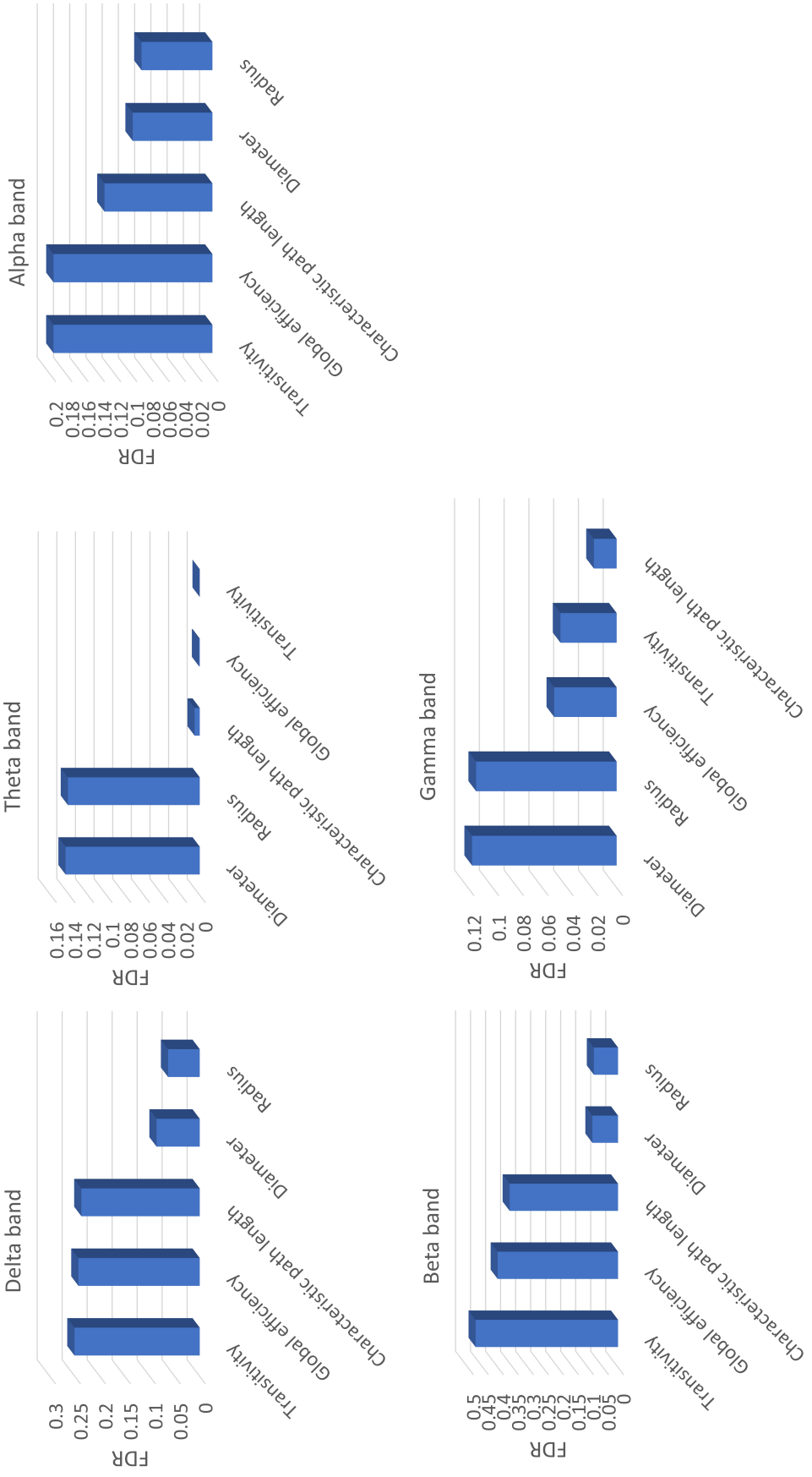

FIGURE 3.11: FDR ranking of the five features in each frequency band with neutral stimulus using time-points-averaged PLV approach.

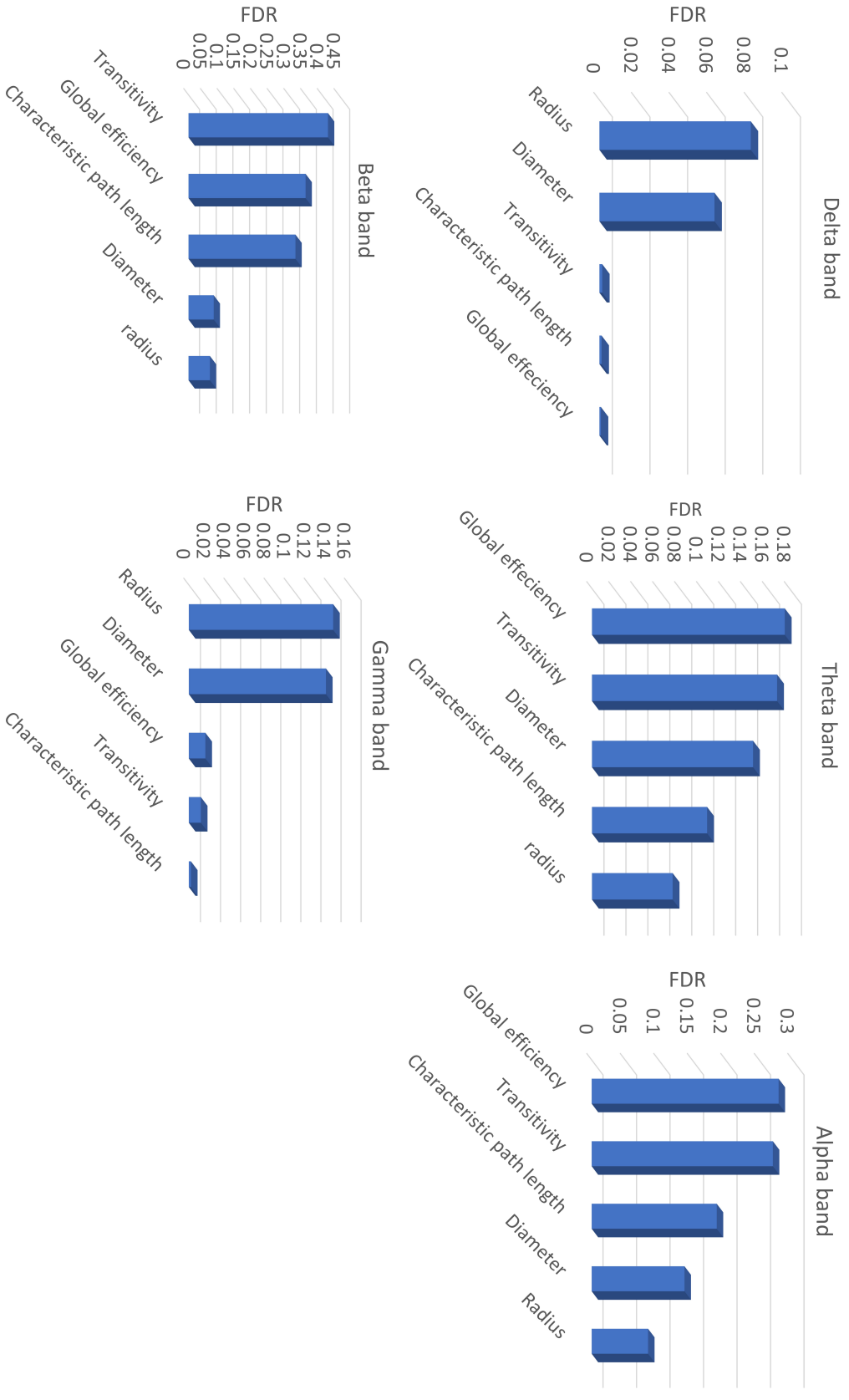

FIGURE 3.12: FDR ranking of the five features in each frequency band with fearful stimulus using time-points-averaged PLV approach.

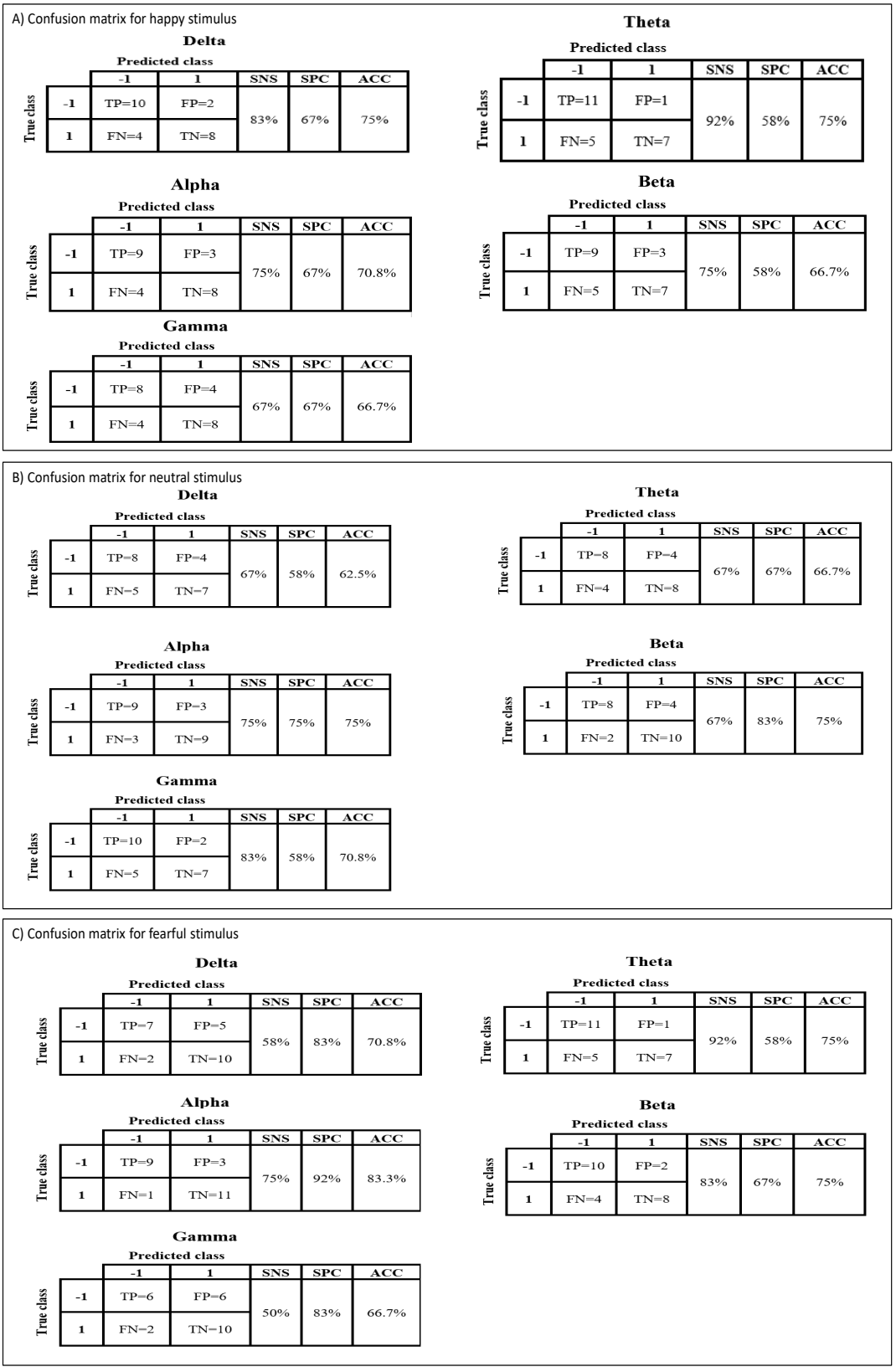

FIGURE 3.13: Confusion matrices of best classification performance using time-points averaged PLV. Panel A, B, and C show each frequency band's results calculated from happy, neutral and fearful stimuli respectively.

3.8 Discussion

This chapter aimed to characterise the difference in task-dependent functional brain networks between ASD and TD. Three proposed PLV-based FBC characterised by global graph-theoretical features within a machine learning framework were explored to find the biomarker to classify ASD children. These approaches were investigated to find the best technique to estimate the FBC from EEG acquiring during ERP experiment. The study found that the three proposed PLV-based FBC—trial-averaged PLV, average trial-averaged PLV, and time-points-averaged PLV achieved considerable results. The best classification performance reached 95.8% ACC, 100% SPC, and 92% SNS using trial-averaged PLV. A comparable result was also observed using average trial-averaged PLV and reached 87.5% ACC, 100% SNS, and 75% SPC. Classification performance using time-points-averaged PLV reached to 83.3% ACC, 75% SNS, and 92% SPC. These results showed a relative superiority of classification performance over the state-of-the-art studies as summarised in Table 3.4.

Kang et al. (2020) conducted a study on resting-state EEG data set of 49 children with ASD and 48 TD using a linear EEG feature— spectral power—and their result was reached up to 85.44% using SVM. Abdolzadegan et al. (2020) explored a set of linear (spectral power, wavelet, and fast Fourier transform (FFT)) and non-linear (fractal dimension, correlation dimension, Lyapunov exponent, detrended fluctuation analysis (DFA) and entropy) EEG features extracted from resting-state EEG data. The study achieved a classification accuracy up to 90.57% using SVM. Grossi et al. (2017) carried out a resting-state EEG study using non-linear EEG features based on multi-scale entropy called multi-scale ranked organising map coupled with implicit function as squashing time algorithm (MSROM/I-FAST) and obtained classification accuracy reached up to 92.8% with a random forest classifier. Ahmadlou et al. (2012) used non-linear EEG analysis—known fuzzy synchronisation likelihood—extracted from a resting-state EEG data set. The study successfully classified ASD using an enhanced probabilistic neural network with classification accuracy up to 95.5%. Khuntia et al. (2019) and Jamal et al. (2014) used the ERP data set recorded during the execution of facial perception tasks—the same data set used in this research. Khuntia et al. (2019) studied the role of face and emotion processing in ASD using multivariate pattern analysis in both time and time-frequency domains using STFT. Classification performance reached 84% using classwise principal component analysis. Jamal et al. (2014) provided the FBC study based on synchrostates analysis and graph theory analysis. Classification ACC reached 94.7%, SNS 85.7%, and SPC 100% using SVM.

As can be seen from Table 3.4, apart from Jamal et al. (2014) and Ahmadlou et al. (2012), most of the studies used linear and non-linear EEG features that were not designed to capture the neural activity over the whole brain, that is, the problem related to the ASD. Ahmadlou et al. (2012) used the non-linear synchronisation method to study the

TABLE 3.4: Comparative studies of EEG-based machine learning for ASD classification.

Author	Data set				Features	Classifier	ACC
	ASD	Age	TD	Age			
Kang et al. (2020)	49	3-6	48	3-6	Combination of spectral power and eye-tracking data	SVM	85.44%
Abdolzadegan et al. (2020)	34	3-12	11	3-12	Spectral power, wavelet transform, FFT, fractal dimension, correlation dimension, Lyapunov exponent, DFA and entropy	SVM	90.75%
Grossi et al. (2017)	15	7-14	10	7-12	MSROM/I-FAST	Random forest	92.80%
Ahmadlou et al. (2012)	9	7-13	9	7-13	Fuzzy synchronisation likelihood	EPNN	95.50%
Jamal et al. (2014)	12	6-13	12	6-13	Graph-theoretical parameters derived from synchrostate	SVM	94.70%
	Data set used in this study						
(Khuntia et al. 2019)	12	6-13	12	6-13	STFT and multivariate pattern of the time-points	Classwise principal component analysis	84.00%
	Data set used in this study						
Current study	12	6-13	12	6-13	Graph-theoretical parameters derived from PLV	SVM	95.80%

FBC within and between seven brain regions (prefrontal, frontal, right temporal, left temporal, central, parietal, and occipital). Jamal et al. (2014) carried out a synchrostate analysis derived from a high-density EEG system which makes it not applicable to young children. In contrast, PLV-based FBC, used in this research, can be perfectly estimated by considering only a limited number of channels. PLV was used to calculate the phase synchronisations between each pair of channels and analyse their characteristics using graph theory parameters. It has several advantages; it is provided a fast and reliable calculation with mathematical simplicity (Bruña et al. 2018). In addition, this study investigated the PLV-based FBC from EEG recording during the execution of face perception tasks, a core deficit in ASD children. Most machine learning-based studies in the literature, except Jamal et al. (2014) and Khuntia et al. (2019), explored ASD abnormalities from resting-state EEG.

One of the key findings of this study was that the significant difference between both populations was observed in the theta and alpha bands. This may be due to the activity of the theta band usually being associated with cognitive and emotional processing and modulations of the alpha traditionally related to memory maintenance (Klimesch 1999). In this context, some studies consistently report a close and strong association between alteration of theta and alpha oscillations and the subject with ASD. Li et al. (2013) stated that the theta power increases, and alpha power decreases after increased task demands, such as presenting less frequent target stimuli in an oddball paradigm. Klimesch (1999) proved that there were changes in the alpha and theta bands in subjects with various neurological disorders when subjects tried to respond to external stimuli.

Moreover, a significant difference between ASD and TD subjects has been found in the alpha and theta bands (Larrain-Valenzuela et al. 2017). Yeung et al. (2014) found that the ASD children had general impairment in recognising facial emotions in the theta-coherence. Khuntia et al. (2019) observed the difference between ASD and TD in the alpha and beta bands.

The results of this study also showed that the global network attributes derived from PLV could effectively classify both groups. However, it is still challenging to generalise the most discriminative feature because the optimal graph metrics vary between PLV approaches and the types of stimuli.

The main limitation of this study was the limited number of samples in the data set. This problem is typical in clinical studies and the medical field. Due to that, the machine learning community devoted a significant effort to establishing techniques for such limitations. LOOCV is one technique employed to reduce the effects of the limited number of samples.

3.9 Conclusion

The task-dependent functional brain connectivity analysis successfully distinguished ASD and TD children. Graph-theoretical features derived from three PLV-based FBC approaches were assessed using several machine learning algorithms—LDA, SVM, KNN and decision tree. The trial-averaged PLV achieved a high classification performance of 95.8% ACC, 100% SPC, and 92% SNS by cubic SVM. Moreover, the global graph-theoretical features of the theta and alpha connectivity may be considered biomarkers for detecting ASD in children.

Chapter 4

Prediction of Cerebral Palsy in Newborns with Hypoxic-Ischaemic Encephalopathy Using EEG-based Functional Brain Connectivity

4.1 Introduction

Chapter 3 successfully validated the phase-based synchronisation adopted within the machine learning framework in classifying children with ASD. Due to this success, the feasibility of this framework in predicting outcomes at two years of age is investigated. In this chapter, the WPLI-based FBC is employed to quantify the phase synchronisation. It is used herein because it is robust against the effect of volume conduction and less prone to other sorts of noise. Hence, it offers a reliable estimation of functional connectivity between different brain regions. WPLI-based FBC is characterised by graph attributes, which are used to identify the topological difference in the brain network of the infant born with HIE and developed CP at two years of age.

The experimental work is divided into several parts. First, the DBP filter is used to decompose the EEG spectra into five traditional brain waves. Then, the WPLI is computed from each frequency range to characterise the overlapping time-frequency brain dynamics associated with CP. The graph attributes are then derived from the FBC network calculated from WPLI. These graphical attributes are used to train and test the RUSBoost classifier to show how useful they could be in practical CP prediction. A schematic outline of the proposed analysis is depicted in Figure 4.1.

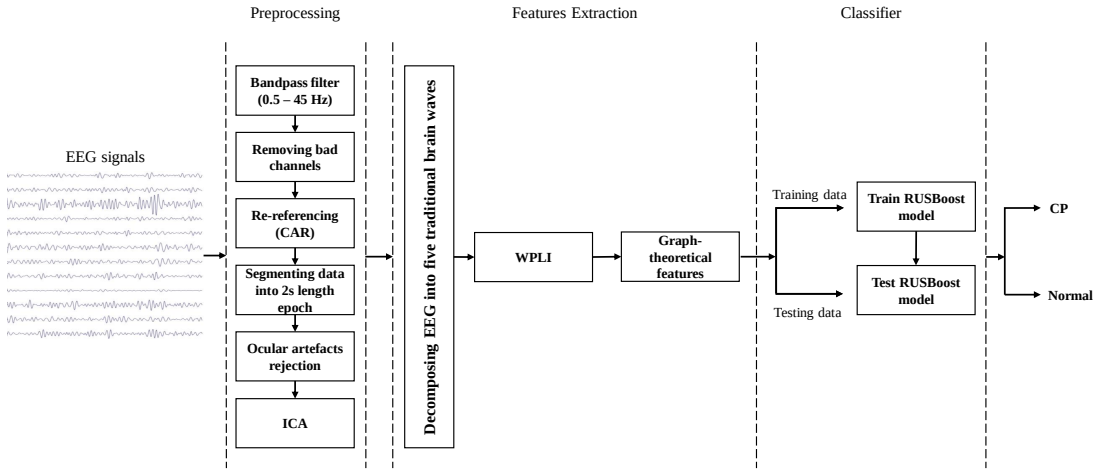

FIGURE 4.1: Schematic outline of the proposed analysis for predicting CP at two years of age. Each time-series recording from each electrode was preprocessed by several preprocessing techniques: filtering, removing bad channels, re-referencing, segmentation and artefacts rejection. Then, the EEG signals were decomposed into five traditional brain waves. After that, the phase-based FBC, particularly WPLI, was calculated, and then the graph-theoretical features were extracted. The extracted features were fed into the machine learning algorithm to perform binary classification of an infant either into CP group or normal ones.

This chapter is organised as follows: section 4.2 describes the EEG data set used in this part of the research. Section 4.3 illustrates the preprocessing techniques adopted for removing the artifices from EEG signals. The feature extraction and analysis schemes are described in section 4.4 and section 4.5, respectively. The machine learning algorithm employed in this chapter is depicted in section 4.6. Section 4.7 presents the analysis of the results. These results are further discussed in section 4.8. Finally, section 4.9 concludes the chapter.

4.2 Experimental Data Description

Thirty term-born infants with HIE treated with hypothermia were prospectively recruited in this study. EEG data were recorded on the neonatal intensive care unit within the first week after birth. At twenty-four months of age, the infants were followed up under the clinical follow-up programme at the University Hospital of Southampton (UHS). A paediatric neurologist carried out the neurological examination at this age. The outcomes were categorised into normal, CP (had abnormalities in posture, movements, tone, and reflexes), or had unspecific signs. The infants were diagnosed as CP

according to the criteria of the Surveillance of CP in Europe Working Group (SCPE 2001). Out of the thirty infants, twenty-nine infants reached two years and completed the follow-up assessment. In this prospective study, twenty infants had normal neurology, six developed CP, and three had unspecific signs at twenty-four months of age, as illustrated in Table 4.1. Secondary analysis of anonymised, routinely collected clinical data were approved by the HRA and Health and Care Research Wales, HCRW (Reference ID 20/HRA/0260; IRAS project ID 278072 University Hospital Southampton R& D protocol number RHM CHI1047).

TABLE 4.1: Clinical characteristics of thirty neonates born with HIE at twenty-four months of age. Based on neurology examination the infants were classified into either normal or having CP.

Subject #	Neurology at age 24 months
subj_1	normal
subj_2	normal
subj_3	normal
subj_4	CP
subj_5	normal
subj_6	CP
subj_7	CP
subj_8	normal
subj_9	normal
subj_10	normal
subj_11	normal
subj_12	unspecificic signs
subj_13	normal
subj_14	normal
subj_15	normal
subj_16	normal
subj_17	normal
subj_18	normal
subj_19	incomplete follow-up
subj_20	normal
subj_21	normal
subj_22	unspecific signs
subj_23	CP
subj_24	normal
subj_25	normal
subj_26	CP
subj_27	CP
subj_28	unspecific signs
subj_29	normal
subj_30	normal

The EEGs were recorded from the infants on the neonatal intensive care unit within the first seven days after birth, during the resting period, with eyes closed for at least 20 minutes. Nineteen surface electrodes (C3, C4, CZ, F3, F4, F7, F8, FZ, FP1, FP2, O1, O2, P3, P4, PZ, T3, T4, T5 and T6) were applied according to the international 10-20 system, as shown in Figure 4.2. Recordings were done by either a Nihon Kohden (sampling frequency 512 Hz, high-pass filter cut-off frequency 0.016 Hz, low-pass filter cut-off frequency 300 Hz) or XLTEK (sampling frequency 512 Hz, high-pass filter cut-off frequency 0.1 Hz, the low-pass filter cut-off frequency 70 Hz) clinical video-EEG system. A

consultant neurophysiologist examined all of the recorded EEGs and extracted a continuous clip with minimal artefacts (the average length of the clips is approximately two minutes).

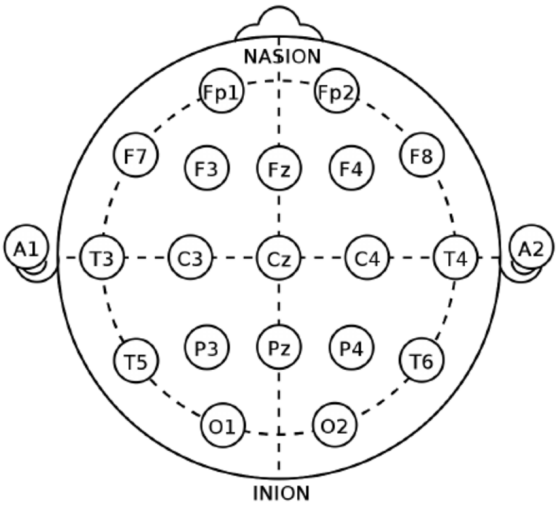

FIGURE 4.2: The 10-20 international system of 19 EEG electrodes placement.

4.3 Data Preprocessing

A two-minute continuous resting-state clip from each EEG electrode was preprocessed to improve the quality of the signal and eliminate any remaining artefacts such as eye movement, muscle, heart activities, line noise, and signal discontinuity. All the data preprocessing was performed via the EEGLAB, an open-source toolbox in MATLAB. The details of preprocessing steps carried out in this study are stated below.

- **Filtering**
  FIR bandpass-filter with the cut-off frequencies at 0.5 Hz and 45 Hz was used to filter EEG signals to mitigate the drifts and direct current components and diminish the high-frequency noises (the detail about FIR filter was described in section 3.2). The filter order was set to 3072 according to the equation 3.1.

- **Removing bad channels**
  The bad channels were identified to make the data amenable to the analysis. EEGLAB automatically picks the bad channels based on two criteria: first, the flat channels, and second, the channels with a large amount of noise determined based on their standard deviation. Subsequently, the bad channels (which were seven) were removed from each subject and not included in further analysis in any subject in the data set under investigation. The remaining twelve channels were: C3, F3, F7, Fz, O1, O2, P3, P4, T3, T4, T5, and T6.

- **Re-referencing**
  A common averaged reference (CAR) was applied to re-reference the data. In CAR, the electrical potential at each electrode is measured by subtracting the average signals of all electrodes from its EEG signal. Through the averaging process, the uncorrelated random noise is minimised as the signal or noise that is common to all electrodes remains on the CAR, whereas the signal that is isolated on one electrode does not appear on the CAR (Ludwig et al. 2009).

- **Epoching**
  A continuous EEG signal recorded from each channel was segmented into a series of epochs (windows) of two-second length according to the typical approaches followed for EEG resting-state analysis (Kulak & Sobaniec 2005). Since EEG is a non-stationary signal in its nature and quasi-stationary only within short intervals, two-second epoch is considered an appropriate length of time to capture the essence of its properties (Sakkalis 2011).

- **Artefacts rejection**
  A semi-automated procedure was performed to remove any epoch contaminated with artefacts. Ocular artefacts, particularly eye movement, were automatically detected through the EEGLAB toolbox by setting the threshold value equal to 55 μV since such artefacts were defined by a value greater than this (Apicella et al. 2013). Thus, each epoch containing values above this threshold was marked as a bad epoch and excluded from further analysis. After this step, the remaining epochs were visually inspected to determine whether they were contaminated by high frequency, line noise, or discontinuity. The corrupted epochs were rejected and eliminated from subsequent analysis. Independent component analysis (ICA) was then applied, using the runICA algorithm implemented in EEGLAB, to remove the remaining artefacts from the signals, such as muscle artefacts and cardiac activity. Thus, the EEG signals from the twelve channels were separated into their twelve constituent independent components (ICs), as the general rule of ICA is to find the N independent components from the N linearly mixed-signal (input channel data). These ICs were then projected back to the EEGs using the estimated separating matrix after the artefact-related ICs were manually eliminated according to the study of Chaumon et al. (2015).

Finally, a total of thirty artefact-free two-second epochs per subject were used in the next stage of the analysis.

4.4 WPLI-Based Functional Brain Connectivity

WPLI is a phase-based functional brain connectivity method used in this study for quantifying phase synchronisation. It was proposed to abate the well-known problem

of PLI and alleviate the sensitivity to noise. Such a problem might exist in the case of small perturbation of phase, which could turn phase lags into leads and vice versa. It would lead to the discontinuity of the measure (Vinck et al. 2011). To overcome this issue, WPLI gives an improved connectivity estimation by weighting the phase difference according to their magnitudes of the imaginary component of the cross-spectrum. Accordingly, the phases differences which are prone to a potential shift in their true signs, attributed by the small noise perturbations, are assigned to a small weight equivalent to the magnitude of the imaginary component. Consequently, they would have a lower impact in quantifying connectivity. Mathematically, WPLI can be defined as:

$$WPLI = \frac{\left|\left\langle \mid \Im(X) \mid sign(\Im(X))\right\rangle\right|}{\left\langle \mid \Im(X) \mid \right\rangle} \tag{4.1}$$

where $\Im(x)$ is the imaginary component of the cross-spectrum X for two real-valued signals Z_1 and Z_2. The cross-spectrum X is computed as:

$$X = Z_1 * Z_2^* \tag{4.2}$$

where Z_1^* and Z_2^* are a complex conjugate of Z_1 and Z_2, respectively. The WPLI value is either one, denoting the presence of synchronisation, or zero, indicating no synchronisation between two signal sources. WPLI quantifies the strength of phase coupling between neural oscillators by estimating the instantaneous phase from the time-series signal. It is crucial to derive the WPLI from narrow-band components in each source to get the intended physical interpretation of the phase. For that reason, herein, the DBP was used to decompose EEG signal into five traditional brain waves in the same manner as stated in section 3.2. Then, these components were subjected to instantaneous phase estimation.

4.5 Extraction of Complex Network Parameters

After calculating the FBC, the graph attributes were derived from the connectivity network. The researchers have suggested that hyper-connection and hypo-connection alteration are associated with CP individuals' brain functions (Gao, Jia, Wu, Yu & Feng 2017). The global network metrics that can capture these two properties are transitivity, global efficiency, radius, diameter and characteristic path length (detailed descriptions of these features were presented earlier in the section 3.4). Thus, these five graph parameters were chosen to be used in this study as they could provide great insight into the information flow in the brain of infants diagnosed later with CP.

The extraction procedure consisted of the following steps to estimate the multivariate brain network features incorporated into a classifier model and then predict the

subject's class accordingly. First, the WPLI connectivity matrix was computed between the twelve channels for each frequency band and epoch. As a result, in each frequency band, thirty connectivity matrices were generated, each connectivity corresponded to one epoch (for example, there were thirty connectivity matrices in the delta band, thirty connectivity matrices in the theta band, and so on.). The generated WPLI matrices were averaged over the epochs to get one connectivity matrix for each frequency band. Then, each connectivity matrix was transformed into a connectivity network, and the graph-theoretical attributes were calculated to quantify its properties. Thus, five graph-theoretical features were obtained for each subject and frequency band. These features were then used to train and test the RUSBoost classifier.

4.6 Classification Techniques for Handling Imbalanced Data Distribution

The data set used in this study consisted of twenty neonates presenting with normal neuromotor outcomes and six with CP. Notably, the classes distribution is imbalanced. This problem is common in the medical domain when instances of one class in the data set outnumber the other class instances. Most of the efforts in the machine learning community have gone into solving this problem by proposing several techniques as described in section 2.5. In this study, the hybrid method called RUSBoost was adopted to discriminate between the two groups as it efficiently alleviates the class imbalance problem. RUSBoost combined random undersampling with a boosting approach. A random under-sampling algorithm works by randomly removing instances from the majority class until the intended balance is achieved (Seiffert et al. 2010). Boosting is an ensemble method that constructs a robust classifier from the several week classifiers (such as a decision tree) by building a model from training data and then formulating a second model to correct the existing error in the previous models. This process is repeated until the training set is predicted correctly (Seiffert et al. 2010). The algorithm of the RUSBoost classifier is depicted in Figure 4.3.

Algorithm RUSBoost

Given: Set S of examples $(x_1, y_1), ..., (x_m, y_m)$ with minority class $y^r \in Y$, $|Y| = 2$
Weak learner, $WeakLearn$
Number of iterations, T
Desired percentage of total instances to be represented by the minority class, N

1 Initialize $D_1(i) = \frac{1}{m}$ for all i.
2 Do for $t = 1, 2, ..., T$
a Create temporary training dataset S'_t with distribution D'_t using random undersampling
b Call $WeakLearn$, providing it with examples S'_t and their weights D'_t.
c Get back a hypothesis $h_t : X \times Y \rightarrow [0, 1]$.
d Calculate the pseudo-loss (for S and D_t):
$\epsilon_t = \sum_{(i,y):y_i \neq y} D_t(i)(1 - h_t(x_i, y_i) + h_t(x_i, y))$.
e Calculate the weight update parameter:
$\alpha_t = \frac{\epsilon_t}{1 - \epsilon_t}$.
f Update D_t:
$D_{t+1}(i) = D_t(i)\alpha_t^{\frac{1}{2}(1+h_t(x_i,y_i)-h_t(x_i,y:y\neq y_i))}$.
g Normalize D_{t+1}: Let $Z_t = \sum_i D_{t+1}(i)$.
$D_{t+1}(i) = \frac{D_{t+1}(i)}{Z_t}$.
3 Output the final hypothesis:
$H(x) = \underset{y \in Y}{\text{argmax}} \sum_{t=1}^{T} h_t(x, y) \log \frac{1}{\alpha_t}$.

FIGURE 4.3: RUSBoost algorithm (Seiffert et al. 2010).

RUSBoost has several advantages, such as computational simplicity, reliability, and short training time, making it a valuable solution for learning from imbalanced data. The classifier training was performed using the classification learner app within the statistics and machine learning toolbox in MATLAB. LOOCV was adopted to evaluate the classifier performance in order to reduce the effect of the limited size of the data set. The performance of the classifier was measured by conventional metrics ACC, SNS, SPC, and receiver operating characteristic (ROC) curve. ROC curve is represented by plotting the SNS versus the (1-SPC). Area Under the curve (AUC) is the area under the ROC curve that gives an idea about how much the model can distinguish between the two classes (Gosain & Sardana 2017). A high AUC indicates the better model in discrimination between two classes and vice versa. In addition, balanced accuracy was used to evaluate the performance of the classifier. It is especially preferred to use when the classes are imbalanced. The balanced accuracy is represented by the arithmetic mean of SNS and SPC.

4.7 Results

This section demonstrates the outcomes of employing the WPLI-based FBC and global graph attributes to find the biomarker using EEG at early infancy for predicting CP

and comparing the results with clinical outcomes at two years. The features vectors were constructed with two different dimensions using the five global graph attributes (transitivity, global efficiency, radius, diameter and characteristic path length) in order to find the best features in the practical identification of CP. At first, the features vector dimension contained each feature from each of the five frequency bands. Each feature from each band was evaluated separately to infer the association between the frequency bands and dysfunction in brain connectivity in neonates diagnosed later with CP. The second features vector dimension involved combining the five graph attributes to investigate whether they could distinguish between the two populations: infants who developed CP and those who have normal neuromotor at two years of age.

LOOCV evaluated the performance of the RUSBoost classifier. A summary of the highest classification performance in each frequency band is given in Table 4.2. The details of the results of all cases were provided in the Appendix A. As aforementioned in section 4.4, the EEG signal was decomposed into narrowband to be subjective for calculating the phase. The Hilbert transform was used to estimate the phase, which can apply to the broadband data. Still, the resulting analytical signal may be difficult to interpret because all the frequencies present in the EEG signal will contribute to the result. The frequencies with more power will contribute more to the resulting signal than those with less power. Thus, to interpret the results in a frequency-band-specific manner, it should filter the data into narrowband frequencies before applying the Hilbert transform (Cohen 2014).

TABLE 4.2: Best classification performance in each frequency bands using WPLI-based FBC.

Frequency band	Case	ACC	SNS	SPC	Balanced accuracy	AUC
Delta	All features	84.60%	67.00%	90.00%	78.50%	0.75
Theta	Radius	76.90%	83.00%	75.00%	79.00%	0.78
Alpha	Global efficiency	73.10%	50.00%	80.00%	65.00%	0.67
Beta	Global efficiency	73.10%	50.00%	80.00%	65.00%	0.51
Gamma	Diameter	50.00%	33.00%	55.00%	44.00%	0.34

It can be seen from Table 4.2 that the most promising result in terms of ACC (84.6%) and SPC (90%) was achieved in the delta band by using the combination of the five graph attributes. In contrast, the SNS did not exceed 67%. Interestingly, there was also a good result in the theta band; ACC was reached to 77%, SNS 83%, SPC 75%, balanced accuracy (79%), and AUC 0.78. Notably, in this case, the regular accuracy was not good enough, but the SNS and the balanced accuracy were good. Since the data set has an imbalanced distribution, accuracy might not be the optimal metric for measuring the performance. The metrics such as sensitivity and AUC could provide a better insight into the performance of a classifier because SNS measures the TPR representing the CP class that was a minority class.

4.8 Discussion

This part of the research carried out a qEEG analysis in a machine learning framework to identify clinical biomarkers that could distinguish between term-born infants with neonatal HIE who developed CP by two years and those with normal neuromotor development. Early identification of those at the highest risk of adverse outcomes enables targeted early interventions and provides family psychological and financial support. WPLI-based FBC of resting EEG signals and graph-theoretical features were explored to provide a multivariate investigation of the pathological abnormality of CP. These features have been used to train and test the RUSBoost classifier.

Significant classification results have been achieved using the combination of all five global graph features and radius calculated from the delta and theta bands, respectively. The highest performance of the classifier reached 84.6% as ACC by combining all features in the delta band. Furthermore, a promising SNS (83%) was obtained using the radius feature in the theta band. These results showed the correlation between alteration in global network topology in CP infant's brain and frequencies bands of the delta and theta. It seems possible that these results are due to the delta and theta bands considered to be factors of mental consciousness and brain damage (Kulak & Sobaniec 2005). This finding is consistent with Koeda & Takeshita (1998), who reported alteration in FBC featured by the intrahemispheric EEG coherence (HCoh). HCoh in the CP children group was significantly higher in the left hemisphere compared with the control in the delta, theta, and beta bands. Kułak et al. (2005) also found a higher interhemispheric coherence (ICoh) in CP children compared with the control group in the delta and theta bands, involving frontal and temporal regions. Kulak & Sobaniec (2005) also showed the significant increase in ICoh in CP children's theta and delta bands.

The methodology and findings of this investigation have been compared to the state-of-the-art research that used qEEG analysis to detect CP brain abnormalities. The summary of these comparisons is shown in Table 4.3, which confirms that it is the first time WPLI-based FBC characterised by graph attributes within the machine learning framework has been used to investigate and predict CP at early infancy. This framework provides advancement and proves the ability of qEEG to objectively and automatedly identify the brain deficits soon after birth. There have been multiple attempts to investigate the brain abnormality associated with CP from EEG, but previous studies never considered the earlier age. For example, Sajedi et al. (2013) studied the efficiency of a non-linear method (fractal dimension) in classification the children with CP from the neurotypical group and their results were significantly better than the results achieved in this chapter. A further strength of this study was laid in using WPL-based FBC, a non-linear method providing a reliable estimation of connectivity between different brain regions. As seen from Table 4.3, most of the reviewed studies used linear qEEG

methods mainly conceived by coherence-based FBC, spectral power and linear complexity. Coherence was the linear connectivity measure adopted in the CP classification; however, it has several limitations. It is a linear measure used with the assumption of signal stationarity, highly sensitive to volume conduction and limited temporal resolution. Compared to coherence, the WPLI is robust against the effect of volume conduction, and it is less vulnerable to other sorts of noise. Even though WPLI uses the imaginary component of coherence (ImCoh) for weighting the phase lag, which is a minor quantity of coherence, it has been shown that ImCoh can diminish the volume conduction effects. Only the real coherence part related quantities are affected by the conduction problem (Hamedi et al. 2016).

Findings of this study demonstrated that FBC features computed at the lower frequency range, mainly the delta and theta bands, could discriminate well between the infants with CP and normal ones. These features could be used as biomarkers for early prediction of CP, which enables the possibility of developing an appropriate intervention strategy to improve the outcomes. The study offers insights into the importance of the global graph parameters in capturing the characteristics of the infants' brain network deficits.

TABLE 4.3: Comparison of the qEEG state-of-the-art methods employed for CP classification.

Authors	Data set	Features	Evaluation method	Findings
Gao, Jia, Wu, Yu & Feng (2017)	Adolescent 14-22 years, CP (n=15) and normal (n=15)	**Microstate** to measure temporal correlation **Omega complexity** to assess spatial correlation	Statistical analysis	**Microstate:** Higher temporal complexity in CPs compared to control **Omega complexity:** Higher global omega complexity in CPs at the alpha band compared to control.
Gao, Wu, Feng & Jia (2017)	Adolescent 14-22 years, CP (n=15) and normal (n=15)	DFA to measure temporal correlation	Statistical analysis	The DFA exponents in alpha and beta bands were significantly attenuated in the CPs compared to controls.
Koeda & Takeshita (1998)	Children 7-15 years, CP (n=12) and normal (n=15)	Spectral power and coherence measures	Statistical analysis	**Spectral power:** No significant difference in spectral power. **Coherence**: Lower ICoh at the occipital region for alpha-band, higher ICoh at the frontal region for theta-band, and Hcoh at the left hemisphere for the delta, theta, and beta bands in the CPs compared to controls.
			Discriminant analysis classifier	Performance of 91.7% ACC, 100% SNS, 83.3% SPC have been reached using the statistically significant features.
Kułak et al. (2005)	Children 6-14 years, CP (n=12) and normal (n=21)	Spectral power and coherence measures	Statistical analysis	**Spectral power**: Significant differences between the CP and control over the left and right hemispheres for the delta, theta, alpha and beta bands. **Coherence**: lower ICoh at the temporal, parietal and occipital regions for the alpha band, lower ICoh at the frontal, central, parietal and occipital regions for the beta band, higher ICoh at the frontal and temporal regions for the theta and delta bands and higher HCoh at right hemisphere for the alpha band in CP patients compared to control.
Kulak & Sobaniec (2005)	Children 6-15 years, CP (n=26) and normal (n=28)	Spectral power and coherence measures	Statistical analysis	**Spectral power**: Significant differences between the CP and control over the left and right hemispheres for the delta, theta, alpha and beta bands. **Coherence**: Lower ICoh at the temporal, parietal and occipital regions for the alpha band in the CPs compared to controls,
Sajedi et al. (2013)	Children 4-14 years, CP(n=26) and normal(n=26)	Spectral power and fractal dimension to measure temporal complexity.	Statistical analysis	**Spectral power**: A higher delta and lower theta and alpha powers were found in CPs compared to controls. **Complexity**: A higher EEG complexity at the interior region for the range (1-30Hz) in CPs compared to controls.
			Enhanced probabilistic neural network classifier	Performance of 94.8% ACC, 92.5% SNS, 97.2% SPC have been reached using the statistically significant features.
Current study	Term-born infants with HIE, CP(n=6) and normal(n=20)	Graph-theoretical features of WPLI-based FBC	RUSBoost classifier	Performance of 84.6% ACC, 67% SNS, 90% SPC, and 0.75 AUC have been reached using the graph-theoretical features.

4.9 Conclusion

The analysis of resting-state FBC in the machine learning framework successfully predicted CP at two years of age from infants with neonatal HIE. The results of this prospective study revealed that the WPLI characterised by the combination of global complex network metrics achieved a good classification performance using RUSBoost classifier reached 84.6% ACC, 67% SNS, 90% SPC and 78.5% balanced accuracy in the delta band. Furthermore, the topological difference in the brain network—particularly in the radius feature—between infants with CP and their neurotypical peers was observed in the theta band with high SNS up to 83% and 79% balanced accuracy. These results indicated that the network attributes could serve as early biomarkers of CP. This part of the study can be viewed as a promising attempt towards the feasibility of qEEG in predicting the CP's brain deficits.

Chapter 5

Investigation of Using Noise-Assistant Multivariate Empirical Mode Decomposition for Quantifying Phase Synchronisation

5.1 Introduction

Chapter 4 described the proposed analysis of phase-based FBC for predicting CP in term-born infants at two years of age. Phase synchronisation methods are mainly based on estimating the phase to quantify the relationship between two time-series. Extracting the phase is considered a crucial step in calculating such phase-based FBC methods. In order to get the phase's intending physical interpretation, it is necessary to extract the phase from the narrowband component (Farahmand et al. 2018). Thus, some form of prefiltering into narrowband is required to decompose EEG signal, which is complex and composed of multiple frequency oscillators.

Traditionally, the DBP filter has been utilised to decompose the broadband signal into discrete predefined frequency ranges. This technique is similar to the methods used in Chapter 4. Even though this approach is convenient and widely used in EEG analysis, it has constraints—such as requiring prior information about filter cut-off frequency. This assumption may raise an issue where the ranges of neural oscillations of interest may vary among subjects, specifically between infants and older individuals (Saby & Marshall 2012). For example, the filter cut-off frequency in the alpha band was chosen to be from 8-12 Hz in (David et al. 2004), from 8-13 Hz in (Breakspear et al. 2004), from 8-14 Hz in (Babiloni et al. 2006), or subdivided into lower-alpha 6-10 Hz and upper alpha 10-14 Hz ranges in (Stam et al. 2003). Furthermore, some studies have shown

that the boundaries of corresponding frequency band ranges could be lower in infants (Saby & Marshall 2012). In addition, using a priori basis is critical for both non-linear and non-stationary data, as one cannot expect a predetermined basis to fit all the non-linear and non-stationary dynamics (Huang et al. 1998).

Thus, in response to these variations and constraints, this study proposes an adaptive analysis approach of phase synchronisation based on EMD algorithms (Huang et al. 1998) precisely NA-MEMD (ur Rehman & Mandic 2011). NA-MEMD is a technique that adaptively decomposes the EEG signals into finite oscillation scales at a time-domain called intrinsic mode functions (IMFs) (Zheng et al. 2014). The frequency range of each scale is varied according to the oscillations inherited in the signal. A prominent advantage of EMD-based algorithms over other decomposition methods (e.g., DBP filter, wavelet, and STFT) is that it does not require a priori selection of the filter cut-offs frequency.

This part of the study aims to examine the effectiveness of NA-MEMD in decomposing EEG signals into their intrinsic components and compare its result in CP prediction with traditional DBP filter to find the best pre-analysis method of phase-based FBC. In this approach, the NA-MEMD is initially applied to decompose EEG signals into narrowband components. Then the WPLI-based FBC is calculated from each intrinsic component, and the graph attributes are computed from each connectivity network. The statistical analysis is then used to evaluate each graph-theoretical feature's capability to discriminate between two groups (CP and normal). This evaluation is carried out for each IMF separately, and the features are used to train and test the RUSBoost classifier. A schematic diagram of the proposed analysis is depicted in Figure 5.1. The results from this chapter have been published in (Bakheet et al. 2021).

The remaining parts of the chapter include section 5.2 which describes the NA-MEMD decomposition method. Features extraction scheme based on NA-MEMD is illustrated in section 5.3. The statistical analysis is described in section 5.4. The results are analysed in section 5.5 and discussed in detail in section 5.6. The conclusion of the chapter is provided in section 5.7.

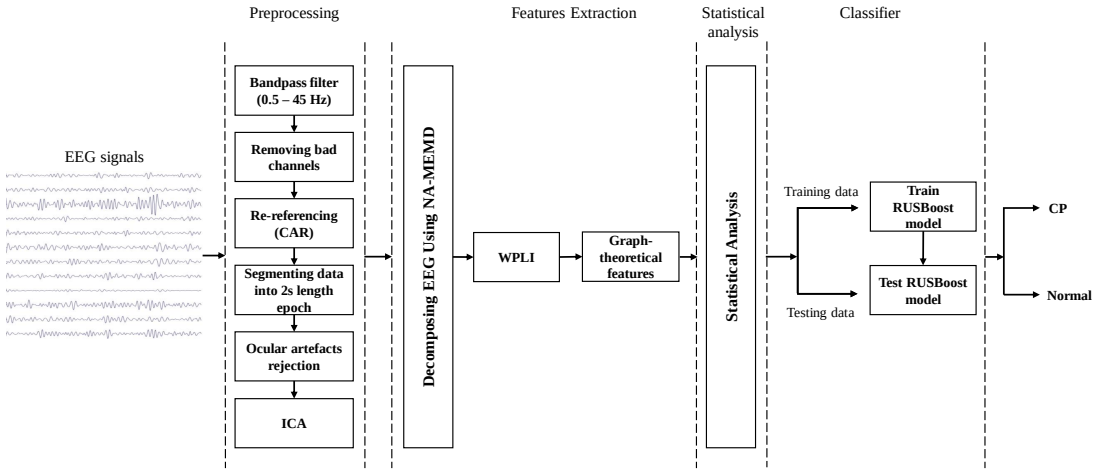

FIGURE 5.1: Schematic outline of the proposed NA-MEMD-based analysis for predicting CP at two years of age. Each time-series recording from each electrode was preprocessed by several preprocessing techniques: filtering, removing bad channels, re-referencing, segmentation and artefacts rejection. Then, the EEG signals were adaptively decomposed into their inherited intrinsic components. After that, FBC was calculated using WPLI, and then the graph-theoretical features were extracted. The statistical analysis was performed to evaluate each graph-theoretical feature's capability in discriminating between two groups (CP and normal). Then extracted features were fed into the machine learning algorithm to perform binary classification of an infant either into CP group or normal.

5.2 NA-MEMD-Based EEG Decomposing Analysis

NA-MEMD is an extended version of EMD, and, in this study, it is used to adaptively decompose the EEG spectra into its intrinsic components. Unlike other traditional decomposing methods such as short-time Fourier (Gabor 1946), wavelet transforms (Mallat 1989) and DBP filter, EMD-based methods do not require a predefined basis of the signals. Instead, they are data-driven time-frequency techniques that adaptively extract the embedded oscillations from the data without determining specific frequency ranges.

Among the available decomposition methods, the well-established wavelet analysis is known as one of the best non-stationary data analysis methods (Huang et al. 1998). However, the predefined basis of, for example, the Morlet wavelet (the most commonly used wavelet in general and in EEG analysis leads to different issues (Sweeney-Reed & Nasuto 2007). First, one cannot guarantee that the predetermined window size of the wavelet will coincide with a stationary period. Good localisation of the low-frequency

oscillations needs a long-time window to identify them and thus a longer period for which signal should be stationary. On the other hand, selecting a small window may lead to missing potential biomarkers in the lower frequency ranges. Such a situation is known as the uncertainty principle, produced from the trade-off between frequency and time. Second, the prior selection of wavelet parameters cannot be expected to fit all the non-linear and non-stationary phenomena. Thus, it could induce spurious harmonic components to spectrally represent the signals, causing energy spreading and leading to faulty results.

EMD-based methods satisfy the necessary conditions for the decomposition to represent a non-linear and non-stationary time series, particularly locality and adaptivity conditions. The locality is most crucial for non-stationarity, in which all events have to be identified by the time of their occurrences. Thus, both the amplitude (or energy) and the frequency are required to be functions of time (Huang et al. 1998). The adaptivity is important for both non-linear and non-stationary data in which the decomposition is adapted to the local variations of the data and hence can fully account for the underlying dynamics of the signals (Huang et al. 1998). Different studies proved that the local and adaptive nature of the decomposition using EMD-based methods is shown to improve time and frequency precision compared to the Morlet wavelet (Huang et al. 1998, Sweeney-Reed & Nasuto 2007).

Applying EMD in analysing EEG signals has attracted attention recently due to its efficiency in extracting the oscillation components from non-linear and non-stationary signals. However, EMD has two main limitations, specifically in analysing multivariate data like EEG, called mode misalignment problems and mode mixing (ur Rehman & Mandic 2011). Mode misalignment refers to the situation that the generating number of IMFs is non-identical between channels, whereas the mode mixing indicates the circumstance when the single IMF contains multi-frequency oscillations. Multivariate empirical mode decomposition (MEMD) algorithm was later proposed to solve the mode-alignment problem by projecting the n-dimensional input signals into different directions in n-dimensional space (ur Rehman et al. 2010). NA-MEMD is a recent version of EMD developed to settle the remaining problem, mode-mixing, by adding white Gaussian noise to n-dimensional channels. The resulting multivariate signals (EEG signals+ white Gaussian noise) are then applied to the MEMD algorithm.

Practically, NA-MEMD decomposes the time-series from high to low-frequency components (IMFs) through the Sifting process in an iterative fashion as following steps:

1. Produce the m-dimensional uncorrelated white Gaussian noise sources with the same length as the input signals.

2. Combine the multivariate input signals with generated multivariate noise in step 1. This yields new multivariate signals with a total dimension $(w = n + m)$, which are then applied to the MEMD algorithm.

3. In the MEMD algorithm, w-dimensional input signals are required to be projected with different directions into w-dimensional space. The procedure of MEMD starts with choosing a proper set of points for sampling on a $(w - 1)$ sphere.

4. Calculate a projection, denoted by $\left\{p^{\theta_k(\mathrm{t})}\right\}_{t=1}^{T}$, of the input signal $\{v(t)\}_{t=1}^{T}$ along the direction vector $\mathbf{X}^{\theta_k}$, for all k (where K is the whole set of direction vectors), giving $\left\{p^{\theta_k(\mathrm{t})}\right\}_{k=1}^{K}$ as the set of projections.

5. Find the time instants $\left\{t_i^{\theta_k}\right\}_{k=1}^{K}$ corresponding to the maxima of the set of projected signals $\left\{p^{\theta_k(t)}\right\}_{k=1}^{K}$, where i indicates the position of maxima point.

6. Get the multivariate envelope curves $\left\{\mathbf{e}^{\theta_k(t)}\right\}_{k=1}^{K}$ by interpolating $\left[t_i^{\theta_k}, v\left(t_i^{\theta_k}\right)\right]$.

7. The mean $m(t)$ of the envelope curves is calculated as $\mathbf{m}(t) = \frac{1}{K}\sum_{k=1}^{K}\mathbf{e}^{\theta_k(t)}$, for all set of K direction vectors.

8. Extract the detail $d(t)$ using $d(t) = x(t) - m(t)$. If $d(t)$ satisfies the stoppage criteria which described in (Huang et al. 1998), apply the above procedure to $x(t) - d(t)$, otherwise apply it to $d(t)$. This process is repeated until all IMFs are extracted and only a residue is left; where the residue corresponds to a signal whose projections do not contain enough extrema to formulate a meaningful multivariate envelope (ur Rehman & Mandic 2011).

9. From the resulting IMFs, only IMFs related to the n-channel input signal are selected, and those related to noise are discarded.

At the end of the NA-MEMD procedure, the input signal can be mathematically represented by the following equation:

$x(t) = \sum_{i=1}^{N} d_i(t) + r_N(t)$

where $x(t)$ is the input signal, $d_i(t)$ is IMF, $r_N(t)$ is residue, N represents the total number of IMFs, and t refers to time.

5.3 Features Extraction based on NA-MEMD

The features were extracted from the infants' data set described in section 4.2. The data set was preprocessed with the same procedure illustrated in section 4.3. The scheme

of features extraction was divided into two parts. The first phase focused on decomposing EEG signals into their intrinsic components using NA-MEMD. The second part involved extracting the fundamental class of features, namely global graph attributes.

- **Step1:** NA-MEMD analysis

1. A multivariate signal was constructed by combining the data points from all infants for each channel separately, yielding twelve different matrices (i.e., one matrix per channel). Each of them has the dimensions of $N_s \times N_t \times N_e$, where N_s denotes the number of subjects (which is 26), N_t indicates the number of temporal samples (which is 1024), and N_e is the number of epochs of each subject (which is 30).
2. Before decomposing the twelve multivariate signals by the NA-MEMD algorithm, each matrix was set up in a two-dimensional time-series of $[N_s \times N_e] \times N_t$ dimensions. Therefore, the alignment among all IMFs across infants and over epochs was ascertained. A similar approach has been used previously by Hu & Liang (2011).
3. The resulting IMF components after the decomposition process was slightly varied between channels. Since the EEG channel that yields the lowest number of IMFs upon decomposition gives ten modes, the first ten IMFs of each channel were considered for feature extraction. Figure 5.2 depicts the sample of extracted IMFs from a channel that gave ten IMFs.

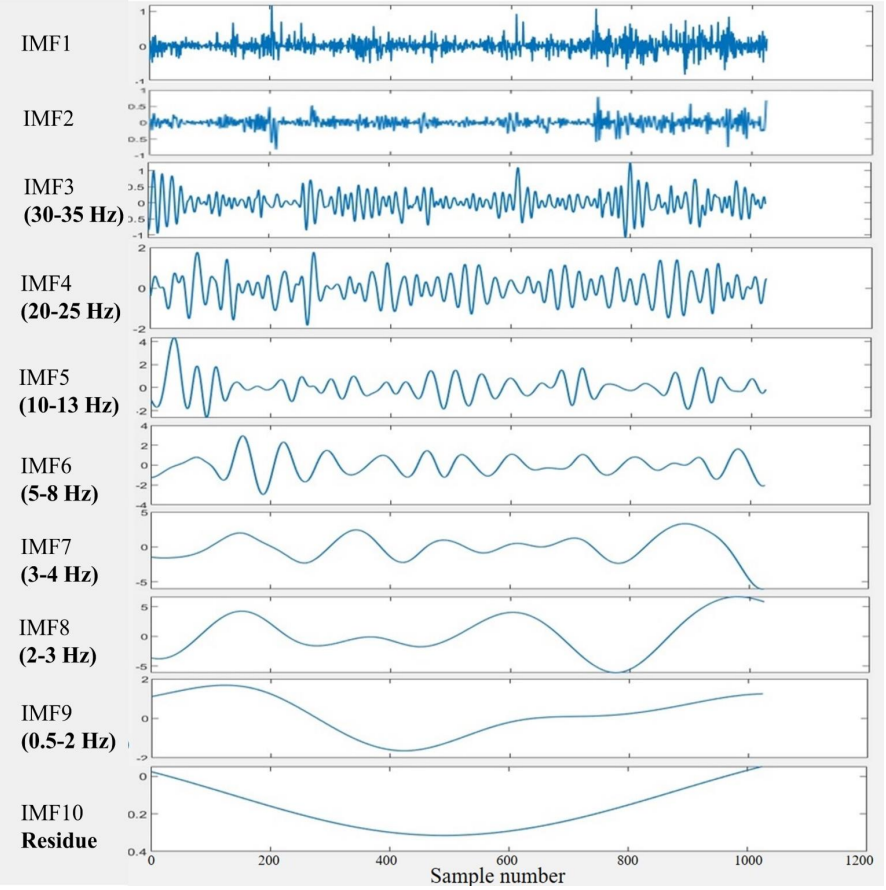

FIGURE 5.2: An example of a set of IMFs resulted from the NA-MEMD decomposition of the two-second EEG signal. IMF1 to IMF2 considered noisy, and IMF10 represented the residue mode. IMF3 to IMF6 frequencies belong to the gamma, beta, alpha and theta bands, respectively, while IMF7, IMF8 and IMF9 all belong to the delta brain wave.

4. The frequencies of each IMF were then acquired by the fast Fourier transform (FFT), and it was found that IMF1 and IMF2 were noisy because they contained different oscillatory components. Thus, these modes were excluded from further analysis. IMF10 was also ignored as it represented the residue mode of some EEG channels, which might give unreal information about the signal. The scales of the remaining IMFs were localised approximately around the following ranges: IMF3 (30 - 35 Hz), IMF4 (20 - 25 Hz), IMF5 (10 - 13 Hz), IMF6 (5 - 8 Hz), IMF7 (3 - 4 Hz), IMF8 (2 - 3 Hz), IMF9 (0.5 - 2 Hz).

- **Step2:** Features extraction

1. Before extracting the five graph-theoretical features, each IMF frequency scale alignment among channels was checked. Following that, for each IMF, the instantaneous phases were calculated using the Hilbert transform.

2. WPLI connectivity matrix was calculated using Equation 4.1 between twelve channels for each IMF and each epoch.
3. The generating WPLI matrices were averaged over the epochs, yielding one averaged connectivity matrix for each IMF.
4. Each connectivity matrix was transformed into a complex connectivity network and the graph-theoretical parameters were estimated to quantify its properties. As a result, the total number of features in each IMF was five, namely transitivity, global efficiency, radius, diameter, and characteristic path length. The extracted graph parameters were then used to train and test the model.

5.4 Statistical Analysis

The statistical test was used to evaluate the discriminatory capability of the graph-theoretical features in differentiating between the two groups (infants who developed CP and those who did not). The evaluation was carried out for each feature calculated from each IMF separately. Kruskal–Wallis (Theodorsson-Norheim 1986) is a non-parametric test computing the medians of each class in each feature to determine if the samples have the same distribution. It was selected to use in this research due to the group samples strongly deviated from the normal because the sample size is small and unequal (Hoffman 2019). Kruskal–Wallis was conducted to test the null hypothesis for each feature, stating that samples of the two classes (CP and normal) come from the same distribution. In general, the difference between groups is statistically significant when the p-value falls below a threshold known as the level of significance (α), usually equal to 0.05. Hence, a lower p-value (below the significance level) rejects the null hypothesis and indicates a significant difference between the two classes. The test was carried out using the MATLAB statistics toolbox.

Benjamini–Hochberg method (Benjamini & Hochberg 1995) was employed to adjust the significant threshold of the p-value. Such adjustments are required if several independent tests are simultaneously conducted (known as multiple comparisons). Benjamini–Hochberg is introduced to control the false discovery rate that is less stringent with the increased gain in power. It is used alternative to the Bonferroni correction (which is control family-wise error in a rigorous criterion and compute the adjusted P values by directly multiplying the number of simultaneously tested hypotheses) for a low proportion of false-positive instead of guarding against making any false positive conclusion (Chen et al. 2017). The index of the corrected p-value was calculated as follows:

$$k = max\{i : p_{(i)} \leq \frac{i}{m}q\} \tag{5.1}$$

where k is the index of the significant p-value, i is the rank of p-value, m is the total number of test, and q is the pre-specific upper bound of false discovery rate (herein $q = 0.05$).

Practically, the Kruskal-Wallis test was used to assess the discriminant capabilities of the five graph-theoretical features computed from each IMF (42 p-values: 6 features × 7 scales). By utilising the false discovery rate correction, the p-value was corrected to 0.02.

5.5 Results

This section outlines the results of employing the NA-MEMD to decompose the spectral components from EEG signals and its application in the early CP prediction among high-risk infants born with HIE. The effectiveness of the five graph attributes (transitivity, global efficiency, radius, diameter, and characteristic path length) and their combination in discriminating between two populations (infants who developed CP at two years and the normal ones) were evaluated by the Kruskal-Wallis test and the RUSBoost classifier. Table 5.1 summarises the results of the Kruskal-Wallis test for the set of proposed features. The statistical significant features (have lower p-value) are shown in boldface. It was seen that the difference between the two groups is particularly distinct using the diameter feature computed from IMF5. The boxplot presented in Figure 5.3 indicates that the diameter of the CP group was significantly higher than the normal one.

TABLE 5.1: P-values of the graph-theoretical features. Graph feature that is statistically significant is indicated in boldface.

	Transitivity	Global efficiency	Radius	Diameter	Characteristic path length	All features
IMF3	0.39	0.43	0.5	0.3	0.39	0.94
IMF4	0.95	0.95	0.5	0.33	0.9	0.86
IMF5	0.63	0.54	0.67	**0.02**	0.81	0.71
IMF6	0.47	0.47	0.76	0.25	0.67	0.8
IMF 7	0.25	0.3	0.72	0.95	0.36	0.83
IMF8	0.58	0.58	1	0.39	0.62	0.99
IMF9	0.22	0.25	0.25	0.36	0.25	0.99

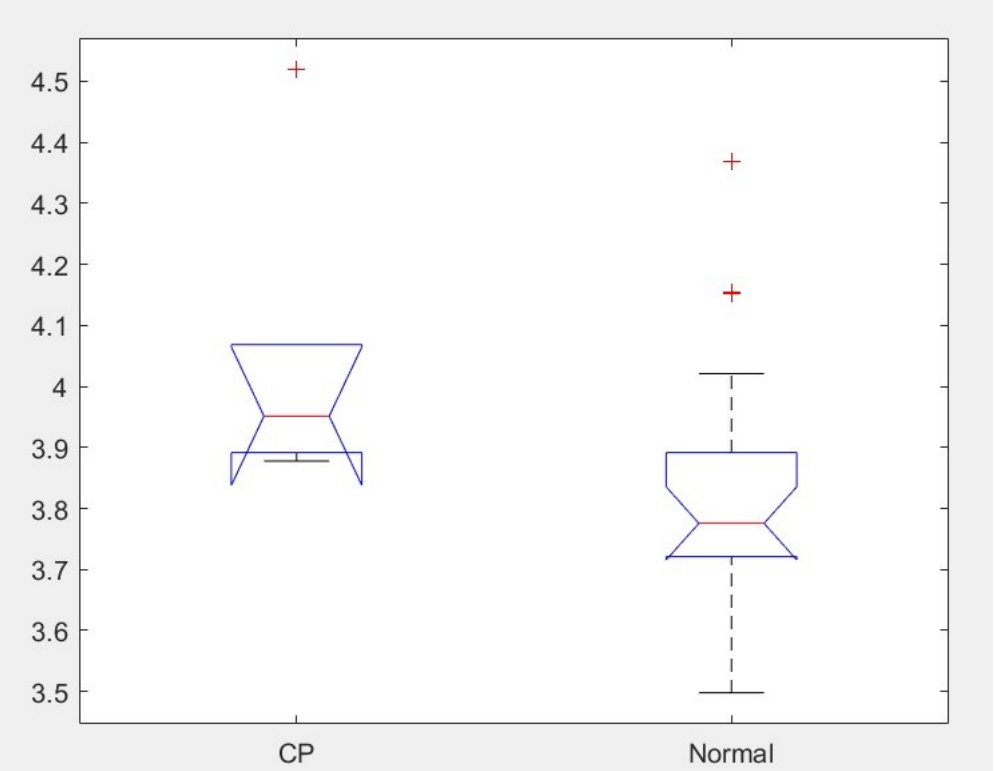

FIGURE 5.3: Box plot of the distribution of the diameter feature extracted from IMF5 component of CP and normal infants. The diameter values of the CP show higher values compared to the normal subjects.

To prevent overfitting, the LOOCV was used to evaluate the performance of the RUSBoost classifier. The highest classification performance for each IMF are summarised in Table 5.2. The detailed results of all cases were provided in the Appendix B. It can be seen from the data in this table that the best classification performance was achieved using transitivity and characteristic path length features computed from the IMF8 (2 - 4 Hz) corresponding to the delta band. The highest classification rate reached 84.6%, SNS (83%), SPC (85%), balanced accuracy (84%), and AUC (0.85) using the transitivity feature. The same ACC was obtained using the characteristic path length attribute but with 67% SNS, 90% SPC, 78.5% balanced accuracy, and 0.81 AUC. Good classification performance was also observed using the global efficiency feature calculated from IMF8, reaching 80.8% ACC, 67% SNS, 85% SPC, 76% balanced accuracy, and 0.9 AUC. Similar classification performance was obtained from IMF5, IMF6 and IMF7 corresponding to the alpha, theta and delta bands, respectively. Particularly, these results were achieved using the transitivity features calculated from IMF7 and the diameter attribute computed from IMF6 and IMF7.

TABLE 5.2: Highest classification performance in each IMF component using WPLI-based FBC.

IMF	Feature	ACC	SNS	SPC	Balanced accuracy	AUC
IMF3	Charactristic path length	69.20%	50.00%	75.00%	62.5%	0.65
IMF4	Global efficiency	53.80%	33.00%	60.00%	46.5%	0.22
	Radius	53.80%	50.00%	55.00%	52.5%	0.74
	Characteristic path length	53.80%	33.00%	60.00%	46.5%	0.27
IMF5	Diameter	80.80%	67.00%	85.00%	76.00%	0.72
IMF6	Diameter	80.80%	67.00%	85.00%	76%	0.79
IMF7	Transitivity	80.80%	67.00%	85.00%	76%	0.78
IMF8	Transitivity	84.60%	83.00%	85.00%	84.00%	0.85
	Global efficiency	80.80%	67.00%	85.00%	76%	0.90
	Charactristic path length	84.60%	67.00%	90.00%	78.5%	0.81
IMF9	Transitivity	69.20%	50.00%	75.00%	62.5%	0.49
	Charactristic path length	69.20%	33.00%	80.00%	56.5%	0.44

5.6 Discussion

This study aimed to develop a non-linear analytical methodology using NA-MEMD to quantify the phase synchronisation among neuronal populations in two groups who developed CP at two years and the normal neuromotor group. The networks synchrony were compared between two groups within different narrowband frequency ranges to predict CP early. Mainly, this study employed the global graph attributes derived from the WPLI as features for the RUSBoost classifier after preprocessing with NA-MEMD. The main findings of this study indicated that the best discrimination capability of the graph features was achieved using the diameter attribute. The statistical test showed an increase in the diameter feature estimated from IMF5 of the CP infants compared to the controls. This result implies global hypoconnectivity, indicating that the CP's brain network is less integrated, and accordingly, the information transfer across the network is less efficient. This finding is consistent with the previous studies that found hypoconnectivity between the right and left hemispheres in CP patients using the coherence-based measures (Koeda & Takeshita 1998, Kułak et al. 2005, Kulak & Sobaniec 2005).

The statistical test is usually adopted to aid in comparing different features and choosing the significant one. However, the data set under investigation has a limited and imbalanced number of samples, which may have affected the power of the statistical

test. Thus, this study investigated the capability of each graph feature and their combinations in classifying between two groups using the RUSBoost classifier to obtain additional evidence regarding the more informative features in discriminating between CP and controls. The best classification performance was obtained using diameter, transitivity, characteristic path length and global efficiency, indicating the existence of alteration in the brain network between CP and normal neuromotor groups. This disruption was featured by the network integration and network efficiency of processing the local information. Network integration was characterised by the diameter, global efficiency and characteristic path length, while the local network efficiency was captured by the transitivity.

Association between frequency range and brain network dysfunctions in infants who developed CP was observed in the IMF5, IMF6, IMF7, and IMF8. The features calculated from those components were successfully differentiated between infants who developed CP and the normal groups. The traditional brain waves corresponding to those components were alpha (IMF5), theta (IMF6) and delta (IMF7 and IMF8) bands. The findings seem to be consistent with other studies that reported disruption of CP patient's brain connectivity in the alpha band (Gao, Wu, Feng & Jia 2017, Koeda & Takeshita 1998, Kułak et al. 2005, Kulak & Sobaniec 2005), theta band (Koeda & Takeshita 1998, Kułak et al. 2005, Kulak & Sobaniec 2005) and delta band (Koeda & Takeshita 1998, Kułak et al. 2005, Kulak & Sobaniec 2005). This finding also supports the results of Chapter 4 that found the difference between CP and control group in the delta and theta bands using a traditional BPF and WPLI based FBC.

In contrast to DBP-based analysis, the NA-MEMD-based analysis showed the difference between two classes in the alpha band range. A possible explanation for this discrepancy might be that the NA-MEMD produce narrower frequency ranges, based on the oscillations inherited in the signal, than the DBP filters; hence, it is possible to calculate the WPLI more accurately. On the contrary, although the DBP is a simple digital signal processing algorithm, its results critically depend on the predefined frequency range (Cho et al. 2017). Prior selection of frequency ranges may result in potentially informative brain waves being missed, specifically in the case of infants, due to the well-known variability between them and older individuals in the neural oscillations of interest. Moreover, the predefined basis may not be able to fit all the non-linear and non-stationary phenomena (Huang et al. 1998). This constraint has been settled in the proposed approach using the NA-MEMD method, which decomposes the signals adaptively. Thus, with this method, all meaningful brain dynamics were ascertained to be included in the analysis, and no misleading energy-frequency distribution will result from analysing the non-stationary and non-linear signals. Nevertheless, the advantages of the EMD-based methods have a price of being empirical, not theoretically,

defined. In addition, the NA-MEMD method has a very high computational complexity having a subspace of multivariate independent white noise equal to the original multivariate signal.

On the other hand, the classification performance of DBP-based analysis is relatively lower than NA-MEMD-based analysis except for the beta band. The delta band's best performance using DBP filter was 84.6% ACC, 67% SNS, 90% SPC, 78.5% balanced accuracy, and 0.75 AUC, while the corresponding performance using NA-MEMD was 84.6% ACC, 83% SNS, 85% SPC, 84% balanced accuracy, and 0.85 AUC. It can be seen from this result that the NA-MEMD-based analysis achieved higher performance in terms of SNS, SPC, balanced accuracy, and AUC. The best performance obtained in the theta band using NA-MEMD-based analysis was reached to 80.8% ACC, 67% SNS, 85% SPC, 76% balanced accuracy, and 0.79 AUC compared with 76.9% ACC 83% SNS, 75% SPC, 79% balanced accuracy, and 0.78 AUC achieved using DBP-based analysis. On the other hand, in the alpha band using the NA-MEMD, the best accuracy reached 80.8% ACC, 67% SNS, 85% SPC, and 0.79 AUC but did not exceed 73.1% ACC, 50% SNS, 80% SPC, 65% balanced accuracy, and 0.67 AUC using the DBP filter approach.

In summary, the findings of the study suggested that the NA-MEMD-based analysis used for quantifying phase synchronisation could significantly discriminate between the CP and normal infants using transitivity, global efficiency and characteristic path length in delta band component and diameter in the theta and alpha bands. Furthermore, the results showed that, in general, the NA-MEMD-based analysis gave the high classification performance (except for the beta band)—in the prediction of CP— slightly outperformed the DBP-based analysis. However, due to the data set under investigation has small size and imbalanced, the results of this study are inclusive and need to be validated in large trials with a statistically significant population.

5.7 Conclusion

This study used a novel methodology merging the adaptive decomposition algorithm (NA-MEMD), WPLI-based FBC, graph-theoretical features and machine learning algorithm to predict infants at high-risk to develop CP at two years of age from neonatal EEG. The performance of NA-MEMD-based analysis was compared with DBP-based analysis. The results suggested that NA-MEMD-based analysis could successfully classify two groups with significant performance 84.6% ACC, 83% SNS, 85% SPC, and 0.85 AUC in the delta band using transitivity. The same classification accuracy was achieved using characteristic path length but with with 67% SNS, 90% SPC, 78.5% balanced accuracy, and 0.81 AUC. In addition, good performance was obtained in the theta and

alpha bands. The study postulates that the merging analysis approach of the FBC, particularly WPLI and global graph theory attributes quantified from NA-MEMD could be used to capture the brain deficit related to CP.

Chapter 6

Prediction of Cognitive Outcome in Infants with Hypoxic-Ischaemic Encephalopathy

6.1 Introduction

In the Chapter 4 and 5, the proposed analysis to predict the CP from EEG recording in the first week after birth by comparing the EEG features with clinical outcome at two years was validated. The next stage investigates the potential benefits of using the previous framework to predict the later cognitive outcome at two years of age. This chapter explores the effectiveness of the phase-based FBC estimated by WPLI and graph metrics within the regression-based framework to predict the cognitive outcome in term-born infants with neonatal HIE. The graph-theoretical features derived from WPLI are utilised to determine the association between neonatal EEG and the individual cognitive profiles (completed in a follow-up visit at 24 months of age). As described in Chapters 4 and 5, it is necessary to decompose EEG signals into the narrowband components to properly estimate the phase. Thus, based on the findings of Chapter 5, the NA-MEMD method is adopted in this study to decompose the EEG signals into their intrinsic components. Correlation analysis is performed to ascertain the statistical significance of graph-theoretical parameters of WPLI in finding the association with cognitive scores. Then, the significant features are used to train and test the tree ensemble regression models: boosting and bagging to evaluate their predictability of later cognitive development. A schematic outline of the proposed analysis is depicted in Figure 6.1.

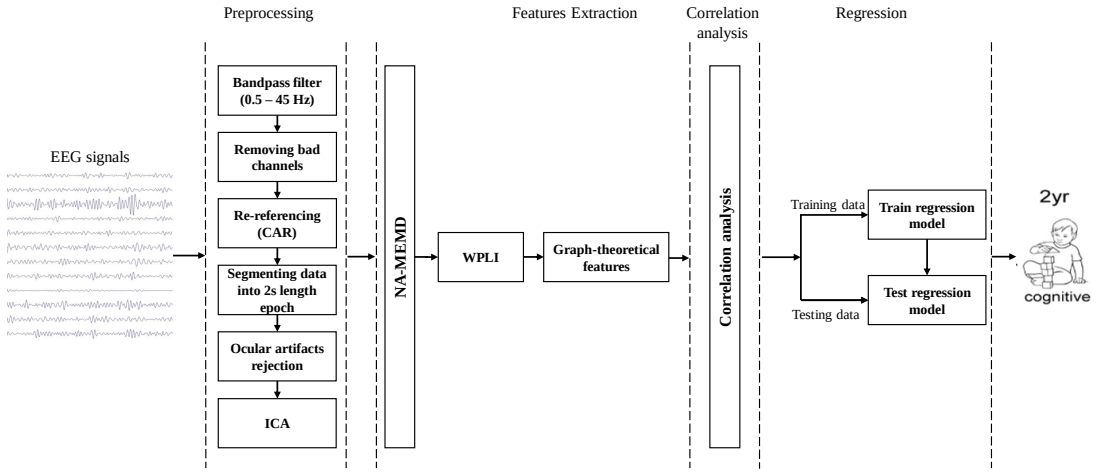

FIGURE 6.1: Schematic outline of proposed analysis for predicting cognitive outcomes at two years of age. Each time-series recording from each electrode was preprocessed by several preprocessing techniques: filtering, removing bad channels, re-referencing, segmentation and artefacts rejection. Then, the EEG signals were adaptively decomposed into their inherited intrinsic components. After that, FBC was calculated using WPLI, and then the graph-theoretical features were extracted. The correlation analysis was used to evaluate the statistical significance of graph-theoretical parameters of WPLI in finding the association with cognitive scores. Then extracted features were fed into the regression models to assess their predictability of later cognitive development.

The remainder of the chapter is structured as follows: brief details about the participants and the recruitment process, followed by a description of the experimental set-up are provided in section 6.2. The procedure of extracting the desired features is illustrated in section 6.3. Correlation analysis and regression models are depicted in section 6.4 and 6.5, respectively. Sections 6.6 and section 6.7 present the results and the discussions of this study, followed by the conclusion in the section 6.8.

6.2 Participants and Experimental Set-up

Thirty term-born infants with HIE treated with hypothermia were recruited into this study. EEG data were recorded on the neonatal intensive care unit within the first week after birth for twenty minutes during resting-state condition with eyes closed by either a Nihon Kohden (sampling frequency 512 Hz, high-pass filter 0.016 Hz, the low-pass filter 300 Hz) and XLTEK (sampling frequency 512 Hz, high-pass filter 0.1 Hz, the low-pass filter 70 Hz) clinical video-EEG system. Nineteen electrodes (C3, C4, CZ, F3, F4, F7, F8, FZ, FP1, FP2, O1, O2, P3, P4, PZ, T3, T4, T5 and T6) placed according to the 10-20 international system were used. Movement or electrode artefact affected the EEG in a substantial proportion of the cases. A consultant neurophysiologist visually

TABLE 6.1: Clinical characteristics at twenty-four months of age of thirty neonates born with HIE. The cognitive outcome of each infant was evaluated using BSITD-III. Ten infants were discharged and did not complete the follow-up assessment.

Subject #	Cognitive scores at age 24 months
subj_1	145
subj_2	Incomplete follow-up
subj_3	100
subj_4	Incomplete follow-up
subj_5	Incomplete follow-up
subj_6	Incomplete follow-up
subj_7	120
subj_8	95
subj_9	95
subj_10	140
subj_11	100
subj_12	120
subj_13	105
subj_14	Incomplete follow-up
subj_15	105
subj_16	130
subj_17	110
subj_18	140
subj_19	incomplete follow-up
subj_20	74
subj_21	105
subj_22	100
subj_23	Incomplete follow-up
subj_24	100
subj_25	125
subj_26	Incomplete follow-up
subj_27	Incomplete follow-up
subj_28	95
subj_29	Incomplete follow-up
subj_30	90

inspected all recorded EEGs. The first period in the EEG that was long enough without any clear significant artefact was always selected (the average length of the clips is approximately two minutes).

A neuropsychological follow-up assessment was conducted at twenty-four months of age using the Bayley Scales of Infant and Toddler Development III (BSITD-III) was used for this purpose. The BSITD-III assesses the three major domains: cognitive, language and motor. The cognitive scale evaluates the cognitive functions on the basis of nonverbal activities, including object relatedness, memory, problem solving, and manipulation (Ouyang et al. 2020). The language scale estimates both receptive and expressive communication. The motor scale assesses the fine motor (e.g. grasping, motor planning and speed) and gross motor (e.g., sitting, standing and balance). Among the thirty infants in this prospective study, twenty infants completed the follow-up assessment when they reached two years of age, as shown in Table 6.1. The BSITD-III cognitive scores from those twenty infants ranged from 74 to 145. The infants with a cognitive score of < 80 were considered to have cognitive decline.

6.3 A Strategic Framework for Predicting Cognitive Score

EEG signals were initially preprocessed using the same techniques described in section 4.3 to improve the quality of EEG signals. The NA-MEMD algorithm was then employed in the same procedure as illustrated in section 5.2 to decompose EEG signals into narrowband components. Since the EEG channel that yields the lowest number of IMFs upon decomposition gives ten modes, the first ten IMFs of each channel were considered for feature extraction. The FFT was used to determine the frequencies of each IMF, and it was found that IMF1 to IMF3 are noisy and contain different oscillatory components. Thus, these modes were excluded from further analysis. IMF10 was also not considered as it represented the residue mode, which might give unreal information about the signal. The scales of the remaining IMFs were localised approximately around the following ranges: IMF4 (15 - 26Hz), IMF5 (10 - 13Hz), IMF6 (6 - 8Hz), IMF7 (3 - 4Hz), IMF8 (1.5 - 3Hz), IMF9 (0.5 - 1.5Hz). Figure 6.2 depicts the sample of extracted IMFs from a channel that gave ten IMFs.

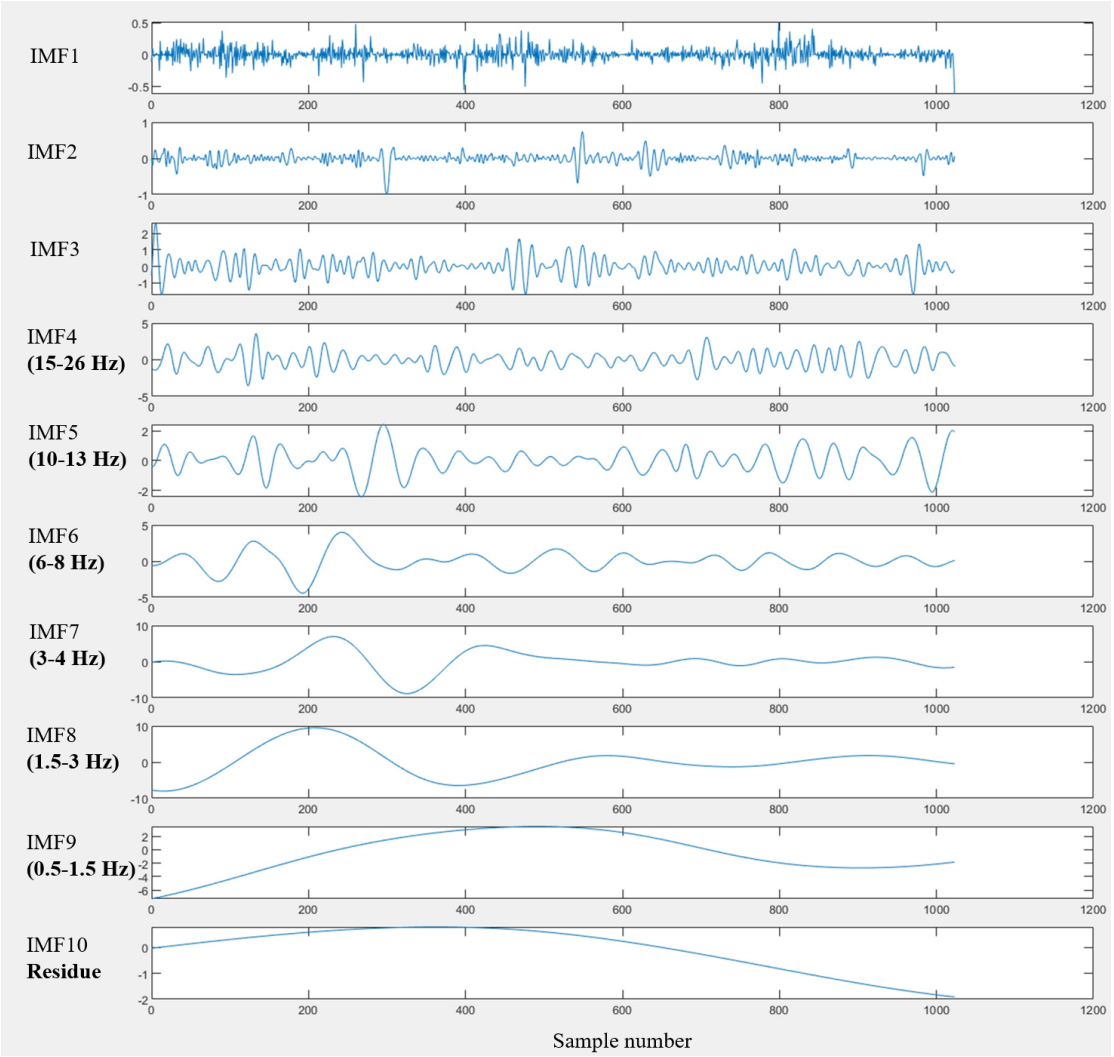

FIGURE 6.2: An example of a set of IMFs resulted from the NA-MEMD decomposition of the 2 s EEG signal. IMF1 to IMF3 considered noisy, and IMF10 represented the residue mode. IMF4 to IMF6 were localized in the beta, alpha, and theta bands, respectively, while IMF7 to IMF9 belonged to the delta band.

Before extracting the five graph-theoretical features, each IMF frequency scale alignment among channels was checked out. The WPLI connectivity matrix was then calculated between twelve channels for each IMF and each epoch. The generating WPLI matrices were averaged over the epochs, yielding one averaged connectivity matrix for each IMF. Then, each connectivity matrix was transformed into a complex connectivity network, and the graph-theoretical parameters were estimated to quantify its properties. The extracted graph parameters were then used to train and test the regression models.

6.4 Statistical Analysis: Correlation Coefficient

Correlation analysis was used to statistically measure the relationship between the predictor variables (EEG features represented by graph-theoretical parameters) and the cognitive scores. Pearson correlation coefficient, denoted by r, was adopted herein for this purpose. Theoretically, the value of r falls in the interval between +1 and -1, with 0 indicates no linear relationship, +1 refers to a perfect positive correlation, i.e., when one variable increases, the other increases too, while -1 indicates a perfect negative correlation, i.e., when one variable increases, the other decreases. In order to identify the high influence predictors, the p-value was computed. Generally, the p-value below 0.05 was considered to indicate a statistically significant relationship between the two variables.

Thus, the Pearson correlation coefficient was utilised in this research to determine the correlation strength between the five graph-theoretical features and the cognitive scores in each IMF (30 p-values: 5 features × 6 scales). A proper adjustment is required if several independent tests are simultaneously conducted. Thus, Benjamini–Hochberg false discovery rate was employed to control multiple comparisons, and the p-value was corrected to 0.04. The correlation analysis was performed using *corrcoef* function in MATLAB's statistics toolbox.

6.5 Regression Model

A regression model was used to predict the later cognitive scores of the infants at high-risk who born with HIE. The model tries to fit the relationship between the EEG features (graph metrics) and the cognitive scores with the least possible error. The tree ensemble regression models were adopted in this study in order to reduce bias and variance in the imbalanced distribution of the data set under investigation—as the cognitive scores ranged between 74 and 145, such that most of the scores clustered above 95 (Figure 6.3).

The basic idea of tree ensemble regression is using several combined models to obtain an improved predictive performance (Moniz et al. 2017). Boosted trees regression and bagged trees regression were the two ensembles models adopted in this study. Bagged tree regression randomly sampled the original data set into different subsets with replacement. Several homogeneous models run independently on each subset in parallel, and the final predictive performance is obtained by combining the estimations of several models. In contrast, the boosted tree is a sequential ensemble method in which several homogenous models train adaptively. Each example in the data set is assigned with weight. The incorrectly classified examples carry more weight than those that are correctly classified. Thus, the successor classifier focuses more on the example with the high weight that the predecessor classifier failed to classify correctly. A more detailed

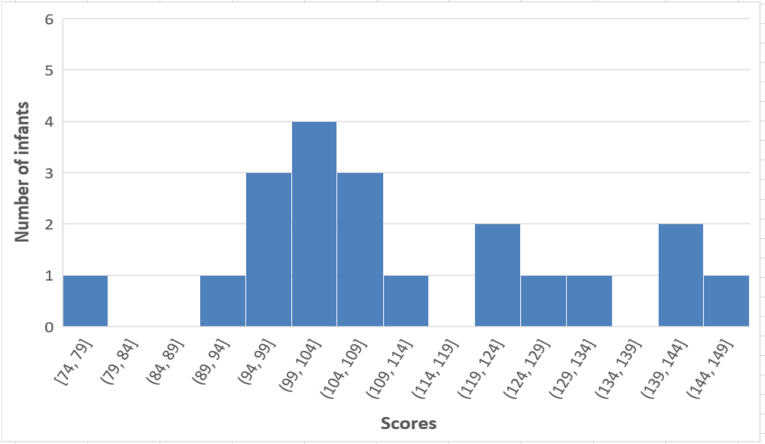

FIGURE 6.3: Cognitive scores histogram. Each bin of the histogram represents the number of infants belonging to a specific scores range. The number of bins count of the histogram represents the broad range of cognitive scores.

description of these models is available in (MathWorks 2021, Moniz et al. 2017). Tree ensembles regression were trained with proposed sets of features separately. Regression learner app within the statistics and machine learning toolbox in MATLAB was used to train the selected models.

LOOCV was used to assess the models' performance to avoid the biased estimation of the prediction performance; more details can be found in section 2.5. The performance of regression models was evaluated by the traditional measures known as root mean square error (RMSE), mean absolute error (MAE) and R-squared. RMSE is the most frequently used metric. It refers to the square root of the averaged squared difference between the predicted score resulting from the regression model and the actual one. Lower RMSE indicates the better model's performance. MAE is the absolute difference between the predicted value and the target one, and as in the case of RMSE, the lowest value refers to the best model's performance. R-squared is another metric used to evaluate the performance of the regression model. It determines how well the model predicts the specific score by comparing the learned model with the constant baseline model. The constant baseline model is built by taking the mean of training data and drawing the line on the mean. The value of R-squared is usually less than or equal to one where the higher value refers to a better fit between predicted and actual values.

6.6 Results

This section provides some experimental evaluation of the proposed approach for the early prediction of cognitive deficits. The effectiveness of qEEG features—global graph-theoretical attributes derived from WPLI—was evaluated using correlation analysis

and regression models. Table 6.2 shows the p-value results of correlation analysis between graph-theoretical features and cognitive scores in each IMF component.

TABLE 6.2: P-values of the correlation analysis of the graph-theoretical features. Significant features that less than or equal to the Benjamini–Hochberg threshold (0.04) are shown in boldface.

Feature	IMF4	IMF5	IMF6	IMF7	IMF8	IMF9
Transitivity	0.12	0.93	0.33	0.62	**0.03**	0.99
Global efficiency	0.11	0.96	0.28	0.66	**0.02**	0.99
Radius	0.65	0.67	0.89	**0.04**	0.16	0.21
Diameter	0.26	0.63	0.4	0.76	0.76	0.9
Characteristic path length	0.18	0.87	0.43	0.54	**0.04**	0.9

In Table 6.2, the features with the smallest p-value with boldface indicate a statistically significant correlation with the cognitive scores. These features were radius calculated from IMF7 and transitivity, global efficiency, and characteristic path length computed from IMF8.

Correlation plots in Figure 6.4 reveal that the radius and characteristic path length exhibited a significant negative correlation ($r = -0.46$, $p = 0.04$) and ($r = -0.45$, $p = 0.04$), respectively. Transitivity and global efficiency showed a high positive correlation ($r = 0.48$, $p = 0.03$) and ($r = 0.49$, $p = 0.02$), respectively. Considering that these features have significant correlation coefficient, they could greatly influence in predicting the cognitive outcome. Thus, these four features were selected to be used in training and testing the regression models.

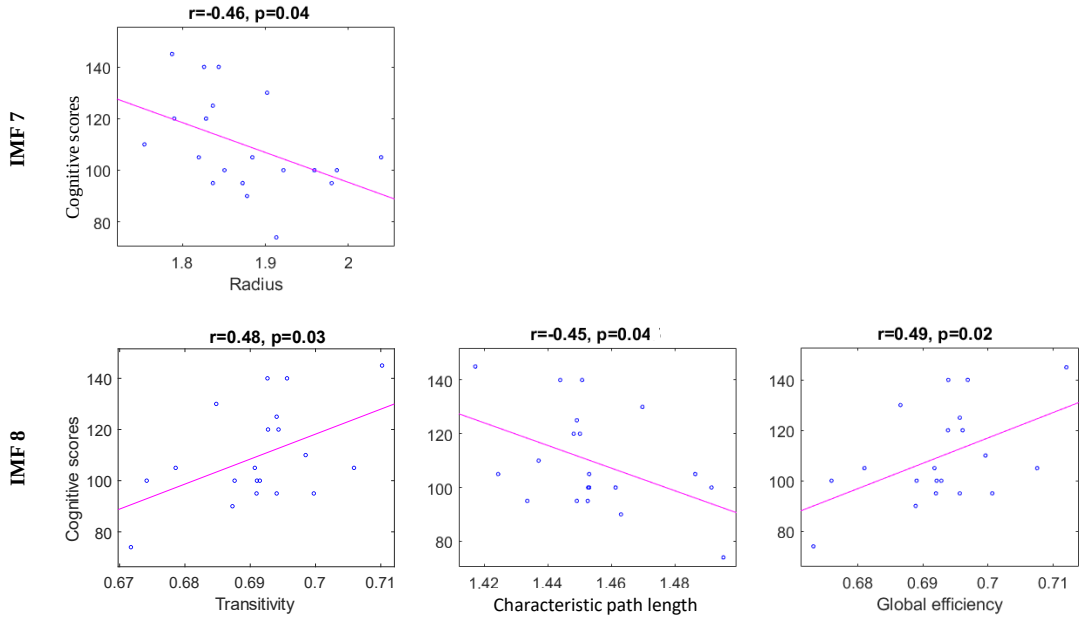

FIGURE 6.4: Scatter plots representing the correlation between the significant graph-theoretical features and cognitive scores.

LOOCV was used to evaluate the models' performance to prevent potential bias from occurring due to overfitting. Table 6.3 summarises the regression models performance of the four selected features and their combinations. It is apparent from Table 6.3 that the best performance—in terms of lowest RMSE, MAE and highest R-squared—was achieved using radius network property from IMF7. The visualisation corresponding to this result represented by the difference between predicted scores and the actual scores is shown in Figure 6.5. The error rate between the predicted values and actual ones of majorities of the individual was generally acceptable as depicted in 6.5. Other features such as transitivity, global efficiency and characteristic path length calculated from IMF8 also gave comparable results. This result implies that the network attributes—mainly radius—could provide valuable information regarding cognitive deficits.

TABLE 6.3: Performance of the tree ensembles regression models using the significant graph-theoretical features.

Scale	Feature	RMSE	MAE	R-Squared	Regression algorithm
IMF7	Radius	16.775	12.7	0.24	Bagged trees
		18.945	14.2	0.03	Boosted trees
IMF8	Transitivity	17.317	13.64	0.19	Bagged trees
		17.802	13.86	0.15	Boosted trees
	Global efficiency	17.26	13.64	0.2	Bagged trees
		17.71	13.82	0.15	Boosted trees
	Characteristic path length	16.98	13.28	0.22	Bagged trees
		17.78	13.85	0.15	Boosted trees
	Combination of transitivity, global efficiency, and characteristic path length	17.11	13.23	0.21	Bagged trees
		17.842	13.897	0.14	Boosted trees

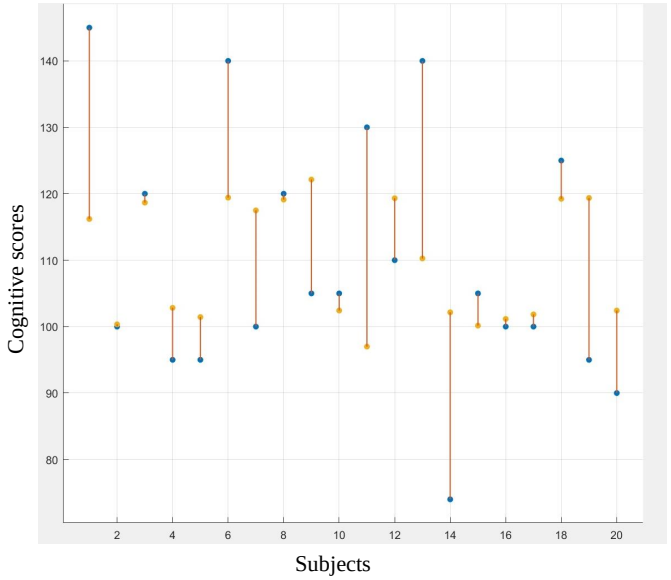

FIGURE 6.5: Response plot of predicted cognitive scores (represented with yellow dots) versus the actual one (depicted with blue dots). Regression-based prediction used the radius graph feature to predict the cognitive scores.

6.7 Discussion

The objective of the present investigation is to explore the effectiveness of employing qEEG analysis in the early prediction of the cognitive outcome at two years of age following the neonatal HIE. The early phase of a child's life is considered a critical stage for cognition, motor, language and social-emotional development owing to brain development and maturation of cortical architecture are most rapidly established in this period (Ouyang et al. 2020). The utilisation of this property helps to provide a tailored intervention seeking to improve the outcome. This study adopted a set of graph-theoretical features—extracted from EEG signals of twenty infants with neonatal HIE during their first week of birth—for early identification of at high-risk infants to develop cognitive impairment. The study aimed to predict the later individual's cognitive functions level assessed at two years of age by BSITD-III. As mentioned earlier, the cognitive scores of the cohort varied between 74 and 145. The score suggests the level of impairment developed at two years. Lower scores than 80 indicate cognitive deficit, and severity worsens with a lower score. While the scores above 80 indicate normal cognition, the level of cognitive functions increases when the score goes high.

The most significant challenge encountered in this study was that the distribution of the data set was biased, with most cognitive scores clustered above 95. Most of the

efforts in the machine learning community have devoted to eliminating current challenges by designing an algorithm that can deal with bias and variance in the data set. Tree ensembles regression, employed herein, is one of the efficient algorithms developed to handle this problem (Moniz et al. 2017). It is designed to train multiple models and then combine their results to improve the performance of the final model.

To the best of the author's knowledge, this research constitutes the first analysis on the impact of graph-theoretical features calculated in the NA-MEMD domain for future cognitive decline prediction. Statistical analysis showed a significant correlation in the delta band connectivity corresponding to IMF7 and IMF8 components using the radius, characteristic path length, transitivity, and global efficiency attributes. A strong negative relationship between the radius and cognitive profile was observed, indicating that the trend of the larger radius was correlated with poor cognitive outcomes. This result suggested that the brain network of infants who later developed with cognitive impairment was less integrated. On the other hand, the negative correlation was also revealed in characteristic path length (a measure of network efficiency), displaying that increase in characteristic path length (i.e., less integrated network) was inversely associated with cognitive scores. This result indicated that the brain network of infants who developed cognitive deficit by two years of age is less efficient in terms of the global information transfer (higher characteristic path length). Moreover, the correlation analysis demonstrated the positive relationship between transitivity and global efficiency and cognitive outcome, i.e., high transitivity and global efficiency, yielding normal cognitive functions (high cognitive scores). These two characteristics are valuable to figure out the plausible configuration of highly efficient brain networks (Fraga González et al. 2016). Thus, it can be inferred that any abnormality in this network could cause the alteration of both graph metrics and, consequently, a drop in cognitive scores. Together with the rest of the results, the proposed analysis suggested that the global graph-theoretical metrics (except diameter) could be used as biomarkers to identify the cognitive impairment early. This finding is consistent with the existing studies of some pathological conditions. Peters et al. (2013) showed increased characteristic path length and decreased global efficiency in children's brain network with ASD. However, in this case, the generalisation of the results could not be inferred because the statistical significance of the results is not sufficient to draw a strong conclusion. This may be caused by limited data available for analysis. The findings of this study provided insight into the feasibility of using the qEEG, particularly the phase-based FBC, as biomarkers for predicting cognitive outcomes. In order to draw the inclusive conclusion, it requires to validate this study with larger sample size.

WPLI revealed the disruptions of brain characteristics related to a cognitive deficit in the delta band. This finding is consistent with the study of Suppiej et al. (2017), where the authors concluded that the high value of the delta spectral power correlated with

poor outcomes in preterm infants at the first year of age. Increased delta activity in EEG of children suffering from learning disorders was also confirmed by Martínez-Briones et al. (2020) and further supported by Barttfeld et al. (2011) study that reported the difference in the delta coherence between children having ASD and the control group.

Two tree ensembles regression models were explored to handle the bias distribution of the data set. The significant graph-theoretical features (transitivity, global efficiency, radius and characteristic path length) calculated from IMF components corresponding to the delta band were used to train and test the regression models. The best performance was observed using bagged tree regression with radius feature (RMSE = 16.78, MAE = 12.07 and R-squared = 0.24).

A key strength of the research was recognised when compared with the state-of-the-art of qEEG studies, shown in Table 6.4. To the best of the author's knowledge, this research is the first prospective study to date performed in neonates (at the first week of birth) investigating the early non-linear qEEG characteristics of WPLI-based FBC and their prognostic value for cognitive outcome at twenty-four months of age. Furthermore, all limited studies existing in literature have used the linear qEEG such as coherence (Kühn-Popp et al. 2016), EEG continuity (West et al. 2005) and spectral power (Cainelli et al. 2021, Suppiej et al. 2017), which may not be optimal to capture the complex characteristics of the EEG spectra. Non-linear methods adopted in this study provided a deep insight into the underlying brain functions and dynamics.

In addition, several studies investigated the overlapping time-frequency activity underlying EEG by analysing the signal using the time-frequency methods that rely on the predefined frequency of traditional brainwaves, as in (Cainelli et al. 2021) and (Suppiej et al. 2017). Prior selection of frequency ranges may result in potentially informative brain waves being missed, specifically in the case of infants, due to the well-known variability between them and the older individuals in the neural oscillations of interest. This constraint has been settled in our proposed approach using the NA-MEMD method, which decomposes the signals adaptively. Thus, all meaningful brain dynamics are ascertained to be included in the analysis with this method.

TABLE 6.4: Comparison of the qEEG state-of-the-art methods employed for predicting cognitive outcome.

Author	Data set	Features	Evaluation methods	Outcome assessment	Findings
Lloyd et al. (2021)	57 preterm infants	EEG grading	Spearman's correlation coefficient	BSITD-III	Statistically significant negative correlation between abnormal EEG grading and BSITD-III subscale (r =-0.354)
Suppiej et al. (2017)	21 preterm infants	Spectral power analysis	Spearman's correlation coefficient	Griffiths Scale of Mental Development	Negative correlation between the delta spectral power and Griffiths scores developmental quotients (r=-0.68, p=0.015). Positive correlation between alpha and beta spectral power and Griffiths developmental quotients (r=0.61, p=0.032).
Cainelli et al. (2021)	26 preterm infants	Spectral power analysis	Bayesian correlation	Wechsler Preschool and Primary Scale of Intelligence III (WPPSI-III) test	Significant association between spectral frequency bands and visual and auditory attention tests.
West et al. (2005)	44 preterm infants	EEG continuity	Linear regression	BSITD-II	Significant correlation between mental developmental indices and continuity feature of EEG at different amplitude setting: 10 and 25 μ V thresholds (r-squared =0.19, P= 0.0032 and r-squared =0.10, p=0.04 respectively).
Kühn-Popp et al. (2016)	32 infants	EEG coherence measures	Correlation analysis Linear regression	Coding-scheme for mental state terms	Significant correlation between left hemisphere coherence and epistemic language at 48 months (r=0.59, p=0.003). Regression analyses showed, left-coherence scores are the most important predictor of epistemic state talk at 48 months.
Current study	20 infants born with HIE	Graph-theoretical features derived from WPLI	Pearson linear correlation coefficient Set of regression models	BSITD-III	Connectivity: Significant correlation between transitivity, global efficiency, radius, and characteristic path length and cognitive outcomes. Reasonable regression performance with radius feature: RMSE (16.775), MAE (12.702), and R-square (0.24)

6.8 Conclusion

In conclusion, the analysis of qEEG successfully predicted the cognitive outcome at two years of age from at high-risk infants born with HIE. FBC calculated by WPLI measures was evaluated by correlation analysis and regression-based machine learning framework. Pearson linear correlation analysis showed a strong correlation between graph-theoretical features of WPLI and cognitive scores. The tree ensembles regression models achieved reasonable performance: RMSE (16.775), MAE (12.702), and R-square (0.24). Therefore, the findings of this study provided insight into the feasibility of using graph-theoretical features derived from the delta band as the biomarker for early predicting cognitive decline. This study can also be considered proof that employing the qEEG features within regression-based machine learning frameworks could capture

the individual variability inherited in infants' developing brains. Moreover, this study lays the groundwork for future investigations into using these features as the biomarkers for predicting individuals at high-risk of developing cognitive impairments-related disorders such as intellectual disability.

Chapter 7

Conclusions and Future Directions

This dissertation was set out to explore the utility of qEEG features in the early classification /prediction of neurodevelopmental disorders. In this chapter, the main conclusions of this work are drawn together and presented in the section 7.1. The challenges and limitations of this dissertation are described in the section 7.2. The possible areas for further research are highlighted in the 7.3. The list of publications is presented in the section 7.4.

7.1 Dissertation Conclusion

This dissertation investigated the novel proposed analysis based on FBC and graph theory to characterise brain functions. Specifically, phase synchronisation based FBC was adopted to show the synchronisation of EEG activity between neuronal networks. The knowledge that the synchrony level can fluctuate in several neurodevelopmental disorders became the basis of this dissertation. The main idea of this approach was to model the resting-state /task dependant brain activity as a network and to compare its topographical properties within a sophisticated machine learning framework between the control groups and those with NDDs. Specifically, complex global network attributes were used to quantify the underlying brain connectivity network topology as they help provide a general insight into network characteristics. The proposed analysis was first validated with the children data set to classify children with ASD and their neurotypical peers using a machine learning classification model. The study of task-dependent FBC successfully distinguished between ASD and TD children, which is met the first objective of the research. The PLV was applied to estimate the FBC by measuring the temporal locking of phases between neural signals, which reflects the dynamic neural interactions underlying the cognitive process. Before calculating the phase, the DBP filter, particularly the FIR filter, was used to decompose the whole EEG spectra into narrowband components. Three different methodologies were adopted for

calculating PLV to find the optimal approach for capturing the difference between two populations in the ERP-based experiment. In this part of the study, the EEG recording was conducted while presenting the face expression stimuli to participants. This experimental set-up was chosen because the researchers have shown that the individual with ASD has a deficiency in social cognitions, which could be represented by emotional facial expression processing. The result of this investigation has revealed that trial-averaged PLV (phase differences calculated at each sample point and then averaging the generated connectivity matrices over the trials) achieved a high classification ACC up to 95.8%, SNS 100% and SPC 92% by cubic SVM. Another important finding was that the difference between the ASD and TD groups was observed in the theta and alpha bands, which met the sixth objective of the research. Generally, the study provided insight into the possibilities of using the global network attributes as biomarkers to classify ASD and TD, which is met the fifth objective of the dissertation. Although the current research comprised a small sample size, it will serve as a base for future studies for classifying /predicting ASD and other NDDs with larger sample sizes and different age populations.

Based on the significant findings from applying the proposed framework in classifying children with ASD from TD ones, the framework was extended to be used in the early prediction of infants who developed CP at two years of age. The resting-state EEG recorded at the first week of birth was analysed using the WPLI based FBC. WPLI was employed in this part of the study due to it is robustness against volume conduction, rendering the phase synchronisation more accurate. The resulting connectivity network was then characterised using the global graph attributes. These graph features were fed into the RUSBoost classifier, which was adopted at this stage to handle the imbalanced data distribution noticed in the infants' data set. The results of this exploration showed that the non-linear qEEG features, represented by the WPLI based FBC, within the machine learning framework could effectively predict the infant who developed CP at two years of age from EEG analysis recording during the first week after birth, which is met the second objective of this dissertation. Despite its exploratory nature, this study offered a good prediction performance in terms of classification accuracy, specificity, balanced accuracy, and AUC (84.6% ACC, 67% SNS, 90% SPC, 78.5% balanced accuracy, and 0.75 AUC) using a combination of all global graph attributes. A good performance in terms of sensitivity, balanced accuracy and AUC was also achieved using the radius feature with 76.9% ACC, 83% SNS, 75% SPC, 79% balanced accuracy and 0.78 AUC. These results showed that the two cases of feature vectors gave a good performance when combining all five graph attributes (transitivity, global efficiency, radius, diameter and characteristics path length) and the radius feature, and this was met the fifth objective. Regarding frequency bands, the results of this study revealed the strong association between the delta and theta bands and dysfunctions of the brain neural network of infants with CP, and this was met the sixth

objective of this research.

Together, these findings suggested the effectiveness of using FBC and global graph attributes as biomarkers for the early prediction of CP. This is the first time this framework was investigated for early prediction of brain disorders and can further contribute to the early, automated and objective prediction of CP to provide tailored intervention that could improve the outcomes and prevent severe impairments. Even though this study can be viewed as a promising attempt towards building an aiding tool for early prediction of CP, more work needs to be carried out with a larger and more balanced data set. On the other hand, this study used a traditional DBP filter, particularly the FIR filter, to decompose EEG signals into narrowband components. This filter has constraints on the filter cut-offs frequencies, which could vary between subjects (adults, children and infants). It might be of interest to investigate the usefulness of other filtering approaches. For this purpose, Chapter 5 proposed a new analysis approach for quantifying the instantaneous phase based on EMD algorithms. Mainly, NA-MEMD was used to adaptively decompose EEG signals into intrinsic components (IMFs) based on the oscillations in the signal. Following that, the WPLI was calculated from each IMF separately. The graph-theoretical features were extracted from the connectivity network, and the statistical test was then used to evaluate the discriminant capability of each graph attribute. After that, the graph features were fed into the RUSBoost classifier to get the predicted class of given data points. This study found that the proposed non-linear analytical methodology using NA-MEMD successfully predicted infants with CP at early infancy with the highest performance reaching 84.6% ACC, 83% SNS, 85% SPC, 84% balanced accuracy, and 0.85 AUC using transitivity feature. The same classification accuracy but with 67% SNS, 90% SPC, 78.5% balanced accuracy, and 0.81 AUC using characteristic path length from the IMF8 corresponding to the delta band range. Furthermore, a good performance in terms of classification ACC, SPC and AUC were obtained using the diameter feature calculated from the IMF5 and IMF6—corresponding to the theta and alpha band, respectively— reaching 80.8% ACC, 67% SNS and 85% SPC, 76% balanced accuracy, and 0.79 AUC from IMF6 and 0.72 from IMF5. These results confirmed the findings from Chapter 4 which stated that the association between frequency ranges and brain deficits in CP was observed in the delta and theta bands. One of the more significant findings from this study was that the NA-MEMD algorithm decomposed EEG into narrower components compared with the traditional DBP filter, optimising the phase estimation. This part of the study, which investigated the use of the NA-MEMD algorithm for quantifying the instantaneous phase and adopted this approach to discriminate between the CP and normal infants, met the fourth objective of this dissertation.

Using insights gained from these results, the proposed analysis was used to study the level of deficits by finding the association between the EEG features and the clinical

scores, mainly focusing on the level of cognitive functions of infants affected by HIE at birth. The proposed framework was utilised to predict the cognitive scores at two years from neonatal EEG recording at the first week of birth. NA-MEMD was used to decompose EEG signals into narrow bands, and the WPLI connectivity matrix was computed from each component. The graph-theoretical features were calculated from each matrix, and the Pearson linear correlation coefficient was used to measure the correlation strength between these graph attributes and cognitive scores. The features with significant correlation were fed into the regression models. Specifically, the tree ensemble regression models were employed to mitigate the effect of the imbalanced distribution of the data set. The results of this investigation showed that the qEEG features (WPLI-based FBC and graph parameters) within the regression framework could offer valuable prognostic information regarding cognitive performance, and this was met the third objective of this research. A significant correlation has been observed between radius, transitivity, global efficiency and characteristic path length calculated from IMF components corresponding to the delta band and the cognitive score, which was clinically assessed at two years of age. The regression analysis showed that the radius feature yielded the best performance (RMSE = 16.78, MAE = 12.07 and R-squared = 0.24). These findings were met the fifth and sixth objectives of this dissertation. This research adds to existing knowledge of early determination of the cognitive functions level during the plastic period of human brain development. It could pave the way for more research that could help provide the tailored intervention that can alter the developmental deficits.

In summary, four different experimental results showed evidence that the qEEG features represented by the FBC and graph theory contain helpful prognostic information for identifying NDDs. The positive outcomes of this study will open up the opportunities to do more extensive studies in early prediction NDDs to transition from the proof of concept stage to being applied clinically in the near future.

7.2 Challenges and Limitations

Undeniably, fulfilling the research objectives—particularly in the EEG analysis— is a challenging task. As the human brain is undoubtedly a highly complex system, understanding the physiology, interconnections, and mapping its connectivity is not straightforward. Furthermore, the major challenge associated with EEG analysis is that it is highly contaminated with artefacts and positively affected by a well-known problem called volume conduction, which occurs because EEG signals are recorded from different electrodes over the scalp, leading to the potential of mixing signals from various sources (Vinck et al. 2011). Consequently, this may lead to distortion of the actual neuronal activities.

Another obstacle encountered in this study has been in gathering sufficient and balanced data. This task is particularly problematic in the medical domain due to the difficulty of finding the required number of participants with the same conditions and of the same age. Notably, this problem is even more complicated in infants, as finding neonates who have the same medical condition takes a long time. Furthermore, dealing with infants and recording their EEG signals is technically very challenging. In this essence, the estimation of sample size that necessary for making the results clinically usable is a critical step in designing research protocol. The sample size must be big enough to be able to infer the statistically significant results, draw the generalised conclusion and make the prediction model more reliable when applied to new individuals (Suresh & Chandrashekara 2012, Riley et al. 2020). At the same time, collecting more experimental data is expensive, time-consuming and exposes more number of subjects to procedure (Hajian-Tilaki 2014, Suresh & Chandrashekara 2012). In fact, the minimum sample size required varies depending on the objectives of the research study. There are several studies that provided the guide for estimating the minimum sample size required in the diagnostic study (Bujang & Adnan 2016, Hajian-Tilaki 2014, Lerman 1996, Suresh & Chandrashekara 2012, Riley et al. 2020).

In addition, in order to predict the emerging neurodevelopmental outcomes in children of two years old from neonatal EEG, the participants ideally need to be followed longitudinally for a minimum of two years. The child must complete the follow-up assessments (set of neurological and developmental tests) required to compare the markers from EEG connectivity at birth with the clinical outcome. Although it helps study the development changes over the lifespan, this longitudinal study presents several difficulties. First, it requires a great deal of time, which may often make it expensive. Moreover, the participant may fail to complete the follow-up assessment due to a variety of reasons such as death, illness, or a change of location; shrinking the sample size as a result.

7.3 Future Works

The research of the early prediction of NDDs is still in its infancy. There is ample room for further progress toward the early and automated identification of such disorders and establishing the aiding tools into the clinical practice to assist the clinicians in their decisions. Some of these future directions are highlighted in the following.

In this dissertation, the proposed framework has been validated in a small sample size. It would be more reliable to ascertain the validity and the efficiency of the framework

using a larger data set with a statistically significant population. This could help confirm the robustness of the models and generalise the outcomes. On the other hand, the infants' data set under consideration has an imbalanced distribution, a well-known problem in the machine learning environment. It would be insightful to further exploit the proposed framework on a more balanced and consistent data cohort or investigate another solution to deal with this problem. Moreover, the infants recruited in this dissertation were at high-risk born with HIE. It would be valuable to explore the varying conditions of birth-time complications such as premature birth.

Further methodological development could be applied to the proposed framework to validate and improve the overall outcomes. For example, exploring different graph attributes is recommended in order to identify more definitive biomarkers of brain functional deficits. Modularity, small-world network property are the example of the those graph features.Further improvement is also suggested to explore various sophisticated machine learning algorithms to determine a model fitting to predict the neurodevelopmental outcome. Random forest, neural network and an evolutionary algorithm are the example of those machine learning algorithms. The proposed framework investigated the statistical correlation between distant brain areas to estimate the functional brain interactions. It might be worthwhile to study the causal interactions between those brain regions with effective connectivity and explore their efficiency in predicting brain abnormalities.

Chapter 6 investigated the utility of the proposed framework, specifically, in cognitive prediction scores on continuous scale. It would be interesting to assess the performance of the framework in predicting the various aspects of developmental delays, such as language and motor skills. Thus, one possible future expansion of this study is to conduct the regression analysis to predict language delay level and the motor state from infants at high-risk infants. Another potential area of future research would be to design the regression model to predict the disorder severity. This might help provide the tailored intervention according to the severity of the disorders.

7.4 Publications

The list of publications that have arisen as part form this dissertation are listed in this section.

1. N. Alotaibi and K. Maharatna, "Classification of Autism Spectrum Disorder From EEG-Based Functional Brain Connectivity Analysis," Neural Comput., vol. 33, no. 7, pp. 1914–1941, Jun. 2021.

2. D. Bakheet, N. Alotaibi, D. Konn, B. Vollmer, and K. Maharatna, "Prediction of Cerebral Palsy in Newborns with Hypoxic-Ischaemic Encephalopathy Using Multivariate EEG Analysis and Machine Learning," IEEE Access, 2021.

3. N. Alotaibi, D. Bakheet, D. Konn, B. Vollmer, and K. Maharatna, "Cognitive Outcome Prediction in Infants With Neonatal Hypoxic-Ischemic Encephalopathy Based on Functional Connectivity and Complexity of the Electroencephalography Signal," Front. Hum. Neurosci., vol. 15, no. 1, pp. 1–19, 2022.

References

Abdolzadegan, D., Moattar, M. H. & Ghoshuni, M. (2020), 'A robust method for early diagnosis of autism spectrum disorder from EEG signals based on feature selection and DBSCAN method', *Biocybernetics and Biomedical Engineering* **40**(1), 482–493.

Adey, W., Walter, D. & Hendrix, C. (1961), 'Computer techniques in correlation and spectral analyses of cerebral slow waves during discriminative behavior', *Experimental Neurology* **3**(6), 501–524.

Ahmadi, A., Kashefi, M., Shahrokhi, H. & Nazari, M. A. (2021), 'Computer aided diagnosis system using deep convolutional neural networks for ADHD subtypes', *Biomedical Signal Processing and Control* **63**(6), 102227.

Ahmadlou, M., Adeli, H. & Adeli, A. (2012), 'Fuzzy Synchronization Likelihood-wavelet methodology for diagnosis of autism spectrum disorder', *Journal of Neuroscience Methods* **211**(2), 203–209.

Allen, K. A. & Brandon, D. H. (2011), 'Hypoxic ischemic encephalopathy: Pathophysiology and experimental treatment', *Newborn Infant Nurs Rev* **11**(3), 125–133.

Alotaibi, N., Bakheet, D., Konn, D., Vollmer, B. & Maharatna, K. (2022), 'Cognitive Outcome Prediction in Infants With Neonatal Hypoxic-Ischemic Encephalopathy Based on Functional Connectivity and Complexity of the Electroencephalography Signal', *Frontiers in Human Neuroscience* **15**(1), 1–19.

Alotaibi, N. & Maharatna, K. (2021), 'Classification of Autism Spectrum Disorder From EEG-Based Functional Brain Connectivity Analysis', *Neural Computation* **33**(7), 1914–1941.

Apicella, F., Sicca, F., Federico, R. R., Campatelli, G. & Muratori, F. (2013), 'Fusiform Gyrus responses to neutral and emotional faces in children with Autism Spectrum Disorders: A High Density ERP study', *Behavioural Brain Research* **251**, 155–162.

Assaf, M., Jagannathan, K., Calhoun, V. D., Miller, L., Stevens, M. C., Sahl, R., O'Boyle, J. G., Schultz, R. T. & Pearlson, G. D. (2010), 'Abnormal functional connectivity of default mode sub-networks in autism spectrum disorder patients', *NeuroImage* **53**(1), 247–256.

Aydore, S., Pantazis, D. & Leahy, R. M. (2013), 'A note on the phase locking value and its properties', *NeuroImage* **74**, 231–244.

Babiloni, C., Brancucci, A., Vecchio, F., Arendtnielsen, L., Chen, A. & Rossini, P. (2006), 'Anticipation of somatosensory and motor events increases centro-parietal functional coupling: An EEG coherence study', *Clinical Neurophysiology* **117**(5), 1000–1008.

Baccalá, L. A. & Sameshima, K. (2001), 'Partial directed coherence: a new concept in neural structure determination', *Biological Cybernetics* **84**(6), 463–474.

Bakheet, D., Alotaibi, N., Konn, D., Vollmer, B. & Maharatna, K. (2021), 'Prediction of Cerebral Palsy in Newborns with Hypoxic-Ischemic Encephalopathy Using Multivariate EEG Analysis and Machine Learning', *IEEE Access* **9**, 137833–137846.

Banker, S. M., Pagliaccio, D., Ramphal, B., Thomas, L., Dranovsky, A. & Margolis, A. E. (2021), 'Altered structure and functional connectivity of the hippocampus are associated with social and mathematical difficulties in nonverbal learning disability', *Hippocampus* **31**(1), 79–88.

Barry, R. J., Clarke, A. R. & Johnstone, S. J. (2003), 'A review of electrophysiology in attention-deficit/hyperactivity disorder: I. Qualitative and quantitative electroencephalography', *Clinical Neurophysiology* **114**(2), 171–183.

Barttfeld, P., Wicker, B., Cukier, S., Navarta, S., Lew, S. & Sigman, M. (2011), 'A big-world network in ASD: Dynamical connectivity analysis reflects a deficit in long-range connections and an excess of short-range connections', *Neuropsychologia* **49**(2), 254–263.

Beare, R., Adamson, C., Bellgrove, M. A., Vilgis, V., Vance, A., Seal, M. L. & Silk, T. J. (2017), 'Altered structural connectivity in ADHD: a network based analysis', *Brain Imaging and Behavior* **11**(3), 846–858.

Benjamini, Y. & Hochberg, Y. (1995), 'Controlling the False Discovery Rate: A Practical and Powerful Approach to Multiple Testing', *Journal of the Royal Statistical Society* **57**(1), 289–300.

Blackburn, C., Read, J. & Spencer, N. (2012), Children with neurodevelopmental disabilities, Technical report, Annual Report of the Chief Medical Officer 2012.

Bos, D. J., Oranje, B., Achterberg, M., Vlaskamp, C., Ambrosino, S., de Reus, M. A., van den Heuvel, M. P., Rombouts, S. A. & Durston, S. (2017), 'Structural and functional connectivity in children and adolescents with and without attention deficit/hyperactivity disorder', *Journal of Child Psychology and Psychiatry* **58**(7), 810–818.

Bos, D. J., Raalten, T. R. V., Oranje, B., Smits, A. R., Kobussen, N. A., Belle, J. V., Rombouts, S. A. R. B. & Durston, S. (2014), 'Developmental differences in higher-order

resting-state networks in Autism Spectrum Disorder', *NeuroImage: Clinical* **4**, 820–827.

Breakspear, M., Williams, L. M. & Stam, C. J. (2004), 'A Novel Method for the Topographic Analysis of Neural Activity Reveals Formation and Dissolution of 'Dynamic Cell Assemblies'', *Journal of Computational Neuroscience* **16**(1), 49–68.

Bruña, R., Maestú, F. & Pereda, E. (2018), 'Phase locking value revisited: teaching new tricks to an old dog', *Journal of Neural Engineering* **15**(5), 056011.

Brunner, C., Scherer, R., Graimann, B., Supp, G. & Pfurtscheller, G. (2006), 'Online control of a brain-computer interface using phase synchronization', *IEEE Transactions on Biomedical Engineering* **53**(12), 2501–2506.

Buckley, A. W., Scott, R., Tyler, A., Mahoney, J. M., Thurm, A., Farmer, C., Swedo, S., Burroughs, S. A. & Holmes, G. L. (2015), 'State-Dependent Differences in Functional Connectivity in Young Children With Autism Spectrum Disorder', *EBioMedicine* **2**(12), 1905–1915.

Bujang, M. A. & Adnan, T. H. (2016), 'Requirements for minimum sample size for sensitivity and specificity analysis', *Journal of Clinical and Diagnostic Research* **10**(10), YE01–YE06.

Byeon, J., Kim, G.-H., Kim, J., Sun, W., Kim, H. & Eun, B.-L. (2015), 'Cognitive Dysfunction and Hippocampal Damage Induced by Hypoxic-Ischemic Brain Injury and Prolonged Febrile Convulsions in Immature Rats', *Journal of Korean Neurosurgical Society* **58**(1), 22.

Cainelli, E., Vedovelli, L., Wigley, I. L. C. M., Bisiacchi, P. S. & Suppiej, A. (2021), 'Neonatal spectral EEG is prognostic of cognitive abilities at school age in premature infants without overt brain damage', *European Journal of Pediatrics* **180**(3), 909–918.

Cao, M., Shu, N., Cao, Q., Wang, Y. & He, Y. (2014), 'Imaging Functional and Structural Brain Connectomics in Attention-Deficit/Hyperactivity Disorder', *Molecular Neurobiology* **50**(3), 1111–1123.

Carson, A. M., Salowitz, N. M. G., Scheidt, R. A., Dolan, B. K. & Van Hecke, A. V. (2014), 'Electroencephalogram Coherence in Children With and Without Autism Spectrum Disorders: Decreased Interhemispheric Connectivity in Autism', *Autism Research* **7**(3), 334–343.

Chaitra, N., Vijaya, P. A. & Deshpande, G. (2020), 'Diagnostic prediction of autism spectrum disorder using complex network measures in a machine learning framework', *Biomedical Signal Processing and Control* **62**(8), 102099.

Chaumon, M., Bishop, D. V. & Busch, N. A. (2015), 'A practical guide to the selection of independent components of the electroencephalogram for artifact correction', *Journal of Neuroscience Methods* **250**(3), 47–63.

Chen, H., Song, Y. & Li, X. (2019), 'A deep learning framework for identifying children with ADHD using an EEG-based brain network', *Neurocomputing* **356**, 83–96.

Chen, S. Y., Feng, Z. & Yi, X. (2017), 'A general introduction to adjustment for multiple comparisons', *Journal of Thoracic Disease* **9**(6), 1725–1729.

Cho, D., Min, B., Kim, J. & Lee, B. (2017), 'EEG-Based Prediction of Epileptic Seizures Using Phase Synchronization Elicited from Noise-Assisted Multivariate Empirical Mode Decomposition', *IEEE Transactions on Neural Systems and Rehabilitation Engineering* **25**(8), 1309–1318.

Cioni, G., Inguaggiato, E. & Sgandurra, G. (2016), 'Early intervention in neurodevelopmental disorders: underlying neural mechanisms', *Developmental Medicine & Child Neurology* **58**(s4), 61–66.
URL: *https://onlinelibrary.wiley.com/doi/10.1111/dmcn.13050*

Coben, R., Clarke, A. R., Hudspeth, W. & Barry, R. J. (2008), 'EEG power and coherence in autistic spectrum disorder', *Clinical Neurophysiology* **119**(5), 1002–1009.

Cohen, M. X. (2014), *Analyzing neural time series data: Theory and practice*, MIT Press.

Covarrubias, L. S. (2017), Connetivity Analysis from EEG Phase Synchronisation in Emotional BCI, PhD thesis, University of Warwick.

D'Albis, M.-A., Guevara, P., Guevara, M., Laidi, C., Boisgontier, J., Sarrazin, S., Duclap, D., Delorme, R., Bolognani, F., Czech, C., Bouquet, C., Ly-Le Moal, M., Holiga, S., Amestoy, A., Scheid, I., Gaman, A., Leboyer, M., Poupon, C., Mangin, J.-F. & Houenou, J. (2018), 'Local structural connectivity is associated with social cognition in autism spectrum disorder', *Brain* **141**(12), 3472–3481.

David, O., Cosmelli, D. & Friston, K. J. (2004), 'Evaluation of different measures of functional connectivity using a neural mass model', *NeuroImage* **21**(2), 659–673.

Dereymaeker, A., Matic, V., Vervisch, J., Cherian, P. J., Ansari, A. H., De Wel, O., Govaert, P., De Vos, M., Van Huffel, S., Naulaers, G. & Jansen, K. (2019), 'Automated EEG background analysis to identify neonates with hypoxic-ischemic encephalopathy treated with hypothermia at risk for adverse outcome: A pilot study', *Pediatrics & Neonatology* **60**(1), 50–58.

Dimitriadis, S. I. (2016), 'Identification of infants at high familiar risk for language-learning disorders (LLD) by combining machine learning techniques with EEG-based brain network metrics', *Clinical Neurophysiology* **127**(7), 2692–2694.

Doyle, O. M., Temko, A., Murray, D. M., Lightbody, G., Marnane, W. & Boylan, G. B. (2010), Predicting the neurodevelopmental outcome in newborns with hypoxic-ischaemic injury, *in* '2010 Annual International Conference of the IEEE Engineering in Medicine and Biology', IEEE, Buenos Aires, pp. 1370–1373.

Doyle-Thomas, K. A. R., Lee, W., Foster, N. E. V., Tryfon, A., Ouimet, T., Hyde, K. L., Evans, A. C., Lewis, J., Zwaigenbaum, L. & Anagnostou, E. (2015), 'Atypical functional brain connectivity during rest in autism spectrum disorders', *Annals of Neurology* **77**(5), 866–876.

Duda, M., Ma, R., Haber, N. & Wall, D. P. (2016), 'Use of machine learning for behavioral distinction of autism and ADHD', *Translational psychiatry* **6**(12), e732.

Duffy, F. H., Shankardass, A., McAnulty, G. B. & Als, H. (2017), 'A unique pattern of cortical connectivity characterizes patients with attention deficit disorders: A large electroencephalographic coherence study', *BMC Medicine* **15**(1), 1–19.

Falkmer, T., Anderson, K., Falkmer, M. & Horlin, C. (2013), 'Diagnostic procedures in autism spectrum disorders: a systematic literature review', *European Child & Adolescent Psychiatry* **22**(6), 329–340.

Farahmand, S., Sobayo, T. & Mogul, D. J. (2018), 'Noise-Assisted Multivariate EMD-Based Mean-Phase Coherence Analysis to Evaluate Phase-Synchrony Dynamics in Epilepsy Patients', *IEEE Transactions on Neural Systems and Rehabilitation Engineering* **26**(12), 2270–2279.

Fingelkurts, A. A., Fingelkurts, A. A. & Kähkönen, S. (2005), 'Functional connectivity in the brain—is it an elusive concept?', *Neuroscience & Biobehavioral Reviews* **28**(8), 827–836.

Fraga González, G., Van der Molen, M., Žarić, G., Bonte, M., Tijms, J., Blomert, L., Stam, C. & Van der Molen, M. (2016), 'Graph analysis of EEG resting state functional networks in dyslexic readers', *Clinical Neurophysiology* **127**(9), 3165–3175.

Friston, K., Harrison, L. & Penny, W. (2003), 'Dynamic causal modelling', *NeuroImage* **19**(4), 1273–1302.

Gabor, D. (1946), 'Theory of communication. Part 1: The analysis of information', *Journal of the Institution of Electrical Engineers - Part III: Radio and Communication Engineering* **93**(26), 429–441.

Gao, F., Jia, H., Wu, X., Yu, D. & Feng, Y. (2017), 'Altered Resting-State EEG Microstate Parameters and Enhanced Spatial Complexity in Male Adolescent Patients with Mild Spastic Diplegia', *Brain Topography* **30**(2), 233–244.

Gao, F., Wu, X., Feng, Y. & Jia, H. (2017), 'Attenuation of temporal correlations of neuronal oscillations in patients with mild spastic diplegia', *Scientific Reports* **7**(1), 14966.

Gaudet, I., Hüsser, A., Vannasing, P. & Gallagher, A. (2020), 'Functional Brain Connectivity of Language Functions in Children Revealed by EEG and MEG: A Systematic Review', *Frontiers in Human Neuroscience* **14**(3).

George, J. M., Pagnozzi, A. M., Bora, S., Boyd, R. N., Colditz, P. B., Rose, S. E., Ware, R. S., Pannek, K., Bursle, J. E., Fripp, J., Barlow, K., Iyer, K., Leishman, S. J. & Jendra, R. L. (2020), 'Prediction of childhood brain outcomes in infants born preterm using neonatal MRI and concurrent clinical biomarkers (PREBO-6): Study protocol for a prospective cohort study', *BMJ Open* **10**(5).

Glass, H. C., Li, Y., Gardner, M., Barkovich, A. J., Novak, I., McCulloch, C. E. & Rogers, E. E. (2021), 'Early Identification of Cerebral Palsy Using Neonatal MRI and General Movements Assessment in a Cohort of High-Risk Term Neonates', *Pediatric Neurology* **118**, 20–25.

Glover, G. H. (2011), 'Overview of Functional Magnetic Resonance Imaging', *Neurosurgery Clinics of North America* **22**(2), 133–139.

Gooskens, B., Bos, D. J., Naaijen, J., Akkermans, S. E., Kaiser, A., Hohmann, S., Bruchhage, M. M., Banaschewski, T., Brandeis, D., Williams, S. C., Lythgoe, D. J., Buitelaar, J. K., Oranje, B. & Durston, S. (2021), 'The development of cognitive control in children with autism spectrum disorder or obsessive-compulsive disorder: A longitudinal fMRI study', *Neuroimage: Reports* **1**(2), 100015.

Gosain, A. & Sardana, S. (2017), 'Handling class imbalance problem using oversampling techniques: A review', *2017 International Conference on Advances in Computing, Communications and Informatics, ICACCI 2017* **7**, 79–85.

Gov.uk (2021), 'Disability Living Allowance (DLA) for children'.
URL: *https://www.gov.uk/disability-living-allowance-children*

Granger, C. W. J. (1969), 'Investigating Causal Relations by Econometric Models and Cross-spectral Methods', *Econometrica* **37**(3), 424.

Griffiths, K. R., Braund, T. A., Kohn, M. R., Clarke, S., Williams, L. M. & Korgaonkar, M. S. (2021), 'Structural brain network topology underpinning ADHD and response to methylphenidate treatment', *Translational Psychiatry* **11**(1), 150.

Grossi, E., Olivieri, C. & Buscema, M. (2017), 'Diagnosis of autism through EEG processed by advanced computational algorithms: A pilot study', *Computer Methods and Programs in Biomedicine* **142**, 73–79.

Gurau, O., Bosl, W. J. & Newton, C. R. (2017), 'How Useful Is Electroencephalography in the Diagnosis of Autism Spectrum Disorders and the Delineation of Subtypes: A Systematic Review', *Frontiers in Psychiatry* **8**, 121.

Haartsen, R., Jones, E. J. H., Orekhova, E. V., Charman, T. & Johnson, M. H. (2019), 'Functional EEG connectivity in infants associates with later restricted and repetitive behaviours in autism; a replication study', *Translational Psychiatry* **9**(1), 66.

Hadders-Algra, M. (2014), 'Early Diagnosis and Early Intervention in Cerebral Palsy', *Frontiers in Neurology* **5**(9), 1–13.

Hadders-Algra, M. (2021), 'Early diagnostics and early intervention in neurodevelopmental disorders—age-dependent challenges and opportunities', *Journal of Clinical Medicine* **10**(4), 1–24.

Hajian-Tilaki, K. (2014), 'Sample size estimation in diagnostic test studies of biomedical informatics', *Journal of Biomedical Informatics* **48**, 193–204.

Hamedi, M., Salleh, S.-H. & Noor, A. M. (2016), 'Electroencephalographic Motor Imagery Brain Connectivity Analysis for BCI: A Review', *Neural Computation* **28**(6), 999–1041.

Han, J., Zeng, K., Kang, J., Tong, Z., Cai, E., Chen, H., Ding, M., Gu, Y., Ouyang, G. & Li, X. (2017), 'Development of Brain Network in Children with Autism from Early Childhood to Late Childhood', *Neuroscience* **367**, 134–146.

Hayashi-Kurahashi, N., Kidokoro, H., Kubota, T., Maruyama, K., Kato, Y., Kato, T., Natsume, J., Hayakawa, F., Watanabe, K. & Okumura, A. (2012), 'EEG for predicting early neurodevelopment in preterm infants: An observational cohort study', *Pediatrics* **130**(4).

He, L., Li, H., Holland, S. K., Yuan, W., Altaye, M. & Parikh, N. A. (2018), 'Early prediction of cognitive deficits in very preterm infants using functional connectome data in an artificial neural network framework', *NeuroImage: Clinical* **18**(10), 290–297.

Hoffman, J. I. (2019), Analysis of Variance. I. One-Way, *in* 'Basic Biostatistics for Medical and Biomedical Practitioners', Elsevier, pp. 391–417.

Hu, M. & Liang, H. (2011), 'Intrinsic mode entropy based on multivariate empirical mode decomposition and its application to neural data analysis', *Cognitive Neurodynamics* **5**(3), 277–284.

Huang, N. E., Shen, Z., Long, S. R., Wu, M. C., Shih, H. H., Zheng, Q., Yen, N.-C., Tung, C. C. & Liu, H. H. (1998), 'The empirical mode decomposition and the Hilbert spectrum for nonlinear and non-stationary time series analysis', *Proceedings of the Royal Society of London. Series A: Mathematical, Physical and Engineering Sciences* **454**(1971), 903–995.

Iidaka, T. (2015), 'Resting state functional magnetic resonance imaging and neural network classified autism and control', *Cortex* **63**, 55–67.

Islam, M. R., Yin, X., Ulhaq, A., Zhang, Y., Wang, H., Anjum, N. & Kron, T. (2017), 'A Survey of Graph Based Complex Brain Network Analysis Using Functional and Diffusional MRI', *American Journal of Applied Sciences* **14**(12), 1186–1208.

Jamal, W., Das, S., Oprescu, I.-A., Maharatna, K., Apicella, F. & Sicca, F. (2014), 'Classification of autism spectrum disorder using supervised learning of brain connectivity measures extracted from synchrostates', *Journal of Neural Engineering* **11**(4), 46019.

Janssen, T. W. P., Hillebrand, A., Gouw, A., Geladé, K., Mourik, R. V., Maras, A. & Oosterlaan, J. (2017), 'Clinical Neurophysiology Neural network topology in ADHD ; evidence for maturational delay and default-mode network alterations', *Clinical Neurophysiology* **128**(11), 2258–2267.

Jeste, S. & Nelson, C. (2009), 'Event Related Potentials in the Understanding of Autism Spectrum Disorders: An Analytical Review Shafali', *Journal of Autism and Developmental Disorders* **39**(3), 495–510.

Kaisar, S. (2020), 'Developmental dyslexia detection using machine learning techniques : A survey', *ICT Express* **6**(3), 181–184.

Kaiser, M. (2011), 'A tutorial in connectome analysis: Topological and spatial features of brain networks', *NeuroImage* **57**(3), 892–907.

Kamifiski, M. J. & Bfinowska, K. J. (1991), 'A new method of the description of the information flow in the brain structures', *Biological cybernetics* **65**, 203–210.

Kana, R. K., Uddin, L. Q., Kenet, T., Chugani, D. & Müller, R.-A. (2014), 'Brain connectivity in autism', *Frontiers in Human Neuroscience* **8**.

Kang, J., Han, X., Song, J., Niu, Z. & Li, X. (2020), 'The identification of children with autism spectrum disorder by SVM approach on EEG and eye-tracking data', *Computers in Biology and Medicine* **120**, 103722.

Keown, C. L., Shih, P., Nair, A., Peterson, N., Mulvey, M. E. & Müller, R.-A. (2013), 'Local Functional Overconnectivity in Posterior Brain Regions Is Associated with Symptom Severity in Autism Spectrum Disorders', *Cell Reports* **5**(3), 567–572.

Kern, J. K., Geier, D. A., King, P. G., Sykes, L. K., Mehta, J. A. & Geier, M. R. (2015), 'Shared Brain Connectivity Issues, Symptoms, and Comorbidities in Autism Spectrum Disorder, Attention Deficit/Hyperactivity Disorder, and Tourette Syndrome', *Brain Connectivity* **5**(6), 321–335.

Kessler, K., Centre, A. B. & Sciences, H. (2016), 'Brain oscillations and connectivity in autism spectrum disorders (ASD): new approaches to methodology, measurement and modelling.', *Neuroscience and biobehavioral reviews* **71**, 601–620.

Khuntia, A. T., Divakar, R., Apicella, F., Muratori, F. & Das, K. (2019), 'Visual processing and attention rather than face and emotion processing play a distinct role in asd: an eeg study', *bioRxiv* .

Kiiski, H., Jollans, L., Donnchadha, S., Nolan, H., Lonergan, R., Kelly, S., O'Brien, M. C., Kinsella, K., Bramham, J., Burke, T., Hutchinson, M., Tubridy, N., Reilly, R. B. & Whelan, R. (2018), 'Machine Learning EEG to Predict Cognitive Functioning and Processing Speed Over a 2-Year Period in Multiple Sclerosis Patients and Controls', *Brain Topography* **31**(3), 346–363.

Kim, S., Kim, J. S., Kwon, Y. J., Lee, H. Y., Yoo, J. H., Lee, Y. J. & Shim, S.-h. (2021), 'Altered cortical functional network in drug-naive adult male patients with attention-deficit hyperactivity disorder: A resting-state electroencephalographic study', *Progress in Neuro-Psychopharmacology and Biological Psychiatry* **106**(7), 110056.

Klimesch, W. (1999), 'EEG alpha and theta oscillations reflect cognitive and memory performance: a review and analysis', *Brain Research Reviews* **29**(2-3), 169–195.

Klimkeit, E., Rinehart, N. & Bradshaw, J. (2008), 'Neurodevelopmental Disorders', *International Encyclopedia of Public Health* **3**(10), 512–521.

Koeda, T. & Takeshita, K. (1998), 'Electroencephalographic coherence abnormalities in preterm diplegia', *Pediatric Neurology* **18**(1), 51–56.

Kong, A. H., Lai, M. M., Finnigan, S., Ware, R. S., Boyd, R. N. & Colditz, P. B. (2018), 'Background EEG features and prediction of cognitive outcomes in very preterm infants: A systematic review', *Early Human Development* **127**(9), 74–84.

Kühn-Popp, N., Kristen, S., Paulus, M., Meinhardt, J. & Sodian, B. (2016), 'Left hemisphere EEG coherence in infancy predicts infant declarative pointing and preschool epistemic language', *Social Neuroscience* **11**(1), 49–59.

Kulak, W. & Sobaniec, W. (2005), 'Quantitative EEG analysis in children with hemiparetic cerebral palsy.', *NeuroRehabilitation* **20**(2), 75–84.

Kułak, W., Sobaniec, W. & Boćkowski, L. (2005), 'EEG spectral analysis and coherence in children with hemiparetic cerebral palsy', *Medical Science Monitor* **11**(9), 449–455.

Lachaux, J. P., Rodriguez, E., Martinerie, J. & Varela, F. J. (1999), 'Measuring phase synchrony in brain signals', *Human Brain Mapping* **8**(4), 194–208.

Lake, E. M., Finn, E. S., Noble, S. M., Vanderwal, T., Shen, X., Rosenberg, M. D., Spann, M. N., Chun, M. M., Scheinost, D. & Constable, R. T. (2019), 'The Functional Brain Organization of an Individual Allows Prediction of Measures of Social Abilities Transdiagnostically in Autism and Attention-Deficit/Hyperactivity Disorder', *Biological Psychiatry* **86**(4), 315–326.

Lang, E. W., Tomé, A. M., Keck, I. R., Górriz-Sáez, J. M. & Puntonet, C. G. (2012), 'Brain Connectivity Analysis: A Short Survey', *Computational Intelligence and Neuroscience* **2012**, 1–21.

Larrain-Valenzuela, J., Zamorano, F., Soto-Icaza, P., Carrasco, X., Herrera, C., Daiber, F., Aboitiz, F. & Billeke, P. (2017), 'Theta and Alpha Oscillation Impairments in Autistic Spectrum Disorder Reflect Working Memory Deficit', *Scientific Reports* **7**(1), 1–11.

Lau, W. K. W., Leung, M.-K. & Lau, B. W. M. (2019), 'Resting-state abnormalities in Autism Spectrum Disorders: A meta-analysis', *Scientific Reports* **9**(1), 3892.

Lavanga, M., De Ridder, J., Kotulska, K., Moavero, R., Curatolo, P., Weschke, B., Riney, K., Feucht, M., Krsek, P., Nabbout, R., Jansen, A. C., Wojdan, K., Domanska-Pakieła, D., Kaczorowska-Frontczak, M., Hertzberg, C., Ferrier, C. H., Samueli, S., Jahodova, A., Aronica, E., Kwiatkowski, D. J., Jansen, F. E., Jóźwiak, S., Lagae, L., Van Huffel, S. & Caicedo, A. (2021), 'Results of quantitative EEG analysis are associated with autism spectrum disorder and development abnormalities in infants with tuberous sclerosis complex', *Biomedical Signal Processing and Control* **68**(4), 102658.

Lazarev, V. V., Pontes, A., Mitrofanov, A. A. & DeAzevedo, L. C. (2015), 'Reduced Interhemispheric Connectivity in Childhood Autism Detected by Electroencephalographic Photic Driving Coherence', *Journal of Autism and Developmental Disorders* **45**(2), 537–547.

Lerman, J. (1996), 'Study design in clinical research: Sample size estimation and power analysis', *Canadian Journal of Anaesthesia* **43**(2), 184–191.

Léveillé, C., Barbeau, E. B., Bolduc, C., Limoges, É., Berthiaume, C., Chevrier, É., Mottron, L. & Godbout, R. (2010), 'Enhanced connectivity between visual cortex and other regions of the brain in autism: a REM sleep EEG coherence study', *Autism Research* **3**(5), 280–285.

Li, X., Yan, Y. & Wei, W. (2013), 'Identifying Patients with Poststroke Mild Cognitive Impairment by Pattern Recognition of Working Memory Load-Related ERP', *Computational and Mathematical Methods in Medicine* **2013**, 1–10.

Liu, J., Li, M., Pan, Y., Lan, W., Zheng, R., Wu, F.-X. & Wang, J. (2017), 'Complex Brain Network Analysis and Its Applications to Brain Disorders: A Survey', *Complexity* **2017**, 1–27.

Liu, L., Vira, A., Friedman, E., Minas, J., Bolger, D., Bitan, T. & Booth, J. (2010), 'Children with Reading Disability Show Brain Differences in Effective Connectivity for Visual, but Not Auditory Word Comprehension', *PLoS ONE* **5**(10), e13492.

Lloyd, R. O., O'Toole, J. M., Livingstone, V., Filan, P. M. & Boylan, G. B. (2021), 'Can EEG accurately predict 2-year neurodevelopmental outcome for preterm infants?', *Archives of Disease in Childhood - Fetal and Neonatal Edition* **106**(5), 535–541.

Lloyd, R. O., O'Toole, J. M., Livingstone, V., Hutch, W. D., Pavlidis, E., Cronin, A.-M., Dempsey, E. M., Filan, P. M. & Boylan, G. B. (2016), 'Predicting 2-y outcome in

preterm infants using early multimodal physiological monitoring', *Pediatric Research* **80**(3), 382–388.

Ludwig, K. A., Miriani, R. M., Langhals, N. B., Joseph, M. D., Anderson, D. J. & Kipke, D. R. (2009), 'Using a Common Average Reference to Improve Cortical Neuron Recordings From Microelectrode Arrays', *Journal of Neurophysiology* **101**(3), 1679–1689.

Luo, Y., Alvarez, T. L., Halperin, J. M. & Li, X. (2020), 'Multimodal neuroimaging-based prediction of adult outcomes in childhood-onset ADHD using ensemble learning techniques', *NeuroImage: Clinical* **26**(10).

Mahmoud, M. B., Ali, N. B., Fray, S., Jamoussi, H., Chebbi, S. & Fredj, M. (2021), 'Utility of EEG on attention deficit–hyperactivity disorder (ADHD)', *Epilepsy & Behavior* **114**, 107583.

Mallat, S. (1989), 'A theory for multiresolution signal decomposition: the wavelet representation', *IEEE Transactions on Pattern Analysis and Machine Intelligence* **11**(7), 674–693.

Malmivuo, J. & Plonsey, R. (1995), *BioelectromagnetismPrinciples and Applications of Bioelectric and Biomagnetic Fields*, Oxford University Press, New York.

Martínez-Briones, B., Fernández-Harmony, T., Garófalo Gómez, N., Biscay-Lirio, R. & Bosch-Bayard, J. (2020), 'Working Memory in Children with Learning Disorders: An EEG Power Spectrum Analysis', *Brain Sciences* **10**(11), 817.

Maruyama, K., Okumura, A., Hayakawa, F., Kato, T., Kuno, K. & Watanabe, K. (2002), 'Prognostic Value of EEG Depression in Preterm Infants for Later Development of Cerebral Palsy', *Neuropediatrics* **33**(3), 133–137.

MathWorks (2018), Statistics and Machine Learning Toolbox™ User's Guide, Technical report, MathWorks, Natick, MA.

MathWorks (2021), 'Regression Learner App'.

Matlis, S., Boric, K., Chu, C. J. & Kramer, M. A. (2015), 'Robust disruptions in electroencephalogram cortical oscillations and large-scale functional networks in autism', *BMC Neurology* **15**(1), 1–17.

Mayo, M. (2016), 'Decision Tree Classifiers: A Concise Technical Overview'.
URL: *https://www.kdnuggets.com/2016/10/decision-trees-concise-technical-overview.html*

McGuire, B. (2021), 'Nervous System and Spinal Cord'.
URL: *https://www.coursehero.com/sg/anatomy-and-physiology/neuron-structure/*

Mehdizadehfar, V. & Fallah, A. (2016), 'Analysis of Brain Connectivity Patterns in Autistic Children During Watching Emotional Faces', *Iranian Conference on Biomedical Engineering* (11), 23–25.

Mika (2010), 'Brain Connectivity Toolbox'.
URL: *https://sites.google.com/site/bctnet/*

Moeskops, P., Išgum, I., Keunen, K., Claessens, N. H. P., van Haastert, I. C., Groenendaal, F., de Vries, L. S., Viergever, M. A. & Benders, M. J. N. L. (2017), 'Prediction of cognitive and motor outcome of preterm infants based on automatic quantitative descriptors from neonatal MR brain images', *Scientific Reports* **7**(1), 2163.

Moghaddari, M., Lighvan, M. Z. & Danishvar, S. (2020), 'Diagnose ADHD disorder in children using convolutional neural network based on continuous mental task EEG', *Computer Methods and Programs in Biomedicine* **197**, 105738.

Mohammad-Rezazadeh, I., Frohlich, J., Loo, S. K. & Jeste, S. S. (2016), 'Brain connectivity in autism spectrum disorder', *Current Opinion in Neurology* **29**(2), 137–147.

Moniz, N., Branco, P., Torgo, L. & Krawczyk, B. (2017), 'Evaluation of Ensemble Methods in Imbalanced Regression Tasks', *Proceedings of Machine Learning Research* **74**, 129–140.

Monteiro, R., Simões, M., Andrade, J. & Castelo Branco, M. (2017), 'Processing of Facial Expressions in Autism: a Systematic Review of EEG/ERP Evidence', *Review Journal of Autism and Developmental Disorders* **4**(4), 255–276.

Moradimanesh, Z., Khosrowabadi, R., Eshaghi Gordji, M. & Jafari, G. R. (2021), 'Altered structural balance of resting-state networks in autism', *Scientific Reports* **11**(1), 1966.

Morken, F., Helland, T., Hugdahl, K. & Specht, K. (2017), 'Reading in dyslexia across literacy development: A longitudinal study of effective connectivity', *NeuroImage* **144**(Pt A), 92–100.

Morris, C. (2007), 'Definition and classification of cerebral palsy: a historical perspective', *Developmental Medicine & Child Neurology* **49**, 3–7.

Murias, M., Webb, S. J., Greenson, J. & Dawson, G. (2007), 'Resting State Cortical Connectivity Reflected in EEG Coherence in Individuals With Autism', *Biological Psychiatry* **62**(3), 270–273.

Muthuraman, M., Moliadze, V., Boecher, L., Siemann, J., Freitag, C. M., Groppa, S. & Siniatchkin, M. (2019), 'Multimodal alterations of directed connectivity profiles in patients with attention-deficit/hyperactivity disorders', *Scientific Reports* **9**(1), 20028.

Niso, G., Bruña, R., Pereda, E., Gutiérrez, R., Bajo, R., Maestú, F. & Del-Pozo, F. (2013), 'HERMES: Towards an Integrated Toolbox to Characterize Functional and Effective Brain Connectivity', *Neuroinformatics* **11**(4), 405–434.

Northcutt, R. G. (1989), 'Body and Brain. A Trophic Theory of Neural Connections.', *Science* **244**(4907), 993–993.

Orekhova, E. V., Elsabbagh, M., Jones, E. J., Dawson, G., Charman, T. & Johnson, M. H. (2014), 'EEG hyper-connectivity in high-risk infants is associated with later autism', *Journal of Neurodevelopmental Disorders* **6**(1), 1–11.

Organization, W. H. (2011), World Report on Disability, Technical report, Geneva.
URL: *https://www.who.int/publications/i/item/9789241564182*

Ouwehand, S., Smidt, L. C., Dudink, J., Benders, M. J., de Vries, L. S., Groenendaal, F. & van der Aa, N. E. (2020), 'Predictors of Outcomes in Hypoxic-Ischemic Encephalopathy following Hypothermia: A Meta-Analysis', *Neonatology* **117**(4), 411–427.

Ouyang, M., Peng, Q., Jeon, T., Heyne, R., Chalak, L. & Huang, H. (2020), 'Diffusion-MRI-based regional cortical microstructure at birth for predicting neurodevelopmental outcomes of 2-year-olds', *eLife* **9**, 1–20.

Pecora, L. M. & Carroll, T. L. (1990), 'Synchronization in chaotic systems', *Physical Review Letters* **64**(8), 821–824.

Peters, J. M., Taquet, M., Vega, C., Jeste, S. S., Fernández, I. S., Tan, J., Nelson, C. A., Sahin, M. & Warfield, S. K. (2013), 'Brain functional networks in syndromic and non-syndromic autism: a graph theoretical study of EEG connectivity', *BMC Medicine* **11**(1), 54.

Pikovsky, A. S. (1984), 'On the interaction of strange attractors', *Zeitschrift für Physik B Condensed Matter* **55**(2), 149–154.

Pisani, F. & Spagnoli, C. (2016), 'Monitoring of newborns at high risk for brain injury', *Italian Journal of Pediatrics* **42**(1), 48.

Potharst, E. S., Houtzager, B. A., van Sonderen, L., Tamminga, P., Kok, J. H., Last, B. F. & van Wassenaer, A. G. (2012), 'Prediction of cognitive abilities at the age of 5 years using developmental follow-up assessments at the age of 2 and 3 years in very preterm children', *Developmental Medicine & Child Neurology* **54**(3), 240–246.

Rashid, B. & Calhoun, V. (2020), 'Towards a brain-based predictome of mental illness', *Human Brain Mapping* **41**(12), 3468–3535.

Righi, G., Tierney, A. L., Tager-Flusberg, H. & Nelson, C. A. (2014), 'Functional Connectivity in the First Year of Life in Infants at Risk for Autism Spectrum Disorder: An EEG Study', *PLoS ONE* **9**(8), e105176.

Riley, R. D., Ensor, J., Snell, K. I. E., Harrell, F. E., Martin, G. P., Reitsma, J. B., Moons, K. G. M., Collins, G. & van Smeden, M. (2020), 'Calculating the sample size required for developing a clinical prediction model', *BMJ* **368**, m441.

Rolls, E. T., Zhou, Y., Cheng, W., Gilson, M., Deco, G. & Feng, J. (2020), 'Effective connectivity in autism', *Autism Research* **13**(1), 32–44.

Rubinov, M. & Sporns, O. (2010), 'Complex network measures of brain connectivity: Uses and interpretations', *NeuroImage* **52**(3), 1059–1069.

Saby, J. N. & Marshall, P. J. (2012), 'The Utility of EEG Band Power Analysis in the Study of Infancy and Early Childhood', *Developmental Neuropsychology* **37**(3), 253–273.

Sahu, R., Dash, S. R., Cacha, L. A., Poznanski, R. R. & Parida, S. (2020), 'Epileptic seizure detection: a comparative study between deep and traditional machine learning techniques', *Journal of Integrative Neuroscience* **19**(1), 1.

Sajedi, F., Ahmadlou, M., Vameghi, R., Gharib, M. & Hemmati, S. (2013), 'Linear and nonlinear analysis of brain dynamics in children with cerebral palsy', *Research in Developmental Disabilities* **34**(5), 1388–1396.

Sakkalis, V. (2011), 'Review of advanced techniques for the estimation of brain connectivity measured with EEG/MEG', *Computers in Biology and Medicine* **41**(12), 1110–1117.

Sanei, S. & Chambers, J. (2013), *EEG Signal Processing*, John Wiley & Sons Ltd,, West Sussex, England.

Sato, J. R., Hoexter, M. Q., Castellanos, X. F. & Rohde, L. A. (2012), 'Abnormal Brain Connectivity Patterns in Adults with ADHD: A Coherence Study', *PLoS ONE* **7**(9), e45671.

Schreglmann, M., Ground, A., Vollmer, B. & Johnson, M. J. (2020), 'Systematic review: long-term cognitive and behavioural outcomes of neonatal hypoxic–ischaemic encephalopathy in children without cerebral palsy', *Acta Paediatrica, International Journal of Paediatrics* **109**(1), 20–30.

Schreiber, T. (2000), 'Measuring Information Transfer', *Physical Review Letters* **85**(2), 461–464.

Schwartz, S., Kessler, R., Gaughan, T. & Buckley, A. W. (2017), 'Electroencephalogram Coherence Patterns in Autism: An Updated Review', *Pediatric Neurology* **67**, 7–22.

SCPE (2001), 'Surveillance of cerebral palsy in europe: a collaboration of cerebral palsy surveys and registers', *Developmental Medicine and Child Neurology* **42**(12), 816.

Seiffert, C., Khoshgoftaar, T. M., Van Hulse, J. & Napolitano, A. (2010), 'RUSBoost: A Hybrid Approach to Alleviating Class Imbalance', *IEEE Transactions on Systems, Man, and Cybernetics - Part A: Systems and Humans* **40**(1), 185–197.

Shannon, C. E. (1948), 'A Mathematical Theory of Communication', *Bell System Technical Journal* **27**(3), 379–423.

Shao, L., Fu, C., You, Y. & Fu, D. (2021), 'Classification of ASD based on fMRI data with deep learning', *Cognitive Neurodynamics* **15**(6), 961–974.

Slaughter, L. A., Bonfante-Mejia, E., Hintz, S. R., Dvorchik, I. & Parikh, N. A. (2016), 'Early conventional MRI for prediction of neurodevelopmental impairment in extremely-low-birth-weight infants', *Neonatology* **110**(1), 47–54.

Spittle, A., Orton, J., Anderson, P. J., Boyd, R. & Doyle, L. W. (2015), 'Early developmental intervention programmes provided post hospital discharge to prevent motor and cognitive impairment in preterm infants', *Cochrane Database of Systematic Reviews* **2015**(11).

Stam, C. J., Nolte, G. & Daffertshofer, A. (2007), 'Phase lag index: Assessment of functional connectivity from multi channel EEG and MEG with diminished bias from common sources', *Human Brain Mapping* **28**(11), 1178–1193.

Stam, C. J., van der Made, Y., Pijnenburg, Y. A. L. & Scheltens, P. (2003), 'EEG synchronization in mild cognitive impairment and Alzheimer's disease', *Acta Neurologica Scandinavica* **108**(2), 90–96.

Suchetha, M., Madhumitha, R., Sorna Meena, M. & Sruthi, R. (2021), 'Sequential Convolutional Neural Networks for classification of cognitive tasks from EEG signals', *Applied Soft Computing* **111**, 107664.

Sui, J., Jiang, R., Bustillo, J. & Calhoun, V. (2020), 'Neuroimaging-based Individualized Prediction of Cognition and Behavior for Mental Disorders and Health: Methods and Promises', *Biological Psychiatry* pp. 1–31.

Suppiej, A., Cainelli, E., Cappellari, A., Trevisanuto, D., Balao, L., Di Bono, M. G. & Bisiacchi, P. S. (2017), 'Spectral analysis highlight developmental EEG changes in preterm infants without overt brain damage', *Neuroscience Letters* **649**, 112–115.

Sur, S. & Sinha, V. (2009), 'Event-related potential: An overview', *Industrial Psychiatry Journal* **18**(1), 70.

Suresh, K. & Chandrashekara, S. (2012), 'Sample size estimation and power analysis for clinical research studies', *Journal of Human Reproductive Sciences* **5**(1), 7–13.

Sweeney-Reed, C. M. & Nasuto, S. J. (2007), 'A novel approach to the detection of synchronisation in EEG based on empirical mode decomposition', *Journal of Computational Neuroscience* **23**(1), 79–111.

Sysoeva, O. V., Constantino, J. N. & Anokhin, A. P. (2018), 'Event-related potential (ERP) correlates of face processing in verbal children with autism spectrum disorders (ASD) and their first-degree relatives: a family study', *Molecular Autism* **9**(1), 41.

Tenev, A., Markovska-Simoska, S., Kocarev, L., Pop-Jordanov, J., Müller, A. & Candrian, G. (2014), 'Machine learning approach for classification of ADHD adults', *International Journal of Psychophysiology* **93**(1), 162–166.

The National Autistic Society (2016), 'Autism'.
URL: *https://www.autism.org.uk/about.aspx*

Theodoridis, S. (2010), Classifiers Based on Bayes Decision Theory, *in* 'Matlab Introduction to Pattern Recognition', Elsevier, pp. 1–27.

Theodoridis, S. & Koutroumbas, K. (2008), *Pattern recognition*, 4 edn, Academic Press.

Theodorsson-Norheim, E. (1986), 'Kruskal-Wallis test: BASIC computer program to perform nonparametric one-way analysis of variance and multiple comparisons on ranks of several independent samples', *Computer Methods and Programs in Biomedicine* **23**(1), 57–62.

Tonmukayakul, U., Shih, S. T., Bourke-Taylor, H., Imms, C., Reddihough, D., Cox, L. & Carter, R. (2018), 'Systematic review of the economic impact of cerebral palsy', *Research in Developmental Disabilities* **80**, 93–101.

Tottenham, N., Tanaka, J. W., Leon, A. C., McCarry, T., Nurse, M., Hare, T. A., Marcus, D. J., Westerlund, A., Casey, B. & Nelson, C. (2009), 'The NimStim set of facial expressions: Judgments from untrained research participants', *Psychiatry Research* **168**(3), 242–249.

Tran, N. & Miyake, K. (2017), 'Neurodevelopmental Disorders and Environmental Toxicants: Epigenetics as an Underlying Mechanism', *International Journal of Genomics* **2017**, 1–23.

ur Rehman, N. & Mandic, D. P. (2011), 'Filter bank property of multivariate empirical mode decomposition', *IEEE Transactions on Signal Processing* **59**(5), 2421–2426.

ur Rehman, N., Yili Xia & Mandic, D. P. (2010), Application of multivariate empirical mode decomposition for seizure detection in EEG signals, *in* '2010 Annual International Conference of the IEEE Engineering in Medicine and Biology', IEEE, pp. 1650–1653.

Valenti, M., Pino, M. C., Mazza, M., Panzarino, G., Di Paolantonio, C. & Verrotti, A. (2020), 'Abnormal Structural and Functional Connectivity of the Corpus Callosum in Autism Spectrum Disorders: a Review', *Review Journal of Autism and Developmental Disorders* **7**(1), 46–62.

van Laerhoven, H., de Haan, T. R., Offringa, M., Post, B. & van der Lee, J. H. (2013), 'Prognostic Tests in Term Neonates With Hypoxic-Ischemic Encephalopathy: A Systematic Review', *PEDIATRICS* **131**(1), 88–98.

Vinck, M., Oostenveld, R., van Wingerden, M., Battaglia, F. & Pennartz, C. M. (2011), 'An improved index of phase-synchronization for electrophysiological data in the presence of volume-conduction, noise and sample-size bias', *NeuroImage* **55**(4), 1548–1565.

Wang, S., Zhang, D., Fang, B., Liu, X., Yan, G., Sui, G., Huang, Q., Sun, L. & Wang, S. (2021), 'A Study on Resting EEG Effective Connectivity Difference before and after Neurofeedback for Children with ADHD', *Neuroscience* **457**, 103–113.

Wang, Y., Sokhadze, E. M., El-Baz, A. S., Li, X., Sears, L., Casanova, M. F. & Tasman, A. (2016), 'Relative Power of Specific EEG Bands and Their Ratios during Neurofeedback Training in Children with Autism Spectrum Disorder', *Frontiers in Human Neuroscience* **9**(1).

West, C. R., Battin, M. R., Williams, C. E., Dezoete, J. A. & Harding, J. E. (2005), '413 Early Quantitative Electroencephalographic Measures of Continuity are Associated with Neurodevelopmental Outcome at 18 Months in Preterm Infants', *Pediatric Research* **58**(2), 425–425.

World Health Organization (2021), 'Autism spectrum disorders'.
URL: *https://www.who.int/news-room/fact-sheets/detail/autism-spectrum-disorders*

Xue, H., Wang, Z., Tan, Y., Yang, H., Fu, W., Xue, L. & Zhao, J. (2020), 'Resting-state EEG reveals global network deficiency in dyslexic children', *Neuropsychologia* **138**(6), 107343.

Yeung, M. K., Han, Y. M., Sze, S. L. & Chan, A. S. (2014), 'Altered right frontal cortical connectivity during facial emotion recognition in children with autism spectrum disorders', *Research in Autism Spectrum Disorders* **8**(11), 1567–1577.

Yin, W., Li, L. & Wu, F.-X. (2020), 'Deep learning for brain disorder diagnosis based on fMRI images', *Neurocomputing* .

Zeng, K., Kang, J., Ouyang, G., Li, J., Han, J., Wang, Y., Sokhadze, E. M., Casanova, M. F. & Li, X. (2017), 'Disrupted Brain Network in Children with Autism Spectrum Disorder', *Scientific Reports* **7**(1), 16253.

Zheng, Y., Wang, G., Li, K., Bao, G. & Wang, J. (2014), 'Epileptic seizure prediction using phase synchronization based on bivariate empirical mode decomposition', *Clinical Neurophysiology* **125**(6), 1104–1111.

Zwaigenbaum, L. & Penner, M. (2018), 'Autism spectrum disorder: advances in diagnosis and evaluation', *BMJ* **361**.

Appendix A

Results of the Applications of WPLI-based FBC from DBP filter

TABLE A.1: Classification performance in each frequency bands using WPLI-based FBC from DBP in prediction CP.

Frequency bands	Feature	ACC	SNS	SPC	Balanced accuracy	AUC
Delta	Transitivity	76.90%	67.00%	80.00%	73.50%	0.63
	Global efficiency	73.10%	67.00%	75.00%	71.00%	0.70
	Radius	65.40%	67.00%	65.00%	66.00%	0.49
	Diameter	57.70%	33.00%	65.00%	49.00%	0.27
	Charactristic path length	76.90%	67.00%	80.00%	73.50%	0.69
	All features	84.60%	67.00%	90.00%	78.50%	0.75
Theta	Transitivity	57.70%	33.00%	65.00%	49.00%	0.43
	Global efficiency	73.10%	50.00%	80.00%	65.00%	0.48
	Radius	76.90%	83.00%	75.00%	79.00%	0.78
	Diameter	73.10%	50.00%	80.00%	65.00%	0.66
	Charactristic path length	73.10%	50.00%	80.00%	65.00%	0.53
	All features	57.00%	33.00%	65.00%	49.00%	0.56
Alpha	Transitivity	57.70%	67.00%	55.00%	61.00%	0.55
	Global efficiency	73.10%	50.00%	80.00%	65.00%	0.67
	Radius	53.80%	0	70.00%	35.00%	0.31
	Diameter	34.60%	33.00%	35.00%	34.00%	0.26
	Charactristic path length	69.20%	33.00%	80.00%	56.50%	0.65
	All features	61.50%	50.00%	65.00%	57.50%	0.52
Beta	Transitivity	65.40%	50.00%	70.00%	60.00%	0.50
	Global efficiency	73.10%	50.00%	80.00%	65.00%	0.51
	Radius	46.20%	17.00%	55.00%	36.00%	0.28
	Diameter	42.30%	33.00%	45.00%	39.00%	0.30
	Charactristic path length	50%	50.00%	50.00%	50.00%	0.38
	All features	53.80%	67.00%	50.00%	58.50%	0.46
Gamma	Transitivity	46.20%	50.00%	45.00%	47.50%	0.35
	Global efficiency	42.30%	50.00%	40.00%	45.00%	0.35
	Radius	42.30%	33.00%	45.00%	39.00%	0.35
	Diameter	50.00%	33.00%	55.00%	44.00%	0.34
	Charactristic path length	34.60%	33.00%	35.00%	34.00%	0.28
	All features	30.80%	33.00%	30.00%	31.50%	0.16

Appendix B

Results of the Applications of WPLI-based FBC from NA-MEMD

TABLE B.1: Classification performance in each frequency bands using WPLI-based FBC from NA-MEMD in prediction CP.

Frequency bands	Feature	ACC	SNS	SPC	Balanced accuracy	AUC
IMF3	Transitivity	53.80%	67.00%	50.00%	58.50%	0.43
	Global efficiency	50.00%	33.00%	55.00%	44.00%	0.38
	Radius	53.80%	33.00%	60.00%	46.50%	0.44
	Diameter	57.70%	33.00%	65.00%	49.00%	0.48
	Characteristic path length	69.20%	50.00%	75.00%	62.50%	0.65
	All features	38.50%	17.00%	55.00%	36.00%	0.26
IMF4	Transitivity	50.00%	33.00%	55.00%	44.00%	0.30
	Global efficiency	53.80%	33.00%	60.00%	46.5%	0.22
	Radius	53.80%	50.00%	55.00%	52.5%	0.47
	Diameter	42.30%	33.00%	45.00%	39.00%	0.35
	Characteristic path length	53.80%	33.00%	60.00%	46.5%	0.27
	All features	46.20%	17.00%	55.00%	36.00%	0.32
IMF5	Transitivity	42.30%	33.00%	45.00%	39.00%	0.38
	Global efficiency	57.70%	67.00%	55.00%	61.00%	0.53
	Radius	38.50%	33.00%	40.00%	61.00%	0.31
	Diameter	80.80%	67.00%	85.00%	76.00%	0.72
	Characteristic path length	53.80%	67.00%	50.00%	58.5%	0.53
	All features	76.90%	83.00%	75.00%	79.00%	0.76
IMF6	Transitivity	30.80%	17.00%	35.00%	26.00%	0.23
	Global efficiency	30.80%	17.00%	35.00%	26.00%	0.21
	Radius	46.20%	17.00%	35.00%	26.00%	0.22
	Diameter	80.80%	67.00%	85.00%	76.00%	0.79
	Characteristic Characteristic	23.10%	0	30.00%	15.00%	0.07
	All features	57.70%	50.00%	60.00%	55.00%	0.49
IMF7	Transitivity	80.80%	67.00%	85.00%	76.00%	0.78
	Global efficiency	65.40%	50.00%	70.00%	60.00	0.67
	Radius	38.50%	33.00%	40.00%	36.50%	0.32
	Diameter	34.60%	0	45.00%	22.5%	0.14
	Characteristic path length	57.70%	50.00%	60.00%	55.00%	0.54
	All features	53.80%	17.00%	65.00%	41.00%	0.40
IMF8	Transitivity	84.60%	83.00%	85.00%	84.00%	0.85
	Global efficiency	80.80%	67.00%	85.00%	76.00%	0.90
	Radius	65.40%	67.00%	65.00%	66.00%	0.64
	Diameter	42.30%	33.00%	45.00%	39.00%	0.29
	Characteristic Characteristic	84.60%	67.00%	90.00%	78.50%	0.81
	All features	76.90%	83.00%	75.00%	79.00%	0.92
IMF9	Transitivity	69.20%	50.00%	75.00%	62.50%	0.49
	Global efficiency	65.40%	50.00%	70.00%	60.00%	0.55
	Radius	61.50%	33.00%	70.00%	51.50%	0.48
	Diameter	46.20%	17.00%	55.00%	36.00%	0.35
	Characteristic Characteristic	69.20%	33.00%	80.00%	56.50%	0.44
	All features	46.20%	50.00%	45.00%	47.50%	0.40